BACTERIOPHAGE LAMBDA INTEGRATES MICROENVIRONMENTS, INDIVIDUALITY, AND INTERACTIONS TO FORMULATE SUBCELLULAR DECISIONS

A Dissertation

by

JIMMY TRI TRINH

Submitted to the Office of Graduate and Professional Studies of
Texas A&M University
in partial fulfillment of the requirements for the degree of

DOCTOR OF PHILOSOPHY

Chair of Committee,	Lanying Zeng
Committee Members,	Ryland Young
	Craig Kaplan
	Deborah Siegele
Head of Department,	Gregory D. Reinhart

May 2018

Major Subject: Biochemistry

ABSTRACT

Decision-making influences the development of life over multiple levels. Understanding the core mechanisms of this complex process could yield new insights into the treatment of diseases and the evolution of lifeforms. To study the universal subject of decision-making, we investigate the simple bacteriophage lambda model to distill complicated decision-making into fundamental biological questions. Lambda is a virus that infects *E. coli*, choosing between alternative modes of propagation, lysis or lysogeny, as its decision. Despite a history of research spanning decades, the underlying mechanisms of lambda decision-making are unclear. Using fluorescence microscopy for quantitative, high-resolution study, we explore an established paradigm with a new perspective to discover the inner workings of cellular decision-making.

In our studies, we find that phages within single cells behave analogous to advanced organisms within their niches. For lambda, we find that their viral DNA molecules compete with each other inside the cell over replication resources. This allows phages to dominate each other, particularly during lysis, when DNA replication is important. Conversely, cooperation is prevalent during lysogeny, allowing viruses to benefit each other during a different path of development. These behaviors play a role in evolutionary fitness, where both strategic domination and cooperation may minimize the chances of extinction. We then study the spatial organization of phage development in the cell. We build tools to specifically characterize the coordinates of lambda DNA replication, resource sequestration, transcription, and virion assembly. We find that

lambda manipulates its environment by hoarding resources and confining replicated viral genomes spatially. We observe that phage transcripts are localized nearby the phage genomes, and that virion assembly transpires in the same location, resembling a phage factory. Through our analysis, we find that multiple factories arise in cells and may be quantitatively distinct, suggesting this to be the origin of viral individuality. Indeed, we observe that different transcription programs, corresponding to different fates, occur in single cells, corroborating our hypothesis that individual phages can vote for decisions within cells. Finally, we incorporate our quantitative data and new models into computational simulations of this biological process to work towards a more complete quantitative understanding of decision-making.

DEDICATION

I dedicate this work to my mother, Thuy Thi Trinh. I will always love and remember you. Everything that I have done and everything that I have accomplished is a direct result of how you raised me. Your love and nurture has carried me for all of these years to where I am now, and I will never let that go, I will always use what you have given me.

In finishing graduate school, I am accomplishing the biggest milestone of my life so far. I know this is something you would have wanted for me, and it would have been a joyous achievement for us to share together. I miss you and know that you cannot be with me, but I also know that I am not alone and this is a happy occasion for all.

I will continue to do my best moving forward. I will make my decisions with the best intentions, using everything that you have taught me, because the gifts you have given me will last a lifetime. I will always live my life in a manner that will make you proud because I am your loving son, with you as my mother, now and forever. Thank you for everything.

ACKNOWLEDGEMENTS

I would like to thank my advisor, Dr. Lanying Zeng, for her role in my graduate career at Texas A&M. She offered me her guidance, support, and trust as I developed myself over my years in graduate school. It is only with the opportunity to participate in multiple projects and the freedom to engage my research following my own merits that I was able to become the scientist that I am now, fully confident and capable of handling any and all problems. My committee members, Dr. Ryland Young, Dr. Craig Kaplan, and Dr. Deborah Siegele have also contributed immensely towards my success by being encouraging and constructively critical of my work, and for that, I offer my heartfelt appreciation. I give much credit Dr. Kaplan for helping me culture my creative and analytical perspectives, because he is always forcing me to think, to see things in different ways, and to be ever ambitious and uncompromising in my research. I want to specifically thank Dr. Young for transforming me into an expert of phage by sharing his endless knowledge, insight, and passion for all things phage. I also greatly appreciate that Dr. Young offers me opportunities for new projects and collaborations, as I am always open to improving myself. I want to thank Dr. Gábor Balázsi and his lab for their collaboration on my projects, specifically regarding computational modeling. I believe that I have grown significantly from my interactions with them because of their different perspectives and input. I wish to thank the current and former members of the Zeng lab for their data and discussion, which have helped shape my work. In particular, I want to thank Dr. Qiuyan Shao for everything that she has done for me. As my senior in the lab,

she has been an ever-present influence on my research from day one with helpful discussion and critiques. As an expert on all things related to data analysis, she has proven invaluable to strengthening my work and my abilities as well. I want to acknowledge the undergraduates of our lab as a whole, who help with many aspects of research every day. They have livened up the lab and mentoring them has been a valuable experience. Thank you to the students and staff here in the Department of Biochemistry and Biophysics at Texas A&M for their support and assistance with the non-scientific side of graduate school. Finally, I want to extend my gratitude to my family for everything that they have done. Their love and support has guided me to this point in my life and helped me to succeed. For that, I am eternally grateful and hope to continue making them proud.

CONTRIBUTORS AND FUNDING SOURCES

Contributors

This work was supervised by a dissertation committee consisting of Drs. Lanying Zeng, Ryland Young, and Craig Kaplan of the Department of Biochemistry and Biophysics, and Dr. Deborah Siegele of the Department of Biology.

In chapter II, the analysis framework was constructed by Dr. Qiuyan Shao in the Zeng lab. Dr. Tamás Székely and Michael G. Cortez in the lab of Dr. Gábor Balázsi at Stony Brook University built computational models, primarily regarding the interactions of phages and effects of time to cellular decision-making, respectively.

In chapter III, Dr. Qiuyan constructed the analysis framework and performed in-situ experiments. Jingwen Guan conducted additional in-situ experiments.

In chapter IV, the creation and processing of nanodiamonds were performed by Masfer H. Alkahtani in the lab of Philip Hemmer at Texas A&M University and Dr. Arfaan Rampersaud.

All other work performed for the dissertation was completed independently by the student.

Funding Sources

This work was made possible by Texas A&M Agrilife Research and the National Institutes of Health under grant number R01GM107597. This content is solely the responsibility of the authors and do not necessarily represent the official views of Texas A&M AgriLife Research or the National Institutes of Health.

TABLE OF CONTENTS

Page

LIST OF FIGURES

Page

LIST OF TABLES

Page

CHAPTER I

INTRODUCTION AND LITERATURE REVIEW

The act of deciding is one of the most significant and complicated processes that we, as human beings, carry out, profoundly influencing the development of our entire lives. Decision-making is a behavior that extends to all organisms, as all types of life will choose between many different possibilities over the course of their lives. Undoubtedly, decisions at the organism level will affect the organism carrying out its choices, but decision-making is also extremely influential at both the cellular and population levels[1,2]. The decisions made by single cells can guide developmental processes, such as cell differentiation[3], as well as diseases, such as cancers, which cause drastic changes in the organism[4,5]. Additionally, the decisions made by individuals will collectively determine the fate of groups of organisms; this can cause even species and ecosystems to flourish or collapse[6]. Therefore, we can discover important information regarding the treatment of diseases and the evolution of lifeforms by studying decision-making[7,8].

It is somewhat peculiar that researchers have chosen to study the ubiquitous and universal subject of decision-making by using the simple model system of bacteriophage lambda infection. Lambda, a virus that infects *Escherichia coli*, chooses between alternate methods of propagation in its host cell after infection. Although this decision-making process may seem straightforward with little depth to explore and little relation to the more grand designs of complicated lifeforms, it has actually been researched to an

exceptional extent, as the phage lambda paradigm is one of the most-studied systems in biology. As a model system, lambda has played an indispensable role in developing techniques for molecular biology and thus, shaping our knowledge about the fundamental processes of life. Because of its rich research history, it is perhaps reasonable to assume that the lambda system might not have much to offer with regards to new discoveries and innovative ideas. However, the opposite is actually true. It is because of its position as a biological paradigm that allows lambda to be an ideal system in which to develop new technologies and utilize the most progressive approaches. It is through these efforts that we can extract maximal amount of information in order to work towards a complete understanding of one of the simplest decisions occurring in nature.

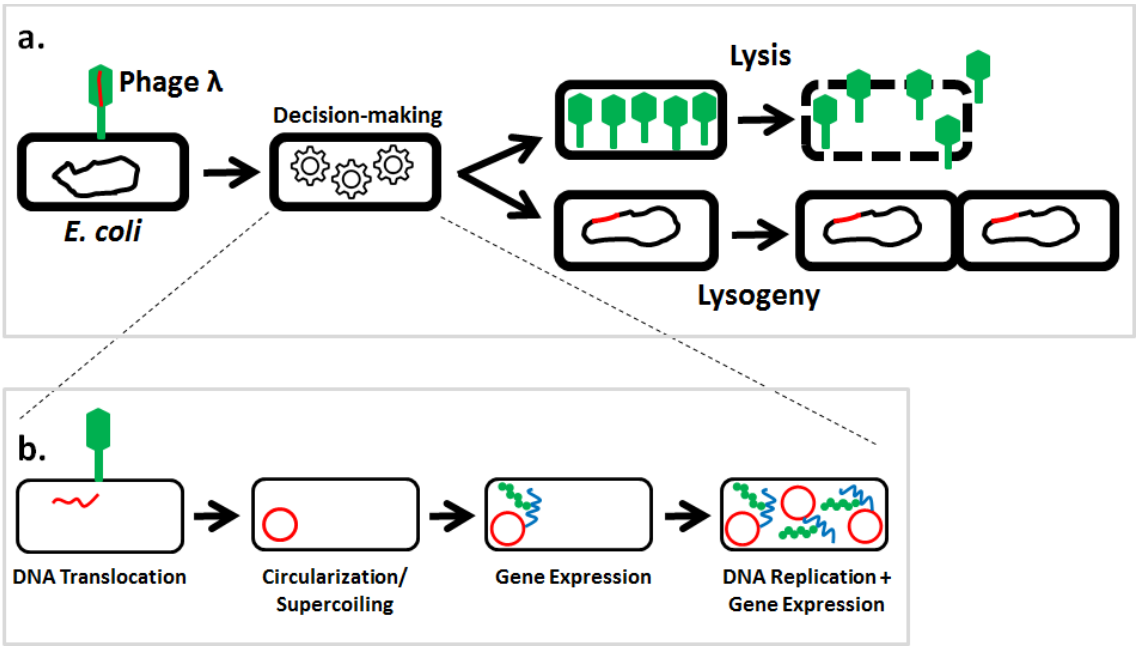

Figure 1.1 Decision-making in bacteriophage lambda.
a. Phage lambda infects its host, *E. coli*, and undergoes a decision-making process, culminating in either lysis or lysogeny. During lysis, lambda clones progeny virions and bursts the host cell to release the new phages. During lysogeny, lambda inserts its DNA genome (red) into the *E. coli* genome and replicates along with its host.
b. Multiple steps occur during decision-making to result in the final cell fate. Linear lambda DNA translocates from the phage capsid into the host cell's cytoplasm. Lambda DNA is then circularized and supercoiled prior to gene expression. Phage gene expression results in phage DNA replication and further gene expression to accumulate proteins and ultimately commit the phage to lysis or lysogeny.

Decision-making in phage lambda development

After infecting *E. coli*, a phage will either undergo lysis, by producing clones of itself and releasing its progeny by bursting the host, or lysogeny, by repressing its lytic functions and integrating into the host's genome to replicate passively (Fig. 1.1a)[9-11]. Lambda development begins after the phage particle encounters the *E. coli* cell and preferentially adsorbs near the polar or mid-cell region of the cell to its receptor (Fig. 1.1a)[12], the maltoporin, LamB[13,14]. Lambda then translocates its linear double-stranded DNA genome into the *E. coli* cytoplasm via mechanisms that are unclear. The cytoplasm is where the phage genome is ligated[15] and supercoiled[16,17] by host proteins, priming it for gene expression (Fig. 1.1b). Host RNA polymerases recognize certain lambda operons and immediate early gene expression then commences from the constitutive promoters, pL and pR, to produce N and Cro from their respective promoters (Fig. 1.2)[9]. Cro is a transcriptional repressor and downregulates pL and pR by binding as a homodimer to operators, oL1, oL2, oL3 and oR1, oR2, oR3 (stronger preference to oL3/oR3), where the oL and oR sets are positioned adjacent to pL and pR respectively[18,19]. N is an anti-terminator which functions by modifying the host's RNA polymerase to allow pL and pR transcription to bypass specific transcriptional terminators downstream of *N* and *cro*, to express the remaining genes in the pL and pR operons, which are important for lambda decision-making and development (Fig. 1.2)[20,21]. The remaining pR operon contains the early genes, including *cII, O, P,* and *Q* as essential genes for decision-making, and the pL operon contains *cIII*. The O and P proteins are required for lambda DNA replication, where O and P are analogous to *E.*

coli DnaA and DnaC respectively[22]. Phage DNA replication is an important step in lambda development, regardless of its cell fate choice (Fig. 1.1b). Many O proteins bind around the lambda origin of replication and interact with the P protein[23]. P interacts with host DnaB, the helicase, to recruit this essential resource to the phage genome to allow for the phage to be replicated[24-26].

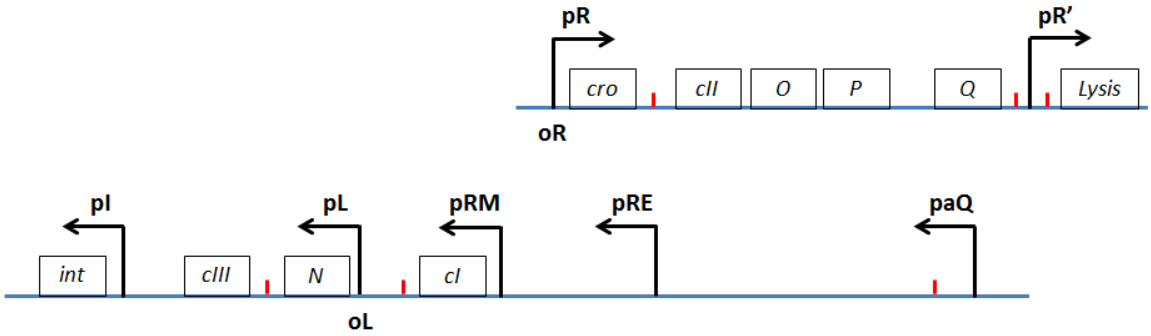

Figure 1.2 Genetic map of lambda immunity region.
The key genes comprising lambda decision-making are shown as boxes. The top section shows rightward transcripts and the bottom section shows leftward transcripts, which are all marked by arrows with promoter names. Red ticks represent transcription terminators. N allows transcription to bypass termination past *N* and *cro*. Q allows transcription to bypass termination past pR′, to continue into the lysis cassette, which consists of the lysis and morphogenesis genes.

Following this initial DNA replication and gene expression, developmental decisions are made by different gene expression pathways. Q is a transcriptional anti-terminator and acts to allow transcription to bypass an early terminator in pR′, the late operon downstream of *Q*[27]. Q acts by binding adjacent to pR′ and then binds to the host RNA polymerase as it is paused, 16 nucleotides downstream of the transcription start site, modifying the enzyme to continue beyond the immediate terminator, 194 nucleotides past the promoter, and downstream blockades (Fig. 1.2)[28,29]. This allows for the expression of morphogenesis genes to produce phage progeny and the lysis genes to complete cell lysis. The *S,R,* and *Rz/Rz1* genes comprise the lysis cassette, and together, the gene products accumulate and lyse the cell after a certain amount of time[30]. One interesting property about Q is that its action has been reported to have a degree of cis preference, where Q anti-terminates pR′ more efficiently on its cognate phage[31,32]. These observations raised some interesting questions about viral individualism to be later explored.

In the alternative path of development, CII and CIII act to prevent the lytic pathway and establish lysogeny. CII acts as a dimer of dimers[33] to bind to cryptic phage lambda promoters, pRE, pI, and paQ, allowing for transcription at these sites[9]. The pRE operon expresses CI, the master repressor of phage gene expression[34]. CI, similar to Cro, binds as a dimer to the oL and oR operators, but with a different preference[35] (1>2>3) and with strong cooperativity between the 1 and 2 sites[36]. CI also loops the DNA by binding the oL and oR regions together via octamerization (Fig. 1.3)[37]. This activity shuts down phage gene transcription from these major promoters, halting further

decision-making. This binding of CI also activates the pRM operon, which self-regulates CI to maintain the lysogeny[38,39]. Higher CI levels cause CI to bind to oR3/oL3 and repress further CI expression from pRM, striking a balance in CI levels[40].

As for the other CII-regulated, promoters, pI controls the expression of Integrase (Int)[41], which acts to integrate the phage genome into the *E. coli* genome at the specific attachment site for lambda, attB[42]; paQ does not appear to encode a protein, but transcription from this promoter downregulates *Q* expression to favor lysogeny over lysis (Fig. 1.2)[43]. CII is actively degraded by the host protease, FtsH[44,45], which inhibits lysogeny, but CIII functions to prevent this by competing as an alternate substrate for the protease, buoying CII levels[46]. Altogether, these different players interact within this genetic circuit, where the actions of CII and Q act as the key decision-makers, committing to the cell to a fate. The expression of the effectors, CI and the lytic proteins then execute the cellular functions to complete the decision.

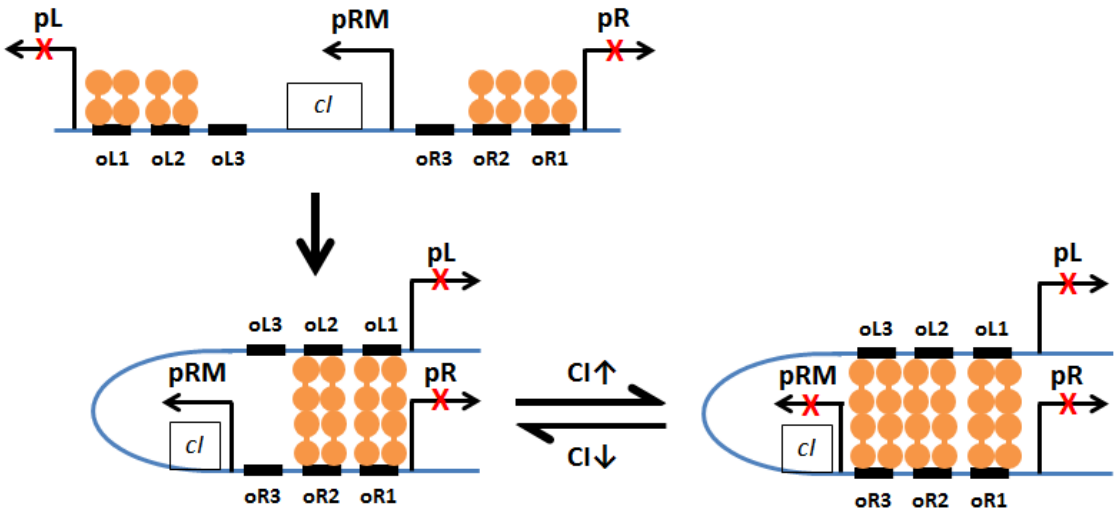

Figure 1.3 Mechanism of CI action.
CI protein dimers (orange) bind to oL and oR operators, specifically oL1/oR1/oL2/oR2, to block transcription from pL and pR. CI binding also activates transcription from pRM to express *cI*. CI has oligomerization domains to form 8-mers and loop DNA, helping to inhibit pL and pR. At high CI levels, CI binds to oL3/oR3 to inhibit further *cI* expression. As CI has lower affinity for oL3/oR3, a decrease in CI levels will cause a reversion to the active pRM state.

Both known and hidden variables affect decision-making

Disparate cell fates occur even when genetically identical phages infect genetically identical host cells, suggesting that decision-making is uncertain or noisy (Fig. 1.4a)[47]. Researchers have performed detailed mathematical modeling using stochastic simulations to show that variations in biochemical kinetics, promoter regulation, and gene expression can capture experimental observations[47,48]. However, it is unclear how random these processes truly are, as it may be possible to determine precise fates at the molecular level. Indeed, for lambda, many important variables have been characterized, including how the multiplicity of infection (MOI)[49], metabolic state of the cell[50], and cell size[51], among other variables, affect the decision-making process. An increase in MOI effectively increases the concentration of viral proteins, as each infecting phage presumably undergoes its own gene expression, and this favors lysogeny[49]. As phage DNA replication occurs over the course of phage infection, replicated phage genomes are also expected to contribute to the viral concentration. Researchers confirmed that the abolishment of phage DNA replication reduces the chances of lysogeny, and naturally, prevents lysis from occurring as well[52]. If the viral concentration affects decision-making, then the size of the cell is predicted to bias the decision by modulating the effective concentration of phage products. This prediction has been validated, with researchers demonstrating that smaller cells favor lysogeny (Fig. 1.4b)[51].

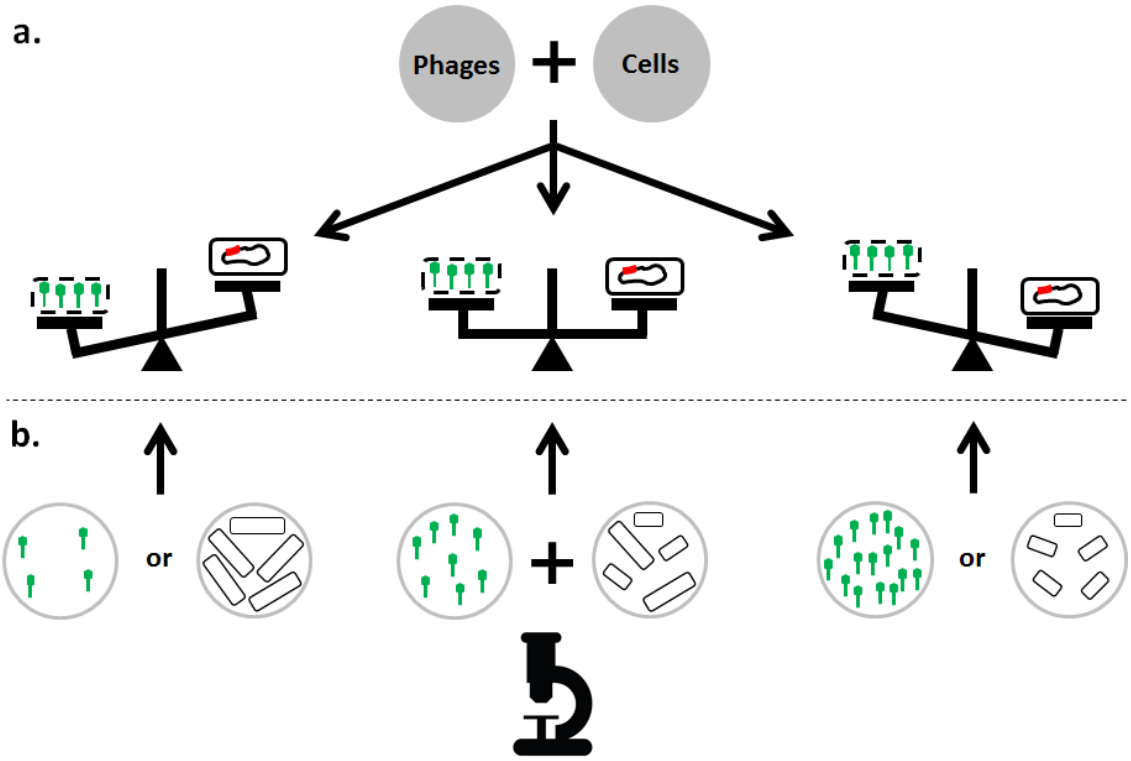

Figure 1.4 Proper resolution reveals deterministic factors behind noisy phenotypes.
a. Infections of *E. coli* by phage lambda can results in a noisy phenotype where the probability of lysis/lysogeny varies. This has been explained to be caused by inherent stochasticity originating from chemical reactions and gene expression.
b. Higher resolution studies decrease the role of stochasticity in decision-making. Microscopy allows for single cell/virus observations of phage infection, showing that the MOI (multiplicity of infection) and cell size have deterministic effects on lambda decision-making.

As phage lambda interacts with numerous host factors, the physiology of the cell also guides decision-making. The expression of CII and Q decide the fate of lambda infection, and their expression can be affected by the physiological state of the host. FtsH degrades CII to alter the decision, and cAMP interferes with FtsH activity, therefore, cAMP levels indirectly bias lambda decision-making. Furthermore, this indicates that pre-existing cellular conditions that define cAMP levels influence decision-making[53,54]. Another important host factor, ppGpp, signals the cell about various stresses. This global cell effector has been suggested to enhance CII-mediated transcription to steer the cell toward lysogeny during starvation[55]. These examples show that underlying cellular processes are not always obvious, but nonetheless exert their influence on decision-making. The apparent role of stochasticity may be even further reduced if more hidden factors can be defined, which would provide much more insight into biological processes.

Further characterization of hidden influential variables could have major implications for how decision-making occurs in advanced systems. Having a systemic understanding of how cells choose to commit to different developmental paths could potentially allow for preventing and treating certain diseases which feature changes in cellular development, such as certain cancers and neurodegenerative conditions[56]. As decision-making occurs at multiple levels and also involves interactions between the agents making choices, it has consequences on how organisms evolve as well[6]. The complex behaviors among individuals shape how populations change over time, so studying decision-making enables researchers to delve into the evolutionary histories of

lifeforms and could help predict future changes[8]. As unintuitive as it seems to utilize bacteriophages to understand this broad decision process, if we distill the nebulous concept of complex decision-making into simpler events, then lambda development resembles a microcosm of the behaviors found in more complicated decision-making circuits.

How fates diverge in decision-making systems

At its most basic interpretation, decision-making circuits can sense different stimuli and produce varying responses accordingly (Fig. 1.5). For organisms capable of higher-order thought, the sensing of stimuli can be thought of in terms of weighing pros and cons of the different outcomes. These stimuli may be chemical in nature, as there are many neurotransmitters that influence the brain's decision-making for organisms with a brain[57,58]. Widely-known examples of these include chemicals such as adrenaline, which alters an animal's physiological state to push it to respond with "fight-or-flight"[59]. The brain senses an outside stimulus and releases the chemical effector to the organs, such as the heart, which then pumps faster.

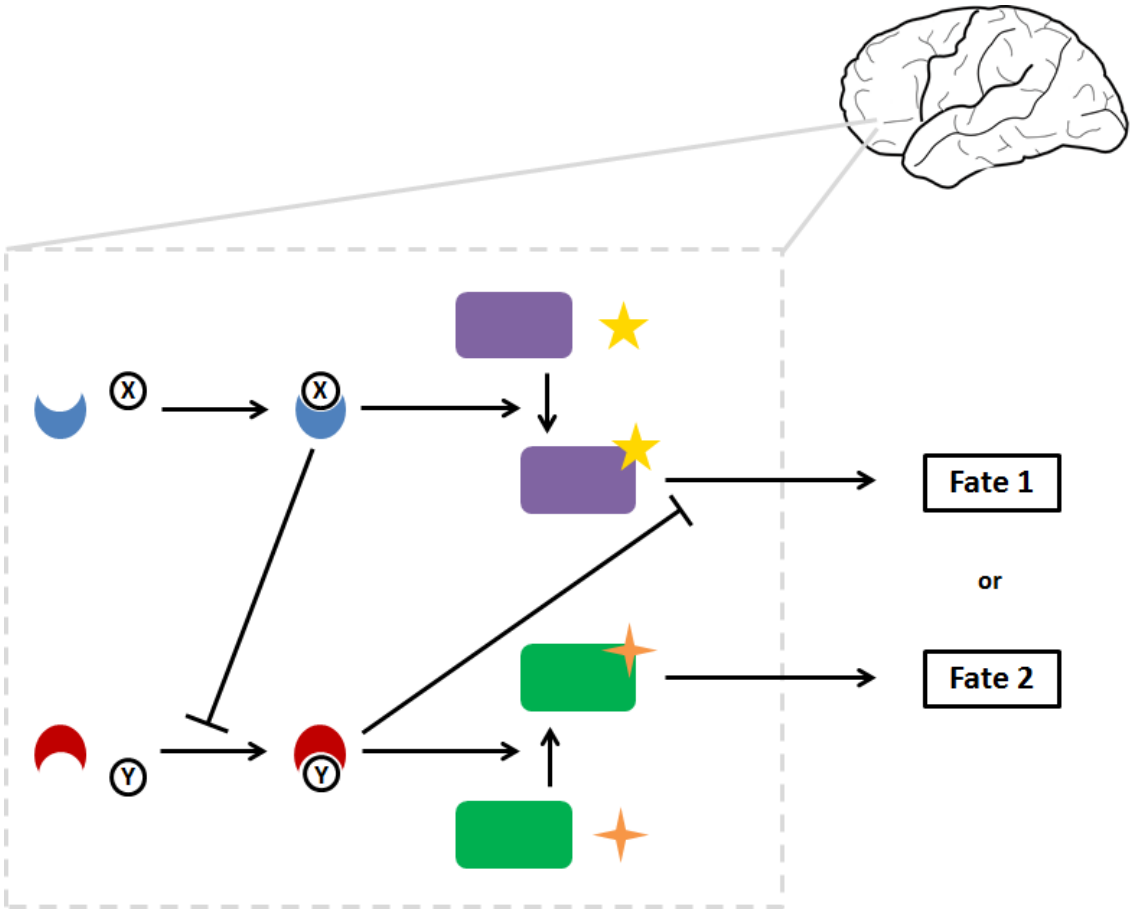

Figure 1.5 Decisions are processed via interacting circuits.
An example of a decision-making circuit is shown. The decision-maker (brain) is able to sense different chemicals (X and Y, which transmit information about the environment) to choose between two fates. In this circuit, blue sensor is able to bind to X and red sensor is able to bind to Y. Blue-X has the ability to promote purple protein to bind to a yellow factor, which activates it. Activated purple protein acts as the effector of Fate 1 and completes Fate 1. Red-Y has the ability to promote green protein to bind to an orange factor, which activates it. Activated green protein acts as the effector of Fate 2 and completes Fate 2. The separate sensors are able to interact, which pushes the circuit towards choosing a single fate. The blue-X element is able to inhibit the formation of red-Y, and red-Y element is able to inhibit the completion of Fate 1.

This signaling also functions at the cellular level, where genetic circuits are programmed to sense environmental changes and then undergo gene expression accordingly. In addition to chemical signals, cells are also programmed to sense and similarly respond to other environmental factors such as temperature, pressure, and proteins[60,61]. This process is termed as signal transduction. Signal transduction begins when a protein sensor receives an environmental signal, such as the binding of proteins or ions to sense various ligands, or undergoing a structural change to sense temperature (Fig. 1.6). The information of this initial stimulus is then transduced, or relayed, through a cascade of interactions by having proteins modify other proteins, perhaps repeated multiple times[62]. In prokaryotes, phosphorylation of proteins is a common method to transmit this information[63]. Ultimately, this cascade will result in a change in gene expression at the transcription, translation, or protein level, to enact a response to the initial stimulus. For example the *ntrB/ntrC* system in *E. coli* is a circuit that reacts to nitrogen availability[64,65]. During nitrogen starvation, the sensors, UT/UR and P_{II}, sense nitrogen levels, and when nitrogen is limited, lead to NtrB autophosphorylation. NtrB transmits this information by transferring this phosphate to NtrC. NtrC is the receiver of the information and activates transcription of glutamine synthetase, which is the effector to the stimulus.

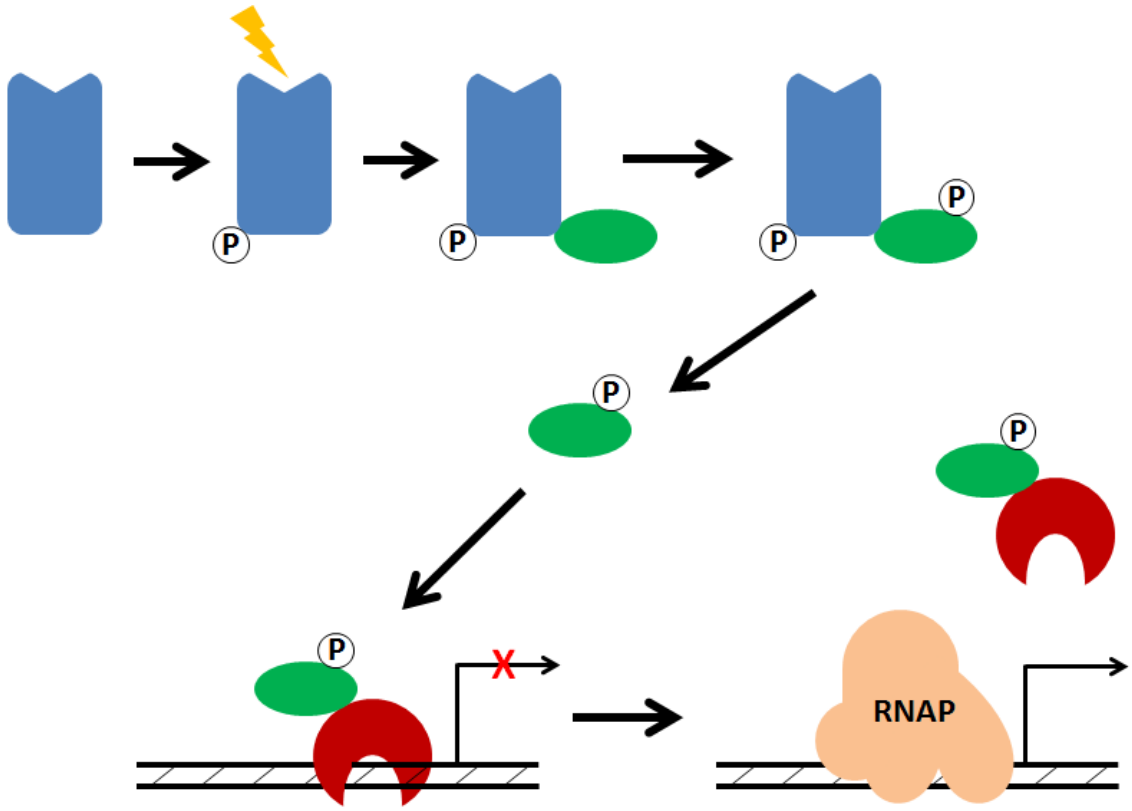

Figure 1.6 Signal transduction causes stimuli to result in biological changes. An example of generic signal transduction is shown. A cellular protein acts as a sensor (blue), and senses an environmental stimulus (lightning). This stimulus phosphorylates the sensor, and allows a secondary protein (green) to bind the sensor. The protein also becomes phosphorylated upon binding the sensor, then unbinds and is able to bind to a transcriptional repressor (red), which causes the repressor to unbind and free the promotor for RNA polymerase to bind and function, completing a response to the stimulus. The response is not limited to transcriptional changes.

More specifically, decision-making typically consists of multiple simple circuits sensing separate environmental cues to elicit different responses, and these circuits interact to an extent to result in cell fate selection (Fig. 1.5)[66]. These different circuits make up networks of sensors and responses, where the output of one circuit can enhance or block along the cascade of other circuits[67]. This interaction could occur at different points along the decision-making circuit, as competing circuits may exert their influence at the step of sensing signals or at any of the steps during commitment to decisions. Recall that phage lambda has separate lytic and lysogenic pathways, where the expression of important, fate-determining genes depends on the ability of the phage DNA to commit to the expression of certain proteins. The lambda genome has multiple genetic circuits that interact, as summarized earlier. Key to decision-making, the phage DNA is the sensor, in essence, of the state of the bacteria. High CII levels may convey that there are multiple phages or a starving cell, and CII itself can transmit this information to pRE, which is the receiver of the information. CI is produced as the response to the cellular information. For lysis, Q transmits information regarding the lack of CII to the pR′, the receiver, which goes on to activate the lysis program (Fig. 1.7). The overall process is more nuanced than just the actions of the final decision operons, but in the end, they are all simple genetic circuits with different feedback pathways amongst each other. It is clear from this perspective that the processes that make up decision-making do not necessarily require any higher order thought or consciousness, as decisions are simply made up of programmed conditional responses.

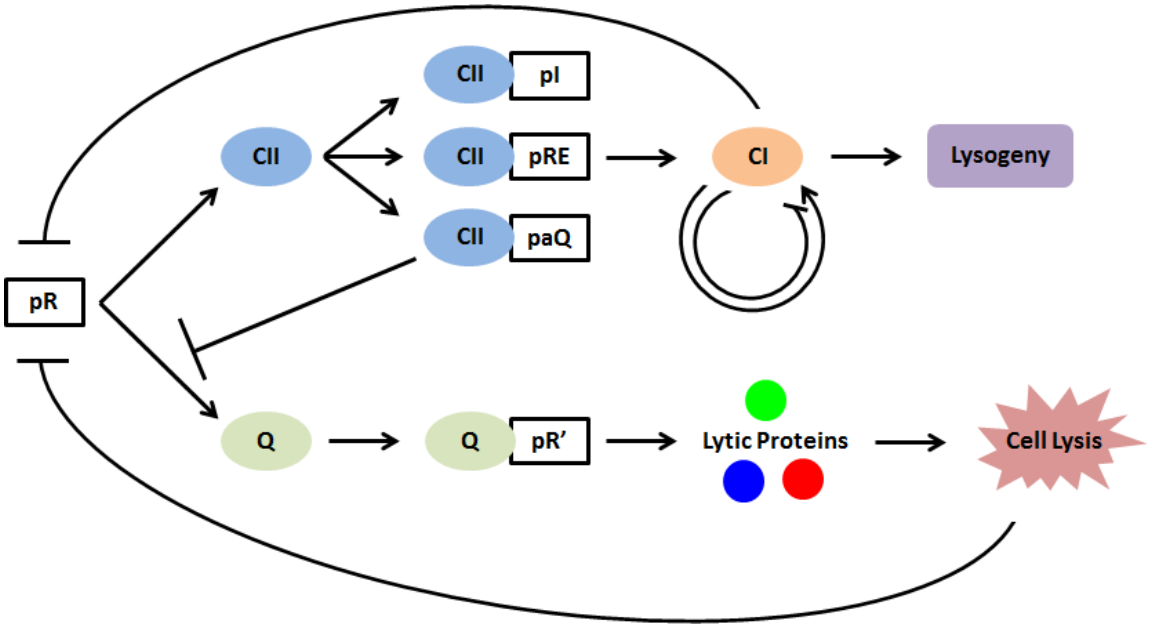

Figure 1.7 Overview of interactions in the lysis/lysogeny genetic circuit.
Promoter pR produces both CII and Q, which work to commit to lysogeny and lysis respectively. Each protein transmits information to the phage DNA about the state of the cell. CII binds to three promoters to enable lysogeny, pI, pRE, and paQ. These promoters are the sensors of CII. CII-mediated pRE activity produces CI, which is the effector that completes lysogeny, and CI inhibits pR and autoregulates its own production. For the lytic pathway, pR′ is the sensor of Q. Q-mediated pR′ activity produces lytic proteins which are the effectors which complete cell lysis, which is the event that inhibits pR. CII-mediated paQ activity interacts with the Q pathway by inhibiting pR from producing Q.

This “logic” bears resemblance to how computers operate, which is an example of decision-making in a fully non-biological system. Consider a computer program that plays chess or some other game. Such programs are made up of code and must be able to understand specific player inputs, analogous to the stimuli as described earlier, and follow up with a move as an output, which is the response or effector in biology, and this is what allows computer programs to undergo decision-making processes. If we explore some generic code from software that process decisions, we would see how their circuits work. Such code would include conditionals, such as “if-then” statements and such, where programs can even be injected with an element of stochasticity through random number generation. Combinations of these lines of code interact together to essentially simulate decision-making as in living beings, although, as computers are fully synthetic, all inputs and outputs are absolutely deterministic. Even though we consider that stochasticity plays an important role in decision-making and in fact, biological processes as a whole, this perceived stochasticity might also ultimately be due to a limit of our resolution as well. Nevertheless, the sensing of stimuli and differential corresponding responses make up the elements of decision-making in both biological and synthetic systems. Phage lambda, and living systems in general, is like any of these cases of decision-making, where its DNA is programmed, through evolution, to receive cellular signals and carry out decisions using simple genetic circuits.

Advantages are gained from proper decision-making

For there to be a decision, differing outcomes must occur, but what is there to be gained from this uncertainty? Lifeforms exist to perpetuate, so proper decision-making should prolong their existence[68]. One common assertion is that decision-making allows for bet-hedging, where multiple possibilities for perpetuation, suitable across multiple conditions, decrease the chance that the lifeform will go extinct, at the cost of maximally efficient propagation under perfect conditions[69,70]. This and other evolutionary behaviors are explored for many systems using game theory, which when applied to biology, is a quantitative analysis of the interactive behaviors between rational players in specific "games," or situations[71]. For example, rats have been trained to make choices with other rats, resembling a game, to study how animals choose to cooperate or not[72]. These studies are not limited to complex organisms with brains either, as this analysis can frame the behaviors of single-cell organisms as well[73,74]. As evolutionary behaviors exist among viruses, game theoretic analyses have also been applied to study simple virus models, which are convenient systems due to their quick generation times[75-77].

In the case of lambda, its decision-making circuit is malleable, and when multiple phages infect a single cell, lysogeny is more likely, contrary to single-phage infections, where lysis is the prevalent outcome[49]. In essence, this behavior may have evolved as a sensor of host availability, to probabilistically switch to means of propagation which does not involve bacterial infection and allow the phage to replicate essentially as a bacterium, when host bacteria are not abundant. To understand this strategy from a game-theoretic point of view, different infecting phages can represent different, identical players when infecting the same cell, each having the same strategy as they are alike (Fig. 1.8). Consider that in this game, lysis offers a great "selfish reward" in the form of progeny phages, but there is a chance that free phages will be released into an environment that will destroy them. Alternatively, lysogeny offers a lesser "collective reward" in the form of integration into a lysogen, such that phages will persist even in conditions that would destroy free progeny phages. Therefore, there would be a cost in not choosing lysis in conditions where progeny would not be destroyed, but also a cost in choosing lysis in conditions where they would be destroyed, and there is limited knowledge of the outside conditions.

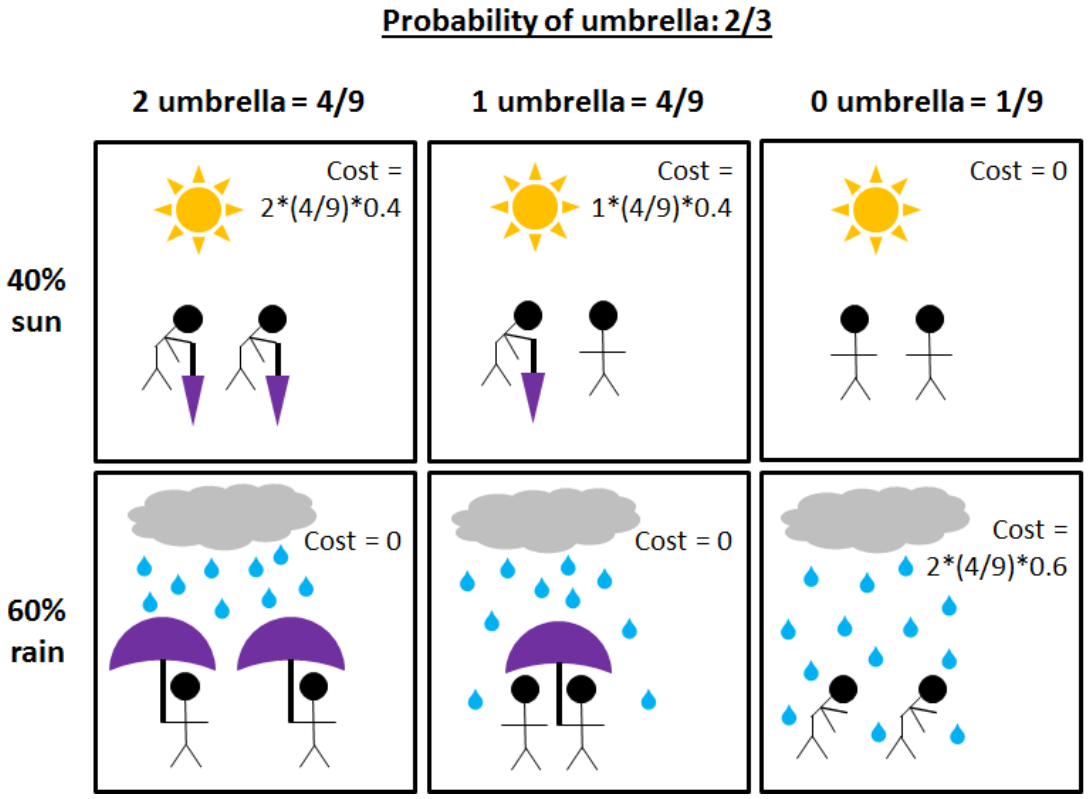

Figure 1.8 Game theoretic analysis of lambda decision-making.
The umbrella game illustrates how a stochastic strategy can minimize cost for phage lambda. In the game, each player decides whether or not to carry an umbrella, and the weather may be sunny or rainy. A player with an umbrella in the sun or without an umbrella in the rain incurs a cost. Under this specific situation (40% sun/60% rain), players with a 2/3 chance of bringing an umbrella minimize net cost per player (0.33 per player), because one umbrella can be shared. A deterministic strategy results in higher net cost (always = 0.4 per player; never = 0.6 per player). For this game, as it relates to lambda, sun is favorable to lysis and rain kills free phage, and is therefore favorable to lysogeny. The umbrella is a shared reward similar to multiple integrations during lysogeny.

The ostensible goal of the game could be to avoid extinction, by minimizing the player's cost, and to outcompete different players, by maximizing rewards. Thus, it is a balancing act when choosing a strategy, as to avoid giving up too much reward while remaining the safest from extinction. A fully deterministic strategy (always lysis or lysogeny) by the infecting phages has an overall cost associated with betting on the environment being favorable for the chosen lytic/lysogenic choice. This strategy wins if the environment never changes, but perfect knowledge does not exist in these games. However, if the strategy is stochastic in lytic/lysogenic decisions, then the overall cost will be lower when the environment is unknown, particularly because lysogeny offers the chance of multiple infecting phages to be integrated. This would protect the phage from a hypothetical cataclysm where all of the progeny virions were destroyed. The tradeoff for minimizing the chances of extinction is that a single lysogenic cell only produces new copies of the phage genome when it replicates its DNA and divides, which would create less new phage genomes than lysing that one cell, which is the difference in rewards. The ideal propensity towards either fate would change based on the conditions the phage evolved in. Note that these games are simplified versions of biological situation, as there are considerably more factors in play in the actual decision-making. This stochastic strategy can also be found in bacteria, where individuals in a population can switch to a persistent, non-growing state which protects against antibiotics[78,79]. This decreases the overall growth rate of the bacteria, but in turn, allows the small persistent subpopulation to survive chance encounters with antibiotics. From these examples, it is clear that decision-making influences the evolution of lifeforms,

making them more fit and able to withstand unknown environmental perturbations within populations.

Characterizing the behaviors of life from viruses

Lambda displays behaviors and strategies which are found in all living beings, despite viruses being labeled as "non-living" by many scientists[80]. This is an interesting dichotomy, as viruses are apparently fully "alive" when existing as a part of their hosts, and are constantly studied to learn about the fundamentals of life[81]. The definition of "life" is currently being defined from the human perspective, making it inherently subjective and based on arbitrary criteria. Research progresses unyieldingly and paradigms shift, meaning that dogmas are never truly set and are always susceptible to being rewritten. Strictly speaking, viruses do not require any traditional lifeforms to propagate, but only an environment similar enough to support their biological functions; this is no different than traditional life, which also has specific environmental demands for successful reproduction and will cease all biological activity if these demands are not met. However, the debate over what constitutes life is not exactly useful, as the processes underpinning biological development occur for viruses, as they do for other lifeforms, regardless of any scientific opinions. Therefore, we may make predictions for viral behaviors following what we know about more complicated living systems to help us learn more about the universal properties of life.

Life is composed of organized processes

Organization is a fundamental part of life. At the population level, individuals within different animal groups have different roles (Fig. 1.9a). Consider colony-forming insects such as ants and termites, which build structured nests and have designated roles and places for different members of the colony[82,83]. Complex organisms are themselves organized into different parts, such as appendages for animals or the different parts of a plant (Fig. 1.9b)[84,85]. The eukaryotic cells which make up these and other similar organisms have separated membrane-bound organelles which spatially segregate different biological processes (Fig. 1.9c)[86]. The nucleus houses the organism's genome and is where the organism transcribes its genes (Fig. 1.9d), and it itself is organized by membraneless subcompartments, like the nucleolus which houses ribosome assembly and other nucleoprotein bodies (Fig. 1.9e). Transcripts must be exported to be translated outside of the nucleus and trafficked via the Golgi body to other locations where the proteins function. Cellular energy is produced in other separate organelles, mitochondria. These examples represent only a fraction of the many layers of organization found in a single eukaryotic cell.

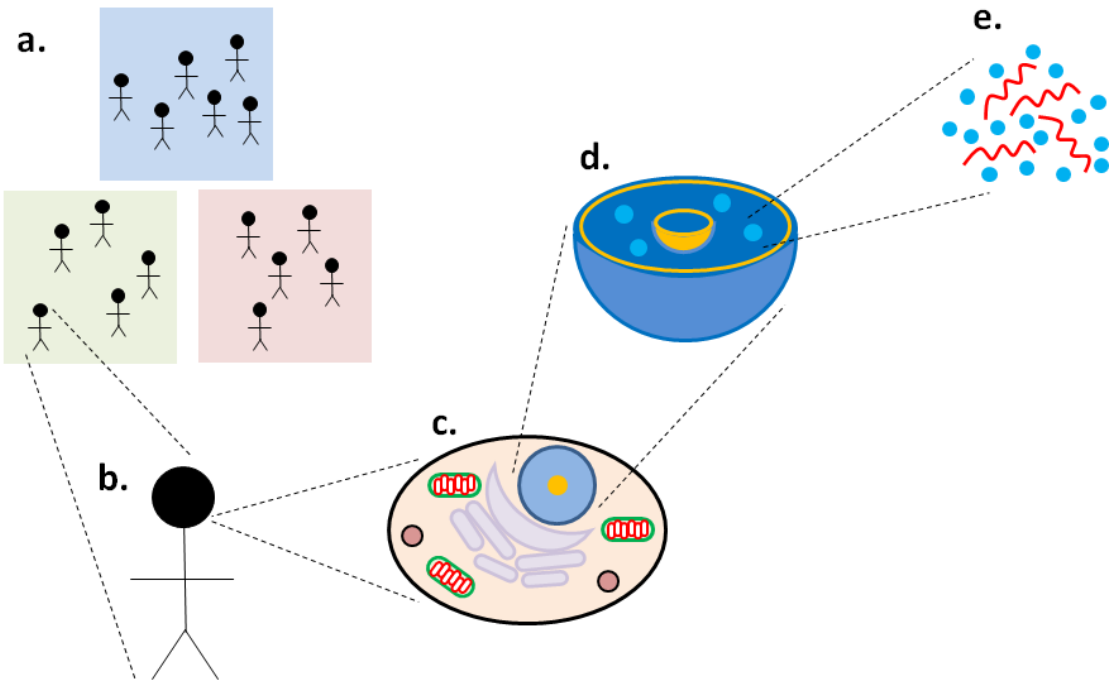

Figure 1.9 Organisms are structured by multiple layers of organization.
For eukaryotes, populations of organisms may be organized into different roles (a). For multicellular organisms, they are typically organized into different body parts (b), and the organism itself is made up of single cells (c). In eukaryotic cells, membranes separate different organelles in the cytoplasm, where each organelle has a specialized function (d). Within membrane-bound organelles, for example, the nucleus, there may be further organization in the form of non-membrane-bound organelles, which are made up of nucleic acids and proteins (e).

In simpler prokaryotic cells, there are no separated organelles, but there is organization at other levels. At the population level, bacteria commonly exist in communities in nature, which are called biofilms (Fig. 1.10). The bacteria secrete an extracellular matrix made up of sugars, proteins, and DNA (known as the EPS) and form a three-dimensional structure[87]. These cells behave differently from cells grown in culture, and there is evidence that different cells in different areas of the biofilm play different roles in maintaining and growing the biofilm[88]. As for the actual bacterial cell, the membrane-bound cytoplasm is surrounded by a peptidoglycan layer (Fig. 1.11). Also consider that the organization for Gram-positive and Gram-negative bacteria differs at this point too, where another outer membrane envelops Gram-negatives. The positions of the cell wall or membranes must be placed correctly to form the cell. This organization is achieved by proteins which move the cellular components to their proper locations, and these proteins are themselves positioned to correctly perform their functions. Take for example *E. coli* peptidoglycan maintenance, where the precursors to the cell wall must be synthesized in the cytoplasm, and then moved to the periplasm to build the cell wall (Fig. 1.11a). The sugars which make up the subunits of the cell wall are manufactured in the cytoplasm and are subsequently localized to the inner membrane via attachment to transport lipids in the membrane. The subunits are then processed into a precursor known as lipid II, which includes processes carried out by inner membrane-localized enzymes[89]. This lipid II must then be flipped into the periplasm, which is accomplished in *E. coli* by the membrane protein MurJ[90,91], to be further processed and incorporated into the cell wall.

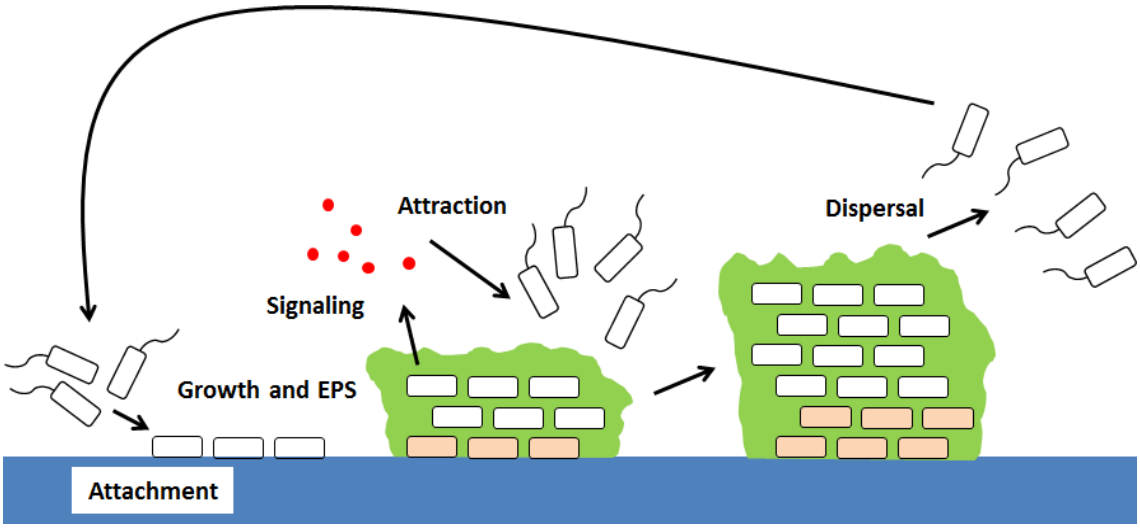

Figure 1.10 Biofilm development and organization.
Biofilms develop when motile bacteria attach to a surface and become non-motile. Cells secrete EPS (extracellular polymeric substances) and grow within it. The biofilm is an organized 3-D structure where different cells in different areas have different metabolic states and roles (orange cells). Biofilms also grow by sending signaling molecules into the environment to attract bacteria to grow the biofilm. The outer layers of biofilm will eventually slough off to disperse motile bacteria back into the environment.

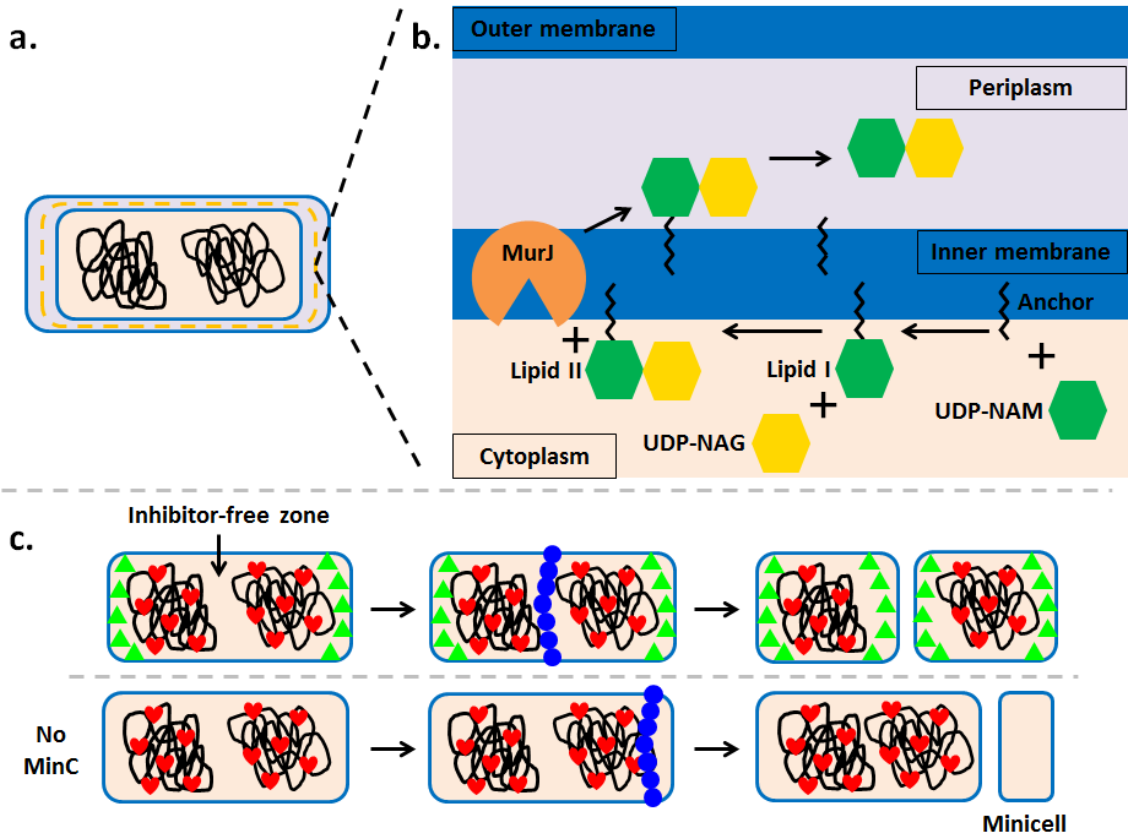

Figure 1.11 Examples of organization in Gram-negative bacteria.
a. In Gram-negative bacteria, an outer membrane surrounds periplasm and the inner membrane, which encloses the cytoplasm. In the periplasm, the peptidoglycan (PG) layer (dashed yellow line) envelops the inner membrane. In the cytoplasm, the bacterial nucleoid is condensed in space.
b. In PG synthesis, PG precursors are organized from the cytoplasm to the periplasm. UDP-NAM, from the cytoplasm, is attached to the inside of the inner membrane via a lipid anchor to form lipid I which is then processed into lipid II via addition of UDP-NAG. Lipid II is then relocated by the flippase, MurJ, into the outside of the inner membrane. The sugars are then freed from the membrane to be incorporated into the PG.
c. Cell division is spatially controlled. SlmA (red hearts) binds to the nucleoid and MinC (green triangles) localizes to the poles to prevent FtsZ (blue circles) from forming a ring anywhere but the midcell to produce properly divided cells. Without MinC, FtsZ is able to form a ring near the poles and cell divisions can produce anucleate minicells.

Even in the cytoplasm, there is extensive organization, despite early assertions that it existed as a "bag of enzymes." Cytoplasmic proteins localize to different areas of the cell to organize different functions[92] and to position the nucleoid[93]. For example, as cells need to divide, organization is vital to position the division machinery and nucleoid in the correct locations[94]. The FtsZ proteins form a ring at the midcell to position cell division[95], because SlmA prevents its formation over the nucleoid, by binding to the nucleoid[96], and the MinCD proteins are localized to the poles to inhibit the FtsZ ring from forming near the cell poles[97]. The *E. coli* nucleoid is condensed and organized into separate halves prior to division, such that the genome is away from the divisome[93,98]. The disruption of this organization, specifically the Min system, produces anucleate, non-viable minicells[99,100]. The biological molecules in the bacterial cytoplasm are subjected to heterogeneous diffusion based on their sizes and the metabolic state of the cell, where larger objects are more constrained[101]. This may cause certain components to become differentially organized. There are also a variety of shapes for different bacteria, and these bacterial shapes also tied to organization. In *C. crescentus*, a curved bacterium, the CtpS protein interacts with the CreS protein to regulate specific curvature in cells by differentially accumulating in specific areas of the cell, forming the different shapes of cells[102-104]. From this selection of examples, it is clear that there are many strategies and purposes for organizing biological processes within cells.

Viruses have their own methods of organization, which may or may not closely resemble the types of organization found in their host cells. For eukaryotic viruses, such as the commonly known influenza virus in humans, their genomes must translocate to

the host's nucleus for transcription to begin. The assembly of new influenza particles occurs at the plasma membrane however, so the organization of gene expression for the flu virus follows similarly to its host cell, where RNA is exported for subsequent translation[105]. In contrast, for the largest and most complex virus, mimivirus, the infecting virion organizes a virus factory in the cytoplasm of its host amoeba, which houses the viruses' DNA replication, transcription, translation, and assembly processes[106,107]. This occurs because mimivirus carries its own transcription machinery within its virion[108]. Some bacteriophages have also been reported to be capable of cellular organization, in a manner unlike its host cell. The giant Pseudomonas phage 201φ2-1 has been reported to build a single proteinaceous compartment in its host to house its DNA replication and transcription, and it exports transcripts for translation elsewhere in the cytoplasm, similar to the function of a nucleus[109].

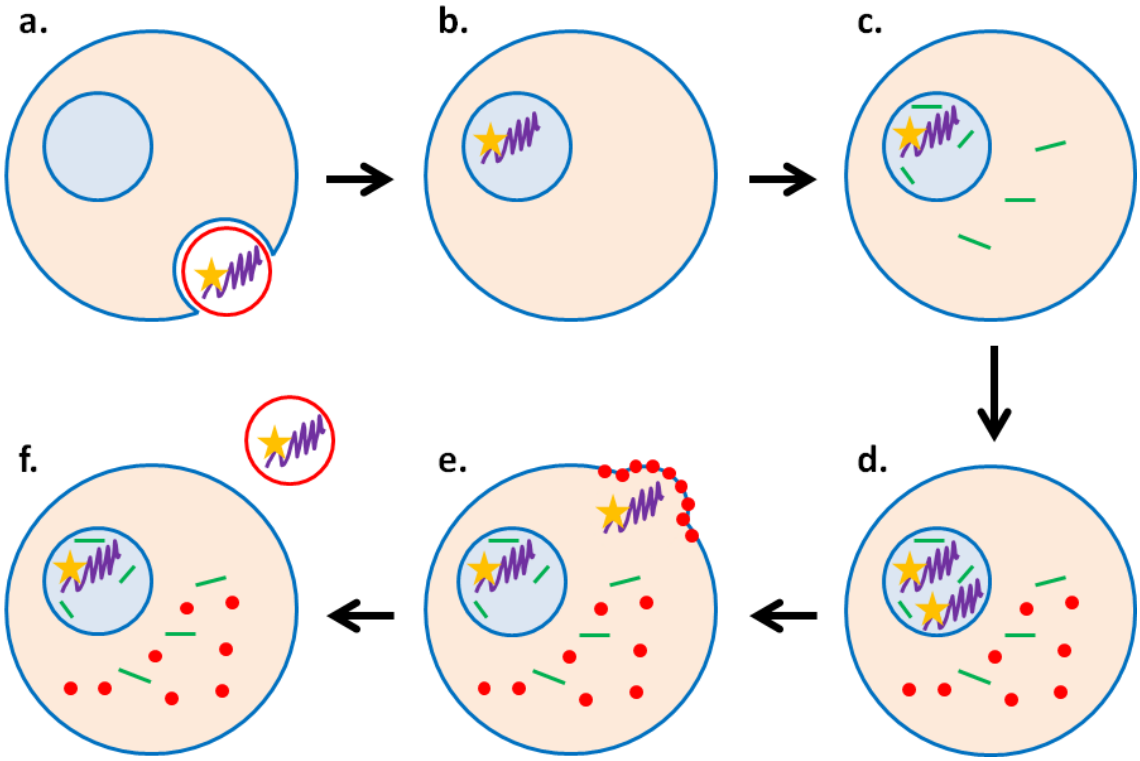

Figure 1.12 Diagram of influenza infection cycle.
Influenza viruses are endocytosed by host cells, and carry their RNA genomes (purple) and RNA polymerases (stars) in their virions (a). After entry, the virus enters the host's nucleus (b) and transcribes its genes and exports its mRNA (green)(c). Translation of viral proteins (red) occurs outside of the nucleus, similar to how the host behaves (d). Certain proteins are re-imported to the nucleus to make new viruses and the viruses assemble near the cell membrane in the cytoplasm (e), before the mature virions are budded off from the host, leaving the host alive (f).

It is not known if phage lambda possesses strategies for self-organization. Spatial organization for lambda likely exists, specifically following reports that lambda shows a preference towards infecting near the cell poles and mid-cells. Studies examining the localization of LamB, phage lambda's receptor, do not suggest that the receptor preferentially accumulates in the phages' adsorption areas[12]. Lambda nonetheless does irreversibly attach to these areas. Therefore, it can be inferred that the phage's DNA would enter the cytoplasm near that area as well. There are also reports that the initial lambda genome is somehow associated to the inner membrane, which would confine and possibly organized the phage in cellular space[110,111]. Given that bacteria themselves display organization at the level of DNA[94], transcription[112], and translation[113,114], and much of the fundamental characterization of these process was accomplished in phage lambda's host, even relatively simple phages like lambda may indeed organize their development using their hosts' components. Given that many cellular processes coalesce for phage development, including DNA replication, transcription, translation, and phage assembly, the cellular components that constitute these processes may be forced to organize together. As previously mentioned, large cellular components do not diffuse as much as smaller ones. The cellular machinery which carry out phage development are numerous and obligatorily attached to each other when they function. This means that multiple phage DNAs and DNA polymerases are attached during replication, RNA polymerases and mRNA transcripts are found on each phage genome, ribosomes and amino acid chains are found on each transcript, and depending on the state of development, the components of the progeny virions are attached to the phage genomes

as well. This would comprise a massive complex that would likely be subjected to physical constraints in the cell, and may contribute to the organization of phage development. These different strategies for organization greatly influence the development of all lifeforms, and as technology improves to achieve better spatial resolution using microscopy, we may further explore how the environments of smaller, simpler systems behave.

Living beings mutually interact with their environment

A local environment surrounds every living being, which may impart either positive or negative influences toward the development of the organism. Given how important the environment of an organism is to survival, it is fitting that lifeforms have evolved to manipulate their local environments. For the most complex metazoans, this includes behaviors such as building shelters to exclude unfavorable weather or cultivating food. Certain species of ants also perform these same tasks on a smaller scale[115]. Plants are organisms that are generally sessile, so they may alter their environment by redistributing water in the soil to optimize their hydration[116,117]. Budding yeast, a simpler eukaryote, secretes enzymes into its environment to digest disaccharides before importing the resulting monosaccharides[118]. In the prokaryotic world, many bacteria have dedicated secretion systems to alter their environments[119-121], such as releasing toxins to destroy their competitors[122]. Also, recall that many bacteria exist in biofilms. It has been reported that the metabolism of *B. subtlis* biofilms is controlled by spatially organized release of potassium into the environment[88]. This environmental signal changes how cells in different areas of the biofilm take up nutrients, where cells in

different areas are suggested to oscillate metabolic states to allow these separate areas access to nutrients at different times, all based on how their environment changes. It is further suggested that this environmental manipulation permits distant biofilms to communicate with each other to share nutrients or attract other bacteria to grow biofilms[123,124]. Regardless of the complexity of lifeforms, their environment plays a profound role in their life trajectory.

Viruses, too, have been shown to modify the intracellular environment in which they are living. Phage P1 packages proteins which are released into its host upon infection to defend against the host's restriction defense system[125], neutralizing the hostile environment. During T5 infection, the phage produces a protein which blocks its own receptor, which modifies its cellular environment to protect the infecting phage from superinfections by other T5 phages, and additionally, reduces the likelihood that its progeny become inactivated by the receptors on the lysed cell[126]. Phage φ3T releases small molecules when its host lyses which are subsequently taken up by naïve host cells to alter the intracellular environment of new infecting phages, which influences this phage's decision-making[127]. These examples illustrate how lifeforms, from simple to complex, strategically control their environments for optimal development. For lambda, any protein that is expressed can broadly be considered to alter its environment. Lambda prophages produce the rexAB proteins, which constitute an abortive infection system against phage T4 *rII* mutants[128,129]. Here, lambda makes the cellular environment inhospitable to these other phages. In terms of communication, co-infecting lambda phages do effectively sense each other to lysogenize at higher frequencies, which is

accomplished through the sharing of proteins. However, little is known about the details of how many of the other processes might influence lambda, such as how phage lambda changes its environment during DNA replication or transcription, and how these changes manifest themselves regarding lambda decision-making.

Modern approaches to studying bacteriophage biology

Phage lambda, despite the decades of research aimed at studying its decision-making and development, still lacks a highly detailed mechanistic characterization of many aspects of its life. The bulk of lambda research occurred prior to the advent and popularization of single-cell techniques such as fluorescent microscopy, so parameters such as true MOIs were hidden (Fig. 1.13a). Therefore, there is an opportunity to probe this paradigm with new tools, experimenting at single-cell and single-virus levels[130,131]. Modern approaches combined with new lines of thought can refine our understanding of this decision-making paradigm.

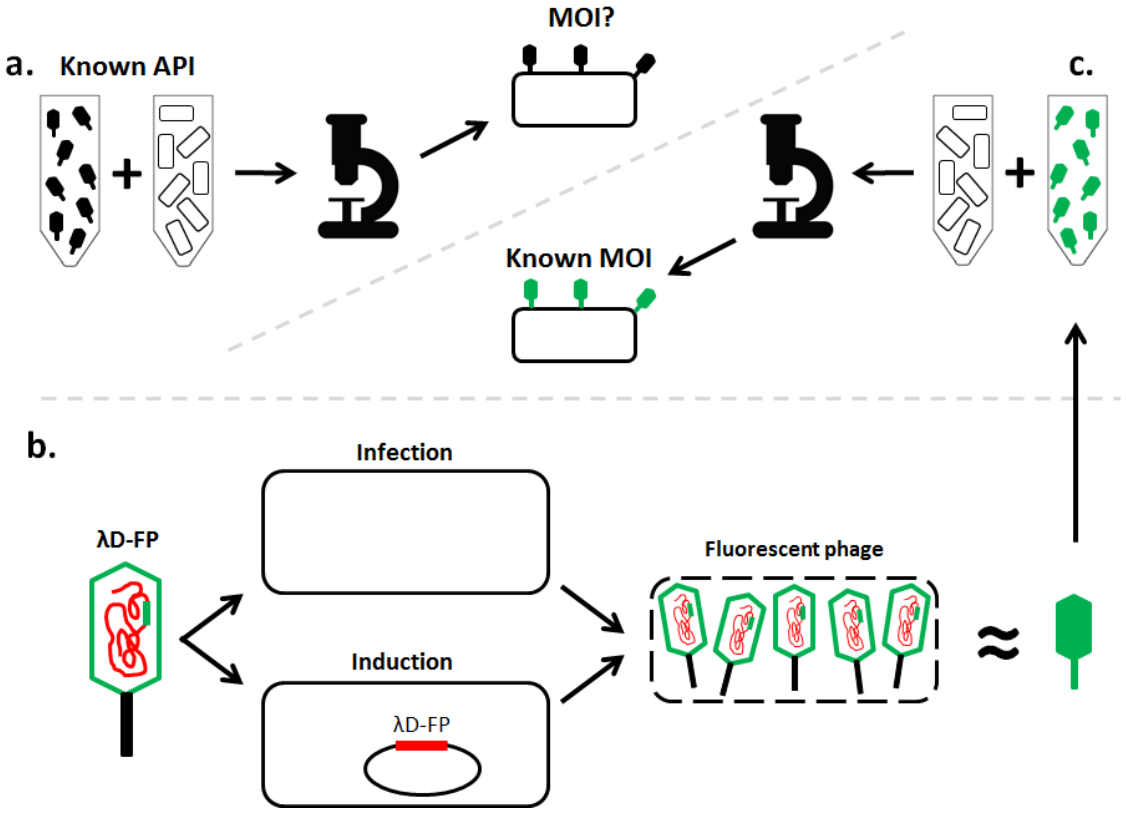

Figure 1.13 Fluorescent phages increases resolution of studies.
a. Standard light microscopes enable single-cell observation of phage infection, but true MOI data are still obscured. This tool does not allow direct visualization of single phages.
b. Genetic engineering is used for phage lambda, modifying the phage *D* gene to produce a D-fluorescent protein fusion. Infections by this modified phage or inductions of this modified prophage produce fluorescent progeny.
c. Fluorescent lambda particles can be observed with fluorescence microscopy to directly observe the numbers of infecting phages to increase the resolution of study.

To address the previous lack of single virus resolution, researchers engineered phage genomes to have fluorescent capsid decorating proteins (λD-FP)[132]. When these phages infect cells or these prophages are induced, they will assemble fluorescent phages, where single phage particles are visible using fluorescence microscopy (Fig. 1.13b). This enables more precise quantitative experimentation and thus, more refined conclusions (Fig. 1.13c). Research utilizing these fluorescent phages with decision-making reporters has uncovered that decisions for lambda are processed at the phage level, not the whole-cell level (Fig. 1.14)[133]. These separate choices are described as phage "votes" for decisions and this idea represented a fresh perspective on noisy decision-making, where hidden, deterministic factors underlie stochastic events when viewed with the proper lens[134,135].

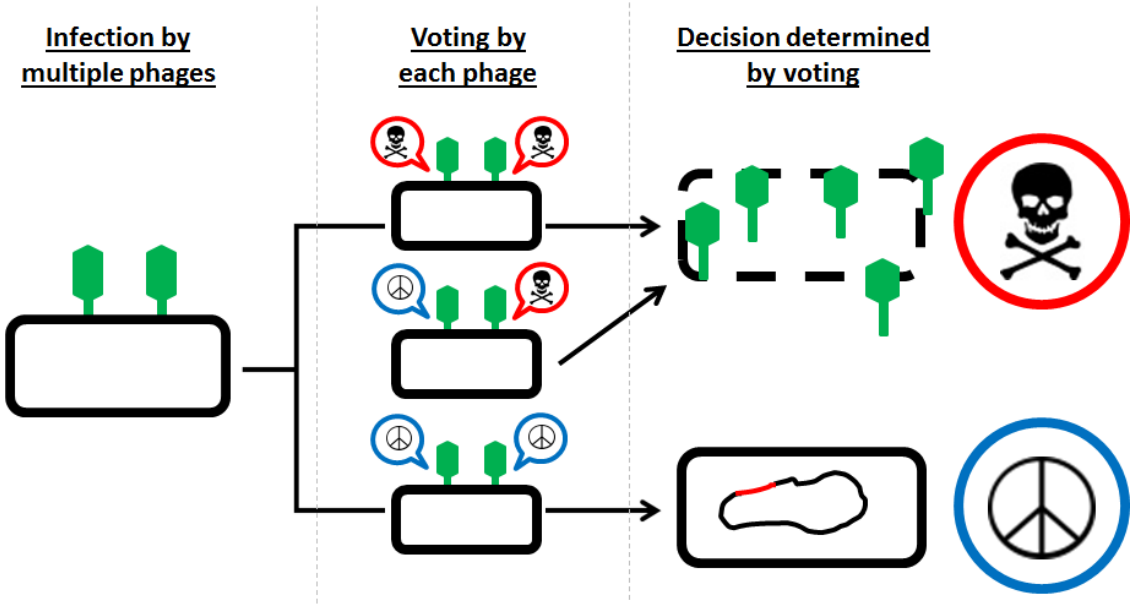

Figure 1.14 Phage lambda voting model for cell fate decisions.
In the lambda voting model, when multiple phages infect a cell, each infecting phage is able to commit to lysis or lysogeny, such that different combinations of votes can occur. Following this model, lysogeny only occurs when there are no lytic votes within the cell, as lytic votes override lysogenic votes to result in lysis.

Naturally, these revelations raise additional questions about how individualism might apply to viruses, where the answers might be revealed through better spatial-temporal analysis[136]. This work also represents an important realization that simple systems can be beautifully complex. These shifts in understanding are monumentally important, because they can also update computational models of biology to better describe the natural world. To gain an accurate mathematical understanding of biological processes, modelers need accurate parameters which are gained through experimentation, and these models, in turn, can inspire even more new experiments. These high resolution experiments allow for better quantitation of biological development and can contribute significantly to progressing computational models. It is through multi-disciplinary approaches like these that will move research closer to a systematic understanding of biological models. Much of the continuation of this work lies in developing the proper tools for extracting the relevant data and targeting the desired processes, preferably whilst being adaptable for subsequent experimentation.

The development of tools should not be limited to the lambda system either. Bacteriophages are the most numerous and diverse biological systems on the planet. In addition to their impact on ecology, where phages interact with bacteria in the outside environment, they may also affect human health. The human microbiome is an emerging field, where its importance is only beginning to be understood. Phages assuredly affect the bacteria that reside within the microbiome, and thus influence any effects of the microbiome. Most phages do not have the breadth of genetic tools as lambda does. Therefore, the development of new technologies to enable single cell/phage studies of

other systems is important for understanding more about phage biology. Although it might be possible to develop genetic tools for different phages, their inherent diversity might make this challenging. Another feasible approach would be to adapt tools to work with the phages themselves. Sequencing data is readily available for phages, and thus, chemical modifications can be developed to react with the actual phage particles or genomes to label them. Fluorescent dyes have been used to label phage DNA[137] or coat proteins[138] to study different processes. By using bioinformatics, chemicals could be developed to conjugate fluorescent particles or dyes to fluorescently label additional phages for studies, in particular, for systems that lack convenient tools. It is through these high resolution studies that new breakthroughs will be made.

Dissertation overview

I looked to the discovery of novel behaviors of fundamental life using high-resolution studies and open-minded approaches as inspiration for my work. I treated this lambda system as if the phage were a living being invading a bacterial world, and used this perspective to guide my studies and thought process. I aimed to craft tools to better understand the origins of biological individuality in bacteriophage lambda. I went beyond single cells and single viruses, to look at single molecules of phage DNAs within single cells, as different individuals, because individual lifeforms must behave together somehow if they encounter each other in their environment. In the following chapters, I will discuss how each new approach generates new narratives and opportunities for both understanding past research and planning new projects.

In chapter II, I explore the aforementioned phage voting model, both to affirm these behaviors and to elaborate upon this phenomenon. By differentially labeling the lysis/lysogeny decision-making reporters of otherwise identical phages, I achieve intracellular resolution of the interactions of viruses to have a direct tool for studying individual phages in the cell. I focus on the different viruses as they progress through their development to understand how the genetic circuits of the phages interact to decide their fates. I find that individuals compete over essential resources differently when developing in different paths, as expected for individuals behaving under different circumstances. I integrate these data into computational models to make predictions about how resources and infection timing affect phage infection. I then use these model predictions to design subsequent experiments in order to verify the accuracy of the predictions.

In chapter III, I investigate individualism in phage development through a spatial-temporal approach. To do this, I build and combine tools which target every step of the phage infection process, expanding upon the initial decision-making reporters. Specifically, I design multiple reporters to study single phage DNAs and replicated phage DNAs in the cell, along with their essential host resources. I characterize how these phages behave in cellular space, which is a perspective not yet explored for lambda. I combine these live-cell reporters with fixed-cell, single-molecule reporters for phage DNA and mRNA transcripts, and also focus on where these molecules reside in the cell. These experiments provide me data to integrate many phage processes, from adsorption to lysis or lysogeny, for spatial characterization, to change how we understand lambda

development. I discuss the consequences of this, regarding how viruses have the agency to uniquely modify their own part of their world to enact different tracts of development.

In chapter IV, I discuss additional technologies I have developed to improve single-cell/single-virus studies of phage biology and apply the natural properties of phages to address problems. I establish a method to attach nanoscale fluorescent diamond particles to phages as a fluorescent label. This new technology provides a proof-of-concept for further development of phage labeling to identify bacterial cells, and could be refined to label new phages that currently lack single-virus tools to enable further studies.

In chapter V, I recapitulate my work and frame it within the context of a bigger picture, discussing what we understood before, what we can be confident in claiming now, and how we might proceed in the future to continue probing the life of phage lambda. It is through these research efforts utilizing the proper tools and appropriate perspectives that I hope to glean more insights into how the simplest of life persists in its own world within ours, and with this knowledge, we may redefine a paradigm.

CHAPTER II

CELL FATE DECISIONS EMERGE AS PHAGES COOPERATE OR COMPETE INSIDE THEIR HOST[*]

Introduction

Decision-making determines the fates of organisms at many levels, from the whole-organism level for multi-cellular beings, where decisions affect how they live and reproduce[2], to the cellular level for all lifeforms, where decisions by single cells can guide development and disease[1,56]. Decisions also have effects at the population level, where perpetuation or extinction hinges on the decision-making of individuals to interact with their neighbors in cooperative and competitive ways to propagate in their environment[6,139]. Therefore, systemic knowledge of cellular decision-making would be instrumental to addressing certain ailments, by potentially manipulating and preventing certain diseases and conditions[7], as well as both understanding the evolutionary history and potentially predicting the evolutionary future of organisms[8,140]. To gain a greater understanding of a complex and ubiquitous concept like decision-making, simple models can be used to simplify and deconstruct its fundamentals[141].

Bacteriophage lambda has served as a paradigm for studying gene regulatory networks, general recombination, bistable switches and other important aspects of

[*] Part of this chapter is reprinted with permission from: "Cell fate decisions emerge as phages cooperate or compete inside their host" by Jimmy T. Trinh, Tamás Székely, Qiuyan Shao, Gábor Balázsi, and Lanying Zeng. Nature Communications. 8, 14341 doi: 10.1038/ncomms14341. 2017 and part of this chapter is reprinted with permission from: "Virus interactions: cooperation or competition?" by Jimmy T. Trinh and Lanying Zeng. Future Microbiology. 12(7), 561-564. 2017. Copyright 2017 by Future Medicine Ltd.

cellular life[10,130,142]. Phage lambda is also a model system for cell-fate developmental decision-making, as it reproduces by infecting its *E. coli* host, undergoing DNA replication and gene expression, culminating in a decision to develop via either the lytic cycle, where the phage assembles clones of itself and induces cell lysis, or the lysogenic cycle, where the phage genome integrates with the host genome to be replicated by the cell, propagating the phage non-destructively[11]. Although the key genes, genetic circuits, and influential variables affecting the decision have been studied thoroughly over decades[9,143], the underlying mechanisms of how the phage integrates these factors to arrive at cell-fate decisions remain nebulous. However, increased resolution of study in recent years has revealed more deterministic factors and deeper mechanisms[130]. For example, advances in technology allowing for observations at the single-cell and single-phage resolution suggest a reduced role of stochasticity, assigning more importance to pre-existing host variation[51] as well as the existence of independent cell-fate commitments within single cells or 'voting' by infecting phages[133]. This voting phenomenon is particularly interesting as it delves into the interplay between some of the simplest, non-living biological entities, raising intriguing questions about how strands of phage DNA interact with one another and how their decisions shape the evolutionary fitness of the phages, similar to how this process occurs in more complex lifeforms like bacteria and eukaryotes[144,145].

In this study, we synthesize a 4-colour fluorescence system at the single-cell/single-virus/single-viral-DNA level that resolves individual phage votes and interactions to study decision-making in live cells at unprecedented resolution. We also build simple computational models that describe how phages interact as individual DNAs inside cells for lytic/lysogenic fates, to help interpret the data towards mechanisms of decision-making and guide our experimental designs. With this complementary experimental/computational approach, we observe interesting subcellular behaviors, providing new insights into the varied developmental strategies at the level of individual phage DNA, which in turn allows us to understand the effect of this evolutionary strategy on the population. This work also has broader implications as a paradigm for how to quantitatively dissect and understand other regulatory gene networks.

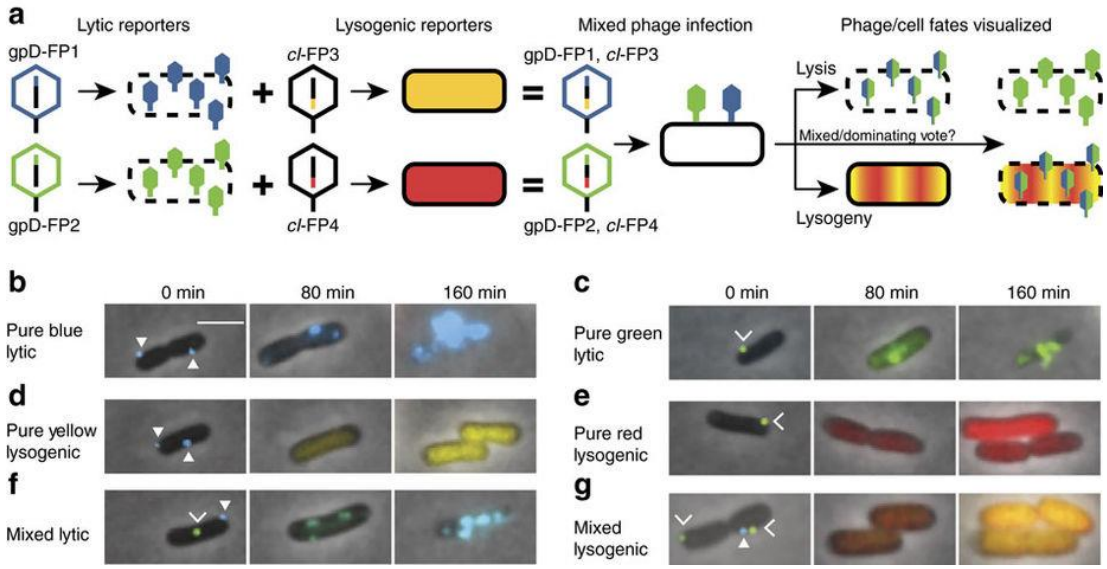

Figure 2.1 Individual phage decisions are visualized using a 4-color fluorescence reporter system.

(a) Lytic reporters are constructed by translationally fusing mTurquoise2 (blue) and mNeongreen (green) to the phage capsid decorative protein, gpD. These phages are visible before infection, and upon lytic decisions, the cells produce progeny phages in the respective colors. Lysogenic reporters are constructed by transcriptionally fusing mKO2 (yellow) and mKate2 (red) to the phage lytic repressor gene, *cI*. Upon lysogenic decisions, cells express the lysogenic reporter color then grow and divide. Combining the lytic and lysogenic reporters produces two new phages, each with separate decision reporters (blue phage with a blue lytic/yellow lysogenic reporter, and green phage with a green lytic/red lysogenic reporter). Cells infected with both phages (dual-color infections) show how individual phages make decisions in cells.

(b–g) The overlay images (phase-contrast and fluorescent channels) of representative cells are shown for various cell fates. In the first frames of the movie (0 min), there are filled triangles pointing at blue phages and carets pointing at green phages adsorbed to cells. For lytic cells (b,c,f), fluorescence develops over time and forms localized spots in the cell (80 min), followed by cell lysis (160 min). The pure blue and pure green (b,c, respectively) lytic cells show only one fluorescence color, but the mixed lytic cells (f) show both blue and green fluorescence, appearing as a cyan color in the overlay image. For lysogenic cells (d,e,g), fluorescence develops uniformly throughout the cells, followed by cell growth and division. The pure yellow and pure red (d,e, respectively) lysogenic cells show only one fluorescence color, but the mixed lysogenic cells (g) show both yellow and red fluorescence, appearing as orange in the overlay image. Scale bar, 2 μm.

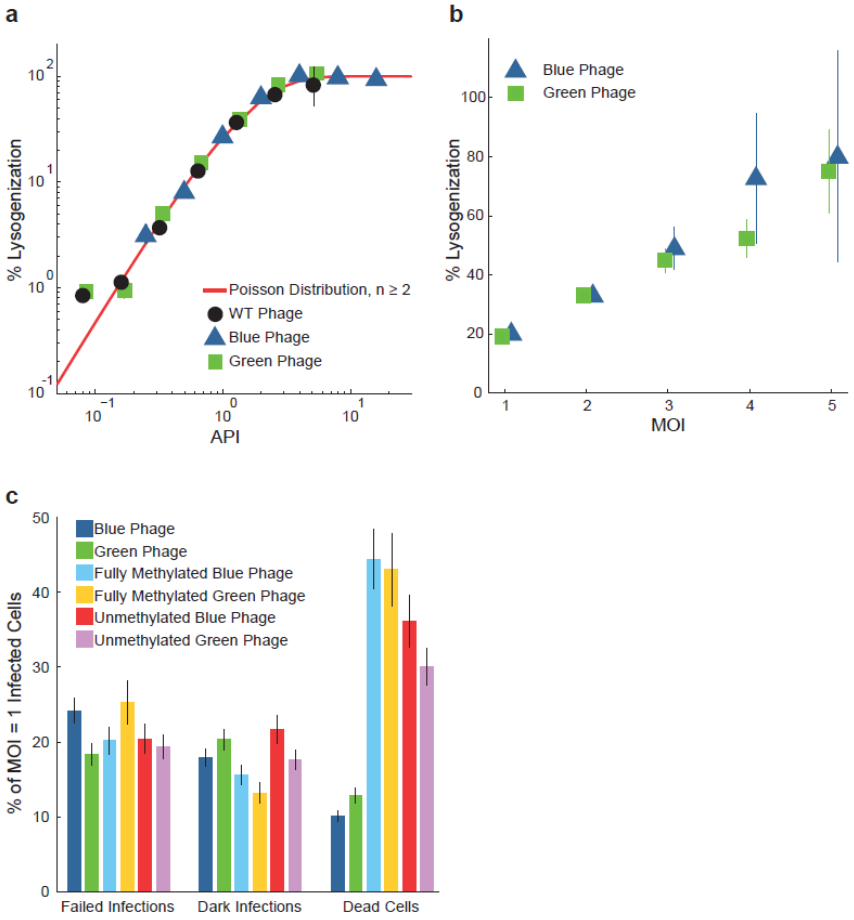

Figure 2.2 Fluorescent phages behave like WT phage.
(a) Fluorescent phages lysogenize like WT phage in bulk. Percentage of lysogeny is plotted against the average phage input (API), showing that fluorescent double reporter phages (blue triangles and green squares represent blue and green phages respectively) are indistinguishable from the wild type (black circles) following the theoretical prediction of Poisson distribution of $n \geq 2$ (red line). Representative plot is shown from 4 biological replicates consisting of 2 technical replicates each. Error bars represent ± s.d. of the technical replicates.
(b) At the single cell level under the microscope, both fluorescent double reporter phages behave similarly to each other, and their lysogenization probabilities increase with multiplicity of infection (MOI). Blue phage data is from movies with N = 179 cells, and green phage data is from movies with N = 200 cells. Error bars represent ± s.e.m.
(c) The failed, dark, and dead cell frequencies for MOI = 1 infections for phages with the normal methylation state (blue and green phages), and fully methylated as well as unmethylated phages. Blue phage data from N = 207 cells, green phage data from N = 164, fully methylated blue phage data from N = 124 cells, fully methylated green phage data from N = 79 cells, unmethylated blue phage data from N = 108 cells, and unmethylated green phage data from N = 150 cells. Error bars represent ± s.e.m.

Results

Subcellular decision-making assayed using a 4-color system

We achieved higher resolution of phage lambda decision-making via fluorescence imaging of phage gene expression using four fluorescent proteins as our reporters, based on their excellent fluorescence properties and separation on the fluorescence spectrum, mTurquoise2 [146], mNeongreen [147], mKO2 [148], and mKate2 [149]. We constructed phages with fluorescent protein genes *mTurquoise2* and *mNeongreen* (denoted blue and green for simplicity), translationally fused to the λ*D* gene, which encodes gpD, a capsid decorative protein assembled in >400 copies on the phage head. This enables the visualization of infecting phages and labels progeny phages[132], reporting the progress of the lytic pathway (Fig. 2.1a). The phages also bear transcriptional fusions of fluorescent protein genes *mKO2* and *mKate2* (denoted yellow and red for simplicity) inserted downstream of the *cI* gene to report lysogeny[131,150], as the *cI* operon is expressed during establishment and maintenance of lysogeny. These transcriptional fusions are expressed as separate proteins to avoid potential interference with CI activity, involving DNA binding and oligomerization[151]. These fluorescent protein genes replace *rexA* and part of *rexB*, genes downstream of *cI*, to preserve the length of the DNA in the operon, as one function of CI is to loop DNA[37,152]. Though *rexB* was suggested to indirectly affect the lytic/lysogenic switch[153], the removal of those genes did not affect lysogenization behavior (Fig. 2.2). These phages report lytic and lysogenic votes separately: the ‘blue phage’, with the blue lytic/yellow lysogenic reporter, and the ‘green phage’, with the green lytic/red lysogenic reporter.

Cells infected with both phages report the decisions of both phages, allowing for the visualization of phage voting (Fig. 2.1a). The two phages are distinguishable from the first frame of the movie (Fig. 2.1b–g, 0 min), and over time, the cells grow, fluorescence develops after cellular decisions occur and the fluorescent proteins mature, allowing us to determine cell fates by the fluorescence signals in the movies (Fig. 2.1b–g). Interestingly, in lytic cells, the lytic reporter forms foci, and in mixed lytic cells, the two lytic reporters co-localize. We speculate that the foci are centers of phage assembly, and that assembling phages utilize both gpD fusions, which are functionally identical.

As the extensive modifications to the phage genomes may have unknown effects on the phages' lysis/lysogeny decision-making behavior, we performed bulk-level and single-cell experiments to characterize the lysogenic response of the phages. Bulk lysogenization showed that the two phages have a similar trend of lysogenic frequency versus average phage input (API, ratio of phage titer to host cell concentration) to wild-type (WT) phage (Fig. 2.2a)[52], and single-cell infection movie analyses found that the phages' lysogenic frequency increases with multiplicity of infection (MOI, number of infecting phages per cell), similar to WT phage expectations (Fig. 2.2b). Taken together, these data suggest that the reporter phages behave like WT phage.

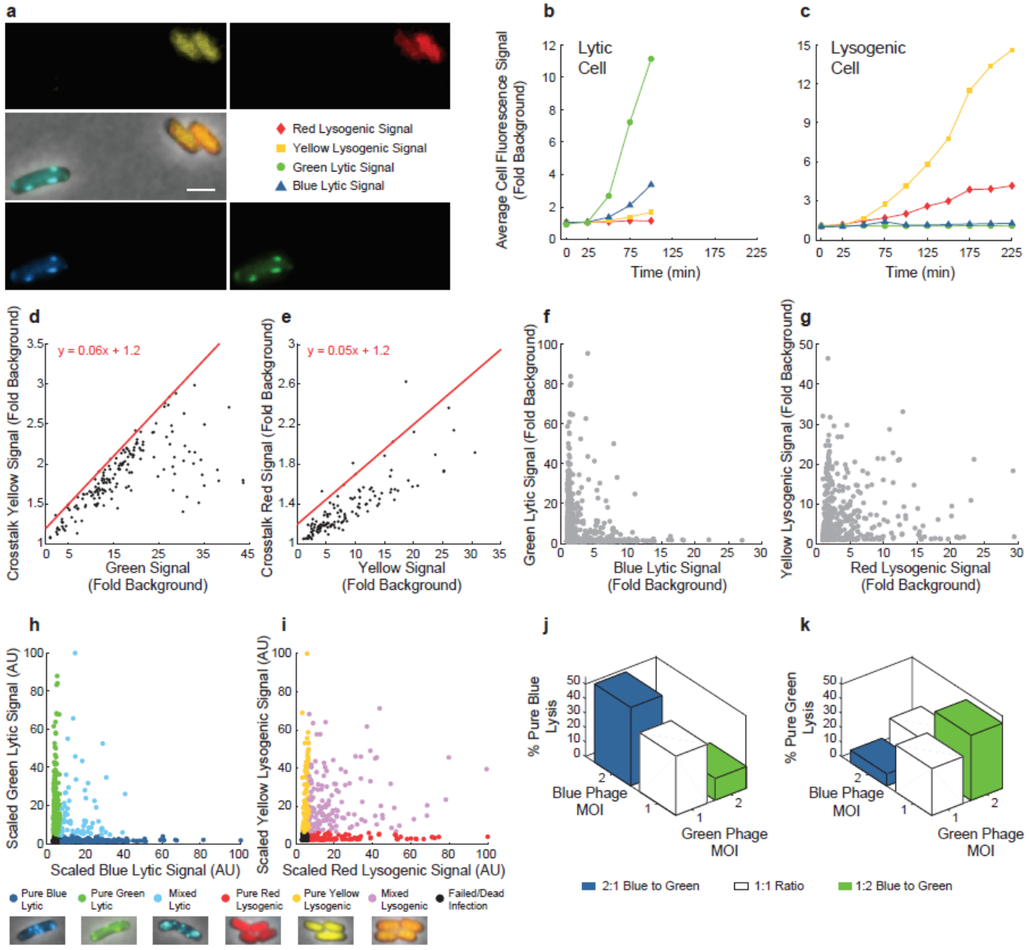

Figure 2.3 Collection and quantification of fluorescent reporter data.
(a) An example of a mixed lytic and mixed lysogenic cell is shown as an overlay image and in each reporter fluorescence channel (blue and green lytic, red and yellow lysogenic).
(b and c) The fluorescence signal in each channel is plotted over time for the example lytic cell (b) and lysogenic cell (c) shown in (a). The signal is defined as the average fluorescence signal within the cell normalized to the average signal of a large cell-free area within the same frame designated as the background.
(d and e) The level of crosstalk of the green into yellow channel (N = 169, green phage) (d) and yellow into red channel (N = 128, blue phage) (e) from pure infections. The crosstalk signals (yellow in d and red in e) are plotted against green and yellow signals from the phages for each cell at the final time point (black dots). The red line shows the upper bound of the crosstalk. The line, which runs above most of the data points, gives a correction factor where 6% of the green signal is subtracted from the yellow signal (d) and 5% of the yellow signal is subtracted from the red signal (e).
(f and g) The fluorescence signals in the reporter channels at the final time point for each cell are plotted by the lytic (f) and lysogenic (g) channels with crosstalk corrections, showing distributions of reporter activities.
(h and i) The highest signal in each channel for lytic/lysogenic cells was scaled to 100 AU and all remaining signals were scaled accordingly. A cutoff value for each channel was assigned to visualize different pure and mixed fates for lytic (h) and lysogenic (i) cells. Representative images of different fates are shown as they appear under the microscope.
(j and k) Percentage of lytic cells showing pure blue (j) and green lysis (k) in total lytic cells infected with specific combinations of phages is plotted against specific phage MOI on the x and y axes. Scale bars = 2μm.

To characterize phage interactions, we performed single-cell infection assays with mixed blue and green phages, collected data from all four fluorescence channels at given times for each cell, and normalized every cell's reporter signals to the background fluorescence (Fig. 2.3a–c). We observed crosstalk from the yellow channel into the red, and from the green channel into the yellow. We quantified the level of crosstalk from pure infection movies, using only one of either phage in the absence of the other (Fig. 2.3d,e), and corrected the signals in mixed-phage infection movies by subtracting the crosstalk from the measured signals (Fig. 2.3f,g). For simplicity, we set the highest intensity for a lytic/lysogenic cell in each of the four channels to 100 AU (arbitrary units) and rescaled all cell intensities accordingly. By assigning a cutoff value for each channel, our program is able to assign preliminary cell fates (Fig. 2.3h,i) which are then verified by eye.

Phages compete in lysis but cooperate in lysogeny

To determine what types of phage interactions are occurring, we analyzed reporter expression patterns in cells infected with both phages (dual-color infections), and we found that a single lytic/lysogenic reporter may dominate or that both phages' reporters may contribute. For each fate, the scenarios of single phage dominance, where only one phage expresses its gpD fluorescent (lytic) or *cI* transcriptional (lysogenic) reporter are defined as 'pure lysis/lysogeny signals,' and cases where both phages express their respective reporters are defined as 'mixed lysis/lysogeny signals.' For lytic cells with dual-color infections, we observed pure lysis at surprisingly high frequency relative to mixed lysis, indicative of possible competitive interactions within the lytic cells. Notably, the number of 'wins' by either phage is similar (45 blue to 41 green), suggesting a scenario where a phage depletes some cellular resource. In contrast to dual-color lysis, lysogenic cells with dual-color infections are less likely to show pure red or yellow lysogenic signals (Fig. 2.4a).

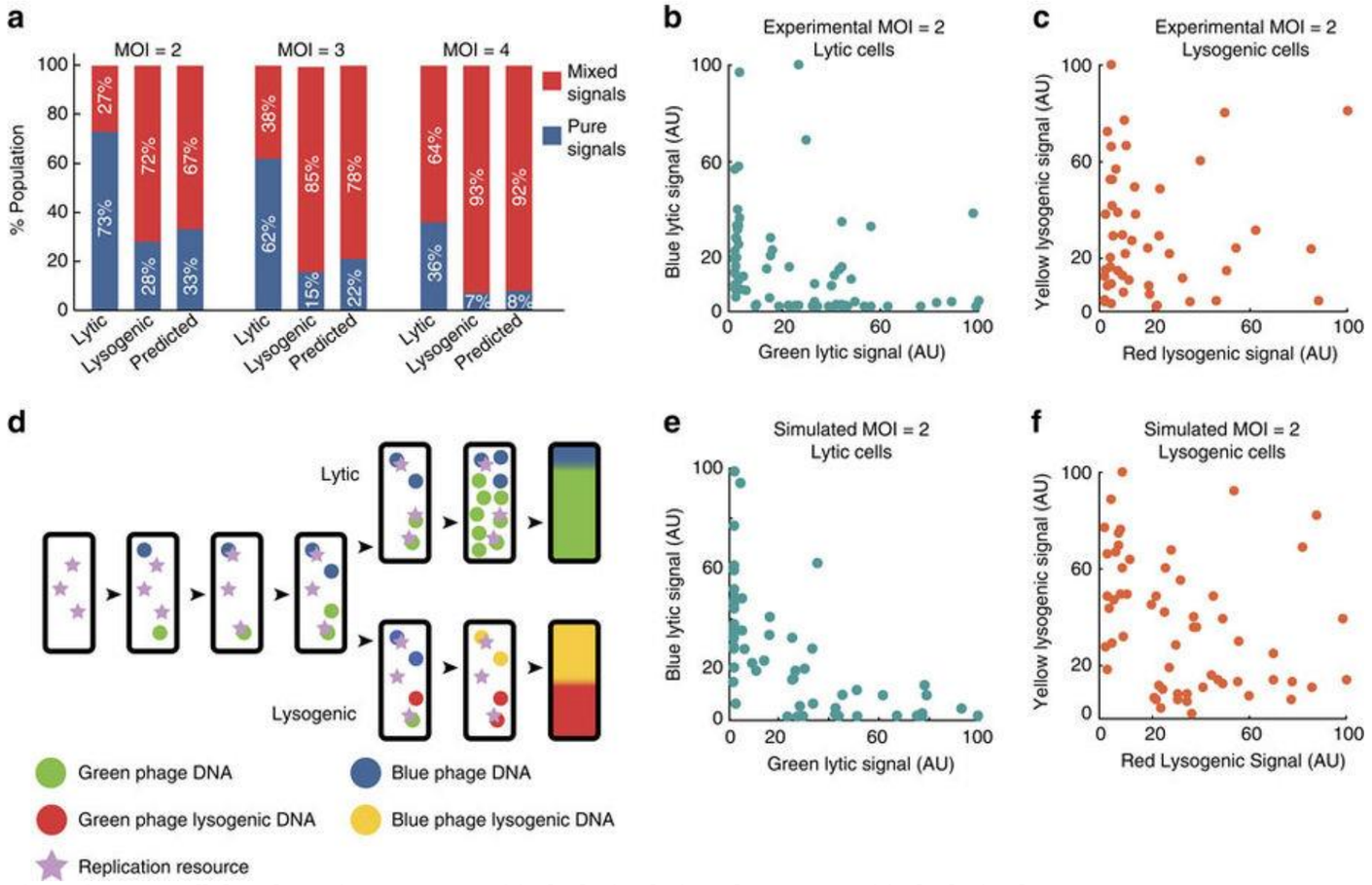

Figure 2.4 Intracellular phages interact competitively during lysis and non-competitively during lysogeny.
(a) Mixed-infected cells at MOI = 2, 3 and 4 are grouped by lytic/lysogenic fates, and furthermore into mixed (both lytic/both lysogenic) and pure (one lytic/lysogenic) fates. The 'predicted' column shows the expected mixed/pure fate populations calculated from observed failed and dark infection frequencies of the blue/green phages. Sample sizes at MOI = 2, 3, 4 are N = 71, 45, and 11 (lytic), and N = 49, 46, and 30 (lysogenic), respectively. (b,c) Cells infected at MOI = 2, one of each phage, grouped as lytic or lysogenic, regardless of mixed/pure signals. For lytic cells (N = 71) (b) we plot their blue/green signals and for lysogenic cells (N = 49) (c) their red/yellow signals. Distributions of products for lytic (mean: 265, median: 30) and lysogenic (mean: 603, median: 159) data's X and Y values are significantly different (mean: K–S test, null hypothesis rejected, D = 0.41, P = 7e-5, median: Mann–Whitney U-test, null hypothesis rejected, U = 3,701, P = 2e-3). (d) Diagram of lytic and lysogenic development models for cells infected by one of each blue/green phage shown. DNAs arrive in the cell, bind a resource to replicate, and retain that resource after replication. In lytic cells, DNAs produce a reporter specific to the phage type. The blue/green reporter levels are recorded at the end of each simulation. For lysogenic cells, DNAs can switch into a lysogen after replicating, and lysogens convert DNA into lysogens and produce reporters. Phage arrival times and resource levels are key parameters varied. (e,f) Simulated cells at MOI = 2, resource level = 3, and average arrival delay = 3 replications are shown for the lytic/lysogenic models (N = 60 for each), resembling the experimental lytic/lysogenic data. Distributions of mean and median products for lytic (mean: 180, median: 22) and lysogenic (mean: 980, median: 490) data points' X and Y values are significantly different (mean: K–S test, null hypothesis rejected, D = 0.56, P = 3e-9, median: Mann–Whitney U-test, null hypothesis rejected, U = 2,457, P = 8e-10).

The pure fates we observe may be a combined result of a failed infection (incomplete ejection of phage DNA into the cell), and/or a dark infection (successfully injected phage sheared off before imaging)[133]. To test this possibility, we calculated the predicted pure and mixed signals based on our measured dark and failed infection frequencies (Fig. 2.2c) and compared them with the measurements (Fig. 2.4a, see Methods for calculations). The pure lytic frequency is far above the predictions, indicating that the 'winning' phage must directly or indirectly suppress the other at some time from infection through lysis. Conversely, the pure lysogenic frequency is consistent with the predictions (Fig. 2.4a), indicating a lack of competition. Additionally, the probability of mixed lysis/lysogeny increases with MOI due to higher probability of successful dual-color infections. Furthermore, within the population of pure lytic infections, when one phage outnumbers the other, the cell has a higher chance to report the lytic cycle of the majority phage (Fig. 2.3j,k), indicating that a higher initial phage copy provides an advantage in gene dosage for a phage to dominate lysis by exponential replication. These data suggest that phage interactions vary with cell-fate decisions, where phages commonly coexist in lysogeny, but predominately vie for dominance in lysis.

If phages interact variably during different cell fates, quantifiable differences should be observed when examining the reporters in lytic and lysogenic cells. In lytic cells, the blue or green fluorescence before lysis represents the level of the decorative capsid protein gpD, indicative of phage burst size. For pure infections, the lytic signals of blue and green phages are well fitted to Gaussian distributions with averages of 19.6 and 19.7, respectively. For dual-color infections of MOI=2 (one of each phage), we grouped these lytic cells by their fates into pure blue or green lysis (dominating) or mixed lysis. The average lytic signals were 17.9 and 17.0 for blue and green dominating infections, respectively, whereas for mixed lysis, the average blue and green signals were lower, at 13.0 and 10.2, respectively. In the lytic signal distribution, we observed that data points commonly reside near the axes with fewer intermediate points, unlike lysogenic signals, so we devised a measure to usefully differentiate between dominating and mixed reporter signals (Fig. 2.4b,c).

We took the product of the two normalized signals (X and Y values) for each data point, so dominated signals have lower values while mixed signals have higher values, due to being on the plot's edges and middle, respectively. By comparing the lytic and lysogenic distributions, we find that their means (lytic: 265, lysogenic: 603, two-sample Kolmogorov–Smirnov (K–S) test, null hypothesis rejected with D=0.41, P=7e-5), and their medians (lytic: 30, lysogenic: 159, Mann–Whitney U-test, null hypothesis rejected with U=3,701, P=2e-3) are significantly different. We also compare the signals over time, where the average lytic fluorescence in pure lysis is greater than in mixed lysis and becomes more significant throughout the infection (Fig. 2.5c,d). Conversely, the fluorescence of lysogenic cells with pure infection (MOI=2) show similar trends to those of dual-color infections (one of each phage) (Fig. 2.5e,f) with slightly higher expression for pure infections, which could be due to a difference in the per-phage DNA copy number between mixed and pure infected cells.

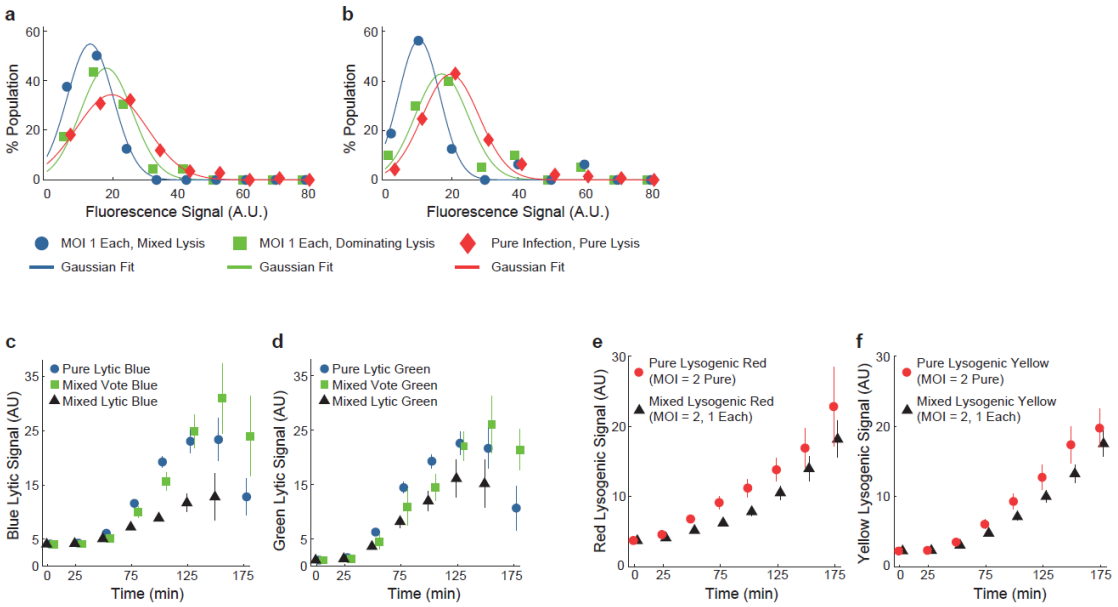

Figure 2.5 Pure and mixed lysis reporter signals behave differently from each other, and from lysogenic signals.

(a and b) Histogram of lytic fluorescence signals before cell lysis and the fitted Gaussian distribution (lines). Lytic cells are grouped into different categories: MOI = 2, one of each phage, mixed lytic (N = 19) (circles, blue and green lytic signals in (a) and (b) respectively); MOI = 2, one of each phage, dominating lytic (squares, blue and green lytic cells in (a) (N = 28) and (b) (N = 24) respectively); pure infections (diamonds, blue and green lytic cells in (a) (N = 168) and (b) (N = 165) respectively).

(c and d) The blue and green lytic signals (c and d respectively) in lytic cells are plotted over time. Lytic cells are divided into groups: pure blue (N = 178) (c) / pure green (N = 179) (d) (circles), mixed lytic (N = 57) blue signal (c) / green signal (d) (triangles), and mixed voting blue lytic (N = 35) (c) / green lytic (N = 20) (d) (squares). Error bars represent ± s.e.m.

(e and f) The yellow and red lysogenic signals (e and f respectively) in lysogenic cells are plotted over time. Lysogenic cells are divided into groups: MOI = 2, pure infections (circles, pure red (N = 11) in (e) and pure yellow (N = 13) in (f), and MOI = 2, one of each phage, mixed lysogens (triangles, N = 35 with red and yellow signals in e and f respectively). Error bars represent ± s.e.m.

Parameter	Value	Units	Meaning	Reasoning
k_1	1e0	s^{-1}	Phage DNA binds DNA pol/replisome	Fast diffusion of proteins
k_2	1e-2	s^{-1}	New DNA production by complex	On the order of minutes
k_3	1e-3	s^{-1}	Replisome unbinds from DNA	Infrequent because replisomes thought to stay bound
k_4	5e-2	s^{-1}	Lytic reporter protein production	Gives reasonable lytic reporter numbers, of gpD
k'_1	1e0	s^{-1}	Lysogenic DNA (unreplicated and replicated) binds DNA pol/replisome	As k_1
k'_2	1e-2	s^{-1}	New DNA production by complexes (unreplicated and replicated)	As k_2
k'_3	1e-3	s^{-1}	Replisome unbinds from lysogenic DNA	As k_3
k'_4	2e-3	s^{-1}	Lysogenic reporter production	Gives reasonable lysogenic reporter numbers
k'_5	2e-2	s^{-1}	Replicated DNA/complex turns into Lysogen	Expected to be on the order of DNA replication
k'_6	1e0	s^{-1}	Forced lysogenization by lysogens	Fast diffusion of CI

Table 2.1 Parameters used in the computational models.

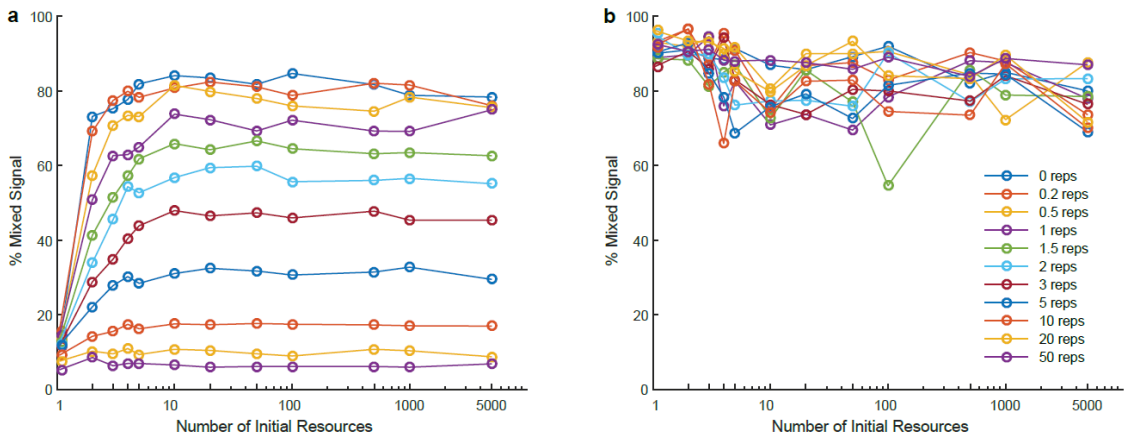

Figure 2.6 Dependence of mixed lysis and lysogeny on infection timing.
(a) Using our chosen replication-limited model, we simulated different permutations of resource levels and arrival delays on our lytic and lysogenic models. Increasing the arrival (in replication cycles) of the second phage decreases the frequency of mixed lysis for all resource levels. This effect plateaus after around 10-20 replication cycles.
(b) Arrival time of the second phage does not have a strong effect on the frequency of mixed lysogeny.

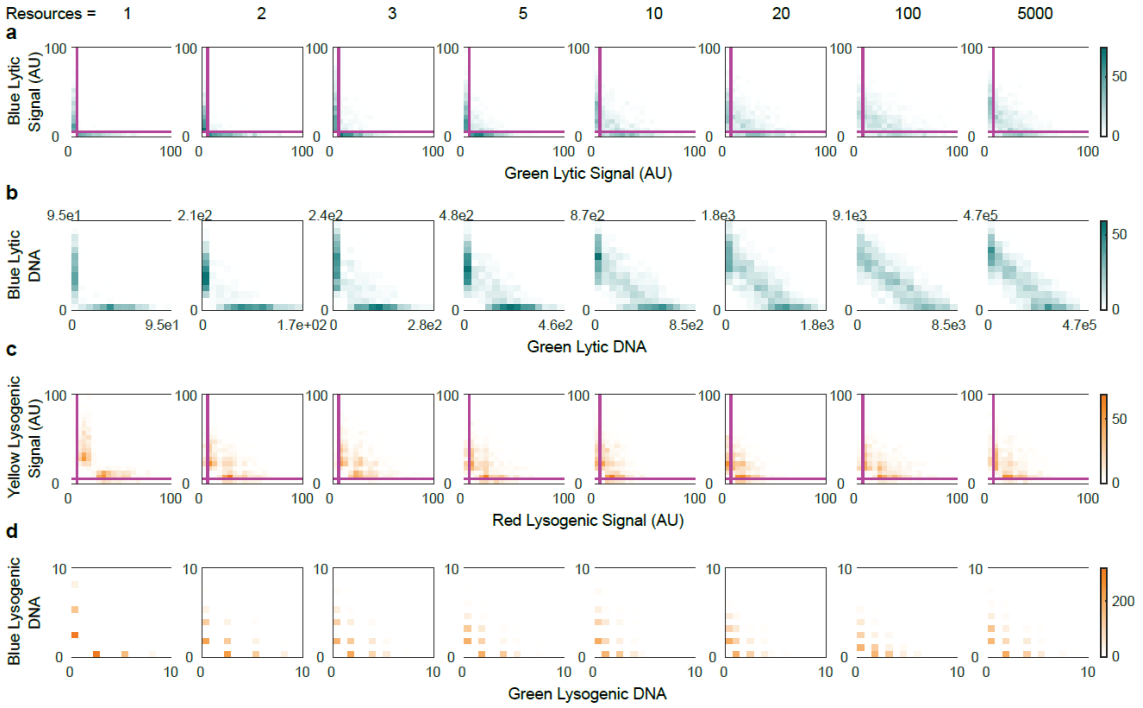

Figure 2.7 Resource level affects DNA and reporter distributions in binding-limited model.

(a-d) The effects of increasing initial resource levels on simulated lytic reporters (a) and DNA numbers (b), and lysogenic reporters (c) and DNA numbers (d) on the simulation end states (N = 1000) using binding-limited parameter set are shown as bivariate histograms. Second phage arrival was fixed at an average of two replications. Axes of (a), (c) are in units of normalized fluorescence signal; axes of (b), (d) are actual simulated DNA numbers.

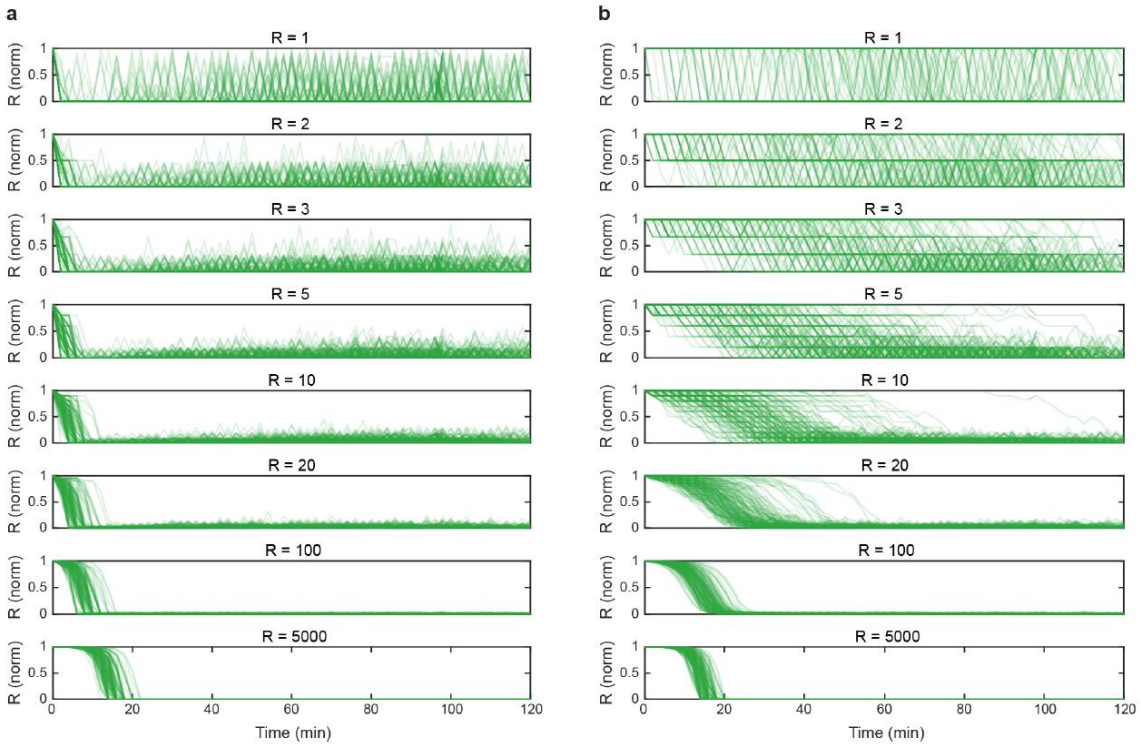

Figure 2.8 Resource usage dynamics changes depending on the model parameters chosen.
Comparison of (a) replication-limited (chosen) with (b) binding-limited parameter sets. The dynamics are more realistic in the replication-limited case, with higher resources being used up later than lower resources.

The experimental data indicate that phages interact at the DNA level, where lysis and lysogeny exhibit different behaviors, so we built computational models to probe how this might occur. These models separate lysis from lysogeny and simulate what would happen when a cell is infected with one of each phage DNA, where the DNAs would replicate and express reporter proteins (Fig. 2.4d). We arrived at our parameter set following rigorous parameter testing, confirming that our model is robust (Table 2.1; Fig. 2.6), but would predictably fail to emulate realistic biological processes under incorrect parameter regimes (Figs 2.7 and 2.8). In both models, one phage DNA enters with a delay, as phage DNA takes a variable amount of time to translocate into the cell[137]. Also, DNA replication requires an undefined resource to proceed, possibly a polymerase or replisome component[154], which stays bound to the DNA as it replicates[155]. Specific to the lysogenic model, there is also an interaction that converts non-lysogenic DNA into lysogenic DNA, summarizing the biological establishment of lysogeny, where *trans*-acting CI from lysogens binds all intracellular phage DNAs rendering them as lysogens by repressing other phage genes (see details in Methods). Representative simulations show similar distributions compared with experimental lytic and lysogenic cells (Fig. 2.4e,f). By changing the key parameters of arrival delay and resource level, we can learn about the differences between lytic and lysogenic development, and about the mechanism of domination.

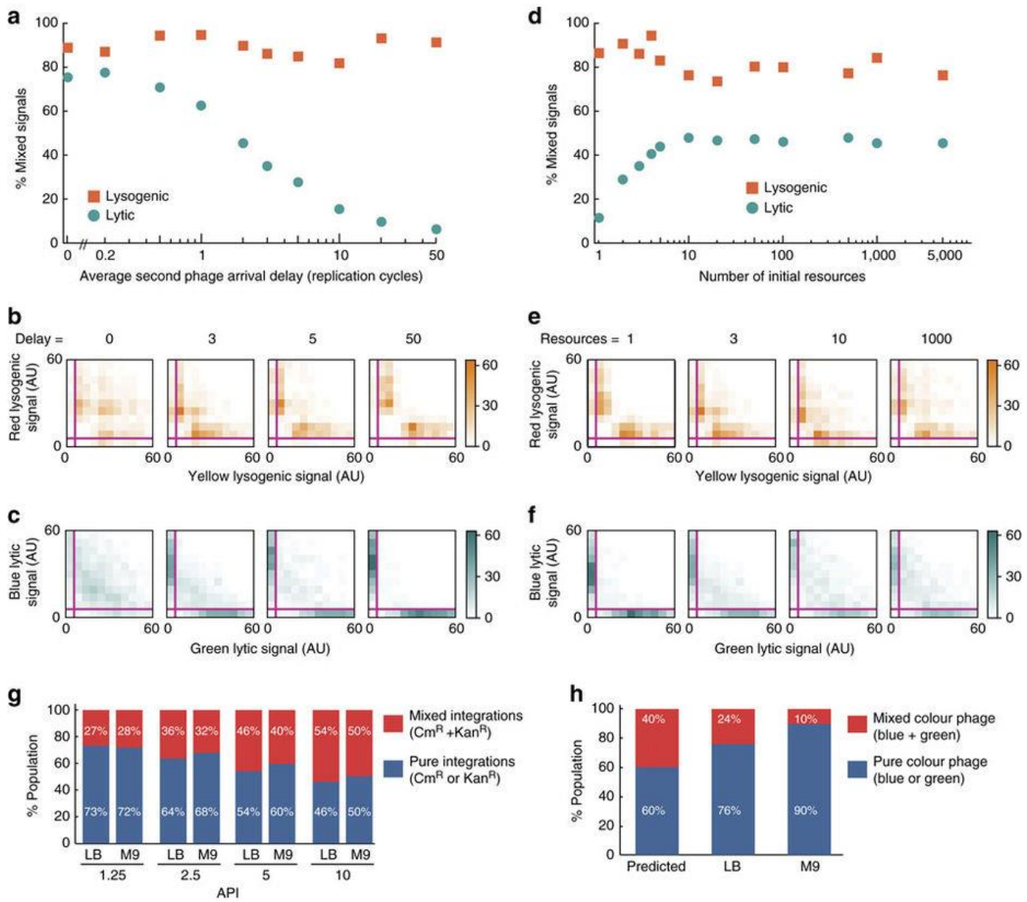

Figure 2.9 Mixed reporter signal frequency decreases with phage DNA arrival time and increases with resource level in lysis but not lysogeny.
(a,d) Mixed reporter signals versus average delay time: (a) for lytic cells (turquoise circles) decrease with delays whereas for lysogenic cells orange squares) they are relatively constant with respect to delays (fixed resource level = 3, 0 cycles means simultaneous arrival). Mixed reporter signals are plotted against initial resource level in d similar to a (fixed delay time = three replication cycles). Simulation data (N = 1,000 for all parameter sets) are normalized to the maximum and minimum of each data set and binned (20 bins), where trajectories ending with lytic/lysogenic signal 45% along both axes are classified as mixed signals for all histograms.
(b,c) Bivariate histograms of lysogenic (b) and lytic (c) reporter levels from simulations at given arrival delays. Magenta lines represent the pure-mixed threshold (5%) for each reporter.
(e,f) Bivariate histograms of lysogenic (e) and lytic (f) reporter levels from simulations at given resource levels. Magenta lines represent the pure-mixed threshold (5%) for each reporter.
(g) Percentage of pure (one antibiotic resistance, KanR or CmR) and mixed lysogens (both antibiotic resistances) from a bulk lysogenization assay using mixed WT phages is plotted as a function of API. The mixed lysogeny increases with API, and is similar between media.
(h) Percentage of mixed and pure phage progeny from bulk lysis experiment (using the same blue and green phage mixture as in the infection movies) is shown compared with predicted values for different growth media, LB (N = 1,522) and M9 (N = 1,844). Predicted values assume no competition, and mixed population increases in richer LB medium.

In the lytic model, simulations show that the ratio of DNA levels, and, therefore, lytic reporter levels, of different phage species depend heavily on the relative arrival times of the phage DNAs. At long delays the proteins are often very unbalanced, where one species dominates, and the data points cluster near the axes with few mixed signal points (Figs. 2.9 and 2.10). With shorter delays, the mixed signal population in the simulations increases. The resource level also affects which species dominates, as with lower resources, the data are shifted towards the axes, whereas mixed signals increase with higher resource levels (Fig. 2.9d,f; Fig. 2.10a,b). This suggests that competition occurs during DNA replication, where in lysis, one phage has runaway replication to dominate the other. For lysogenic cells, the model predicts that the level of mixed signals is higher than in lysis, and that it is less sensitive to changes in resource level and phage arrival delay (Fig. 2.9a,b,d,e; Fig. 2.10c,d,g,h). Both models have identical mechanisms for DNA replication, but the lysogenic model predicts less competition for low resources and similar phage DNA numbers for all resources (Fig. 2.10), which is biologically relevant, as lysogenic establishment requires few phage DNA copies and halts DNA replication[9,49]. These models are, therefore, consistent with our experimental observations regarding different interactions in lysis versus lysogeny, predicting that fast resource depletion is a means of competition.

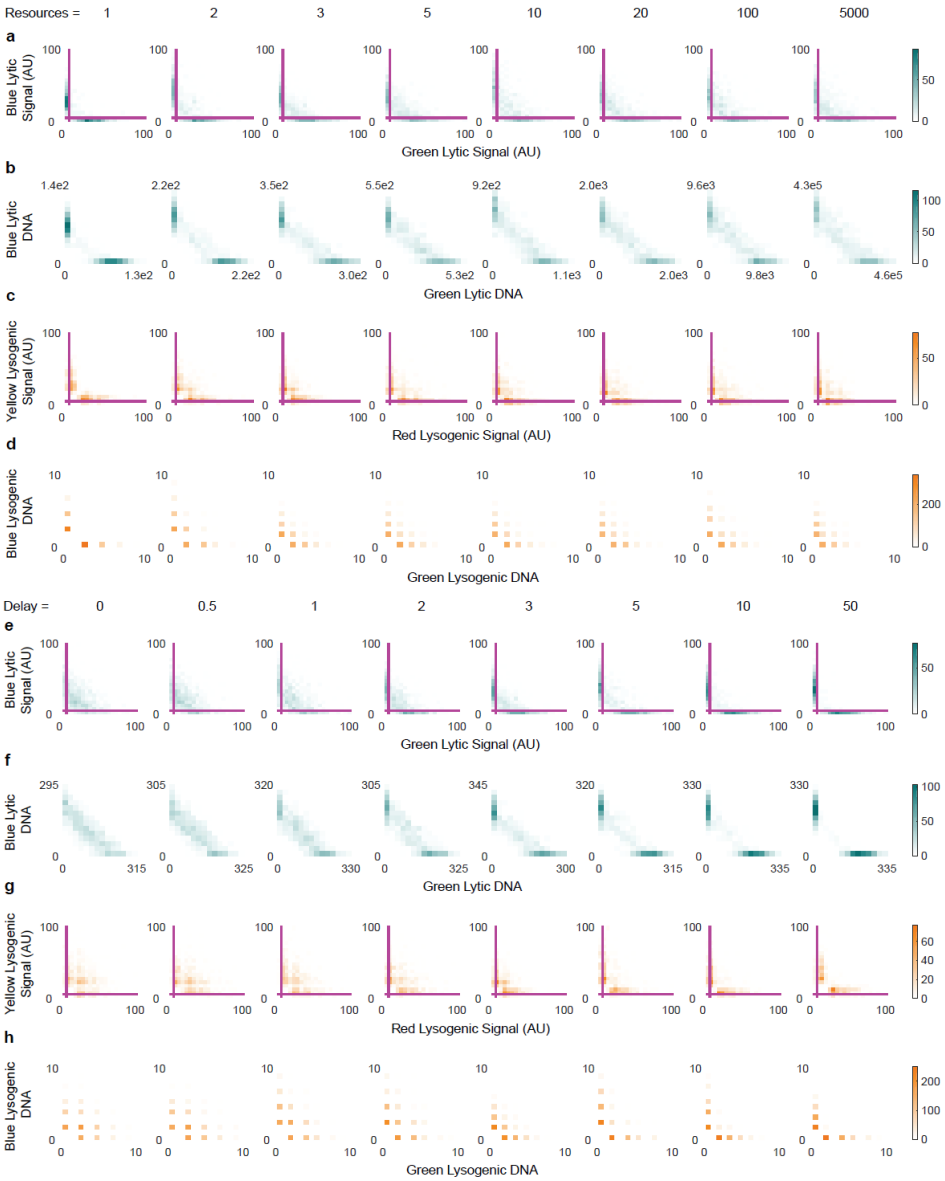

Figure 2.10 Resource level and infection timing predicted to imbalance DNA ratio in replication-limited model and influence mixed signal level in lysis, with less effect during lysogeny.

(a-d) The effects of increasing initial resource levels on simulated lytic reporters (a) and DNA numbers (b), and lysogenic reporters (c) and DNA numbers (d) on the simulation end states (N = 1000) using chosen replication limited parameter set are shown as bivariate histograms. Second phage arrival was fixed at an average of three replications. (e-h) The effects of increasing second phage delays (represented as the number of average replication cycles) on simulated lytic reporters (e) and DNA numbers (f), and lysogenic reporters (g) and DNA numbers (h) on the simulation end states (N = 1000) are shown as bivariate histograms. Resources = 3. Axes of (a), (c), (e), (g) are in units of normalized fluorescence signal; axes of (b), (d), (f), (h) are actual DNA numbers.

We performed a bulk lysogenization assay by using a 1:1 mixture of WT phages bearing different antibiotic markers (Kan^R or Cm^R) to infect cells at different APIs, to test how mixed phages propagate when finally integrated into lysogens. The results showed a high frequency of double antibiotic resistant cells, indicating mixed phage DNA integration (mixed lysogeny), which increases with API due to the increasing frequency of mixed-phage infections (Fig. 2.9g). These data are consistent with the lysogenic model's prediction of similar DNA numbers, as mixed lysogeny would be favored in the case of balanced DNA species. This observation holds when the assay is done in either a richer LB or poorer M9 medium, where cells are growing faster or slower, respectively, with similar levels of mixed lysogeny in both media, suggesting that resource limitations in host growth have negligible effect on lysogenic development and interactions. To test mixed lysis, we infected cells in culture tubes with the same mixture of phages used for the infection movies, forcing the lytic decision in infected cells by incubating at 42°C, and grouping the resulting phage progeny in the lysate as mixed or pure phages based on microscopy data. The mixed progeny population was far below the prediction (Fig. 2.9h), supporting phage competition as observed at the single-cell level. When performing this lytic assay in LB and M9 media, we observed that the richer medium resulted in more mixed progeny, indicating that phages compete over resources involved in host growth during lysis.

The high frequency of mixed lysogeny in the bulk experiment suggests that there may be cooperation during lysogenization. Cooperation can be summarized as individuals in a group interacting non-antagonistically to achieve a mutual benefit for the participants. Cooperating individuals can endow function-deficient mutants with the function that they are lacking, as exemplified by swarming bacteria[139]. We tested such cooperative behavior for phages by performing the bulk lysogenization assay as described above using lysogenization-defective mutants of phage lambda, λ*cII*$^{-}$ and λ*P*$^{-}$ (Table 2.2) in mixed-phage infections, by mixing the mutants with the WT phage and also together, then compared their lysogenization behavior to pure infections of each strain without mixing[52,156]. We calculated the frequency of mixed integration lysogens (double antibiotic resistance) and pure integration lysogens (single antibiotic resistance) from colony counts on different antibiotic plates.

When mixed with WT phages, mutant phage integration frequency increases at all APIs relative to the mutant-only infections (Fig. 2.11), and WT phage integration frequency generally increases relative to the WT-only infections (Fig. 2.11b,d). Also of note, the WT phages with different antibiotic markers have the same lysogenization behavior, and are considered as functionally identical (Fig. 2.11a,c). When the mutants are mixed together, they mutually complement lysogenization defects, resulting in increased integration frequencies for both phages (Fig. 2.11e,f). The increases in lysogenic frequency are likely due to the sharing of key lysogenic proteins, and combined with the aforementioned similarity in DNA copies, allow both phages to propagate as lysogens more frequently than was possible in the pure infections. Thus, phages interact cooperatively in lysogeny and show dominating behavior in lysis, indicating that phages do not behave uniformly in a cell.

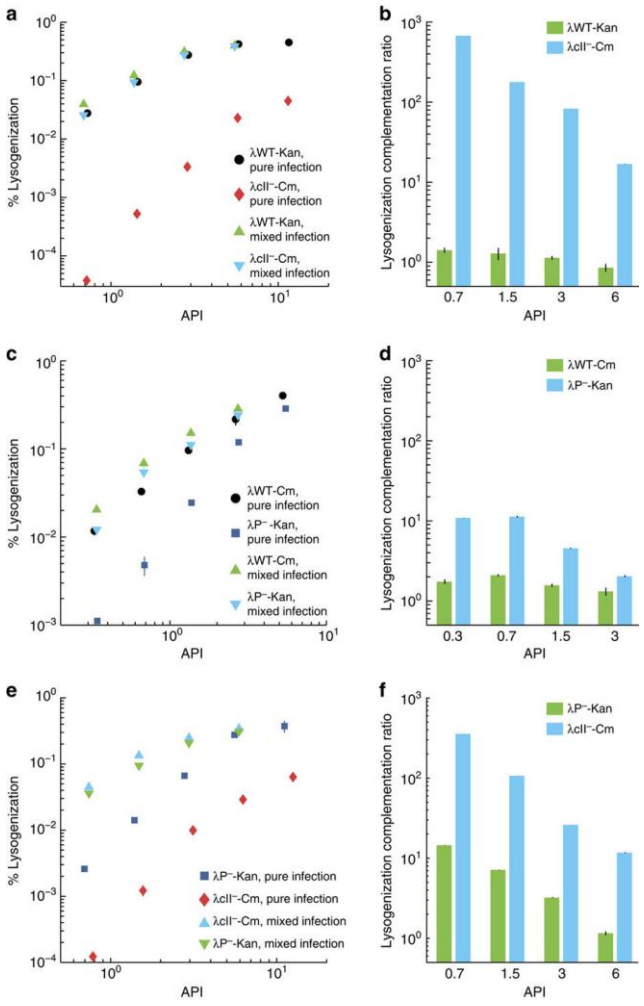

Figure 2.11 Phages cooperate during lysogeny to mutually propagate integration. (a,c,e) Mixed bulk lysogenization using WT phage mixed in a 1:1 ratio with either mutants λcII$^-$ (a) or λP$^-$ (c), and 1:1 ratio mixture of λcII$^-$ and λP$^-$ show complementation of mutant lysogenization defects via co-infection. Lysogenization frequency of pure infections with WT (circles), λcII$^-$ (diamonds), and λP$^-$ (squares) versus API are plotted on a log-log scale. Total phage integrations from mixed infections including lysogens from pure phage integrations and mixed phage integrations are shown (a,c, mutants in down triangles, and WT in up triangles, and e, up and down triangles correspond to different mutants) for each API, referring to the number of mutant or WT phages. (b,d,f) Quantification of change in lysogenization from pure infections to mixed infections. (b corresponds to a,d to c and f to e). Values are calculated for each API by dividing the % lysogenization in the mixed infection by the % lysogenization in the pure infection; the bar represents the fold change in integration frequency, where '1' is no change. WT shows generally positive changes, and the mutants show increased lysogen frequency substantially. Representative plots are shown for each experiment, which were done with at least two biological replicates consisting of two technical replicates each. Error bars represent ± s.d. of the technical replicates.

Phage #	Phage Strains	Comments	
λLZ613	λ*cI*$_{857}$ *bor::Kan*^{R}	"λWT-*Kan*," wild type phage, *Kan*^{R}	Lab Stock
λLZ859	λ*cI*$_{857}$ *bor::Cm*^{R}	"λWT-*Cm*," wild type phage, *Cm*^{R}	Lab Stock
λLZ637 or λ*P*$^{-}$	λ*cI*$_{857}$ *Pam*$_{80}$ *bor::Kan*^{R}	"λ*P*$^{-}$*-Kan*," phage with nonsense mutation in *P*, *Kan*^{R}	Lab Stock
λLZ895	λ*cI*$_{857}$ *cII*$_{68}$ *bor::Kan*^{R}	"λ*cII*$^{-}$*-Kan*," phage with point mutation in *cII*, *Kan*^{R}	Lab Stock
λLZ896	λ*cI*$_{857}$ *cII*$_{68}$ *bor::Cm*^{R}	"λ*cII*$^{-}$*-Cm*," phage with point mutation in *cII*, *Kan*^{R}	Lab Stock
λLZ1367	λ*D-mTurquoise2 cI*$_{857}$*-mKO2 bor::Cm*^{R}	"Blue phage," double reporter, *Cm*^{R}	This work
λLZ1373	λ*D-mNeongreen cI*$_{857}$*-mKate2 bor::Cm*^{R}	"Green phage," double reporter, *Cm*^{R}	This work
λLZ1381	Unmethylated λ*D-mTurquoise2 cI*$_{857}$*-mKO2 bor::Cm*^{R}	"Unmethylated blue phage," *Cm*^{R}	This work
λLZ1380	Unmethylated λ*D-mNeongreen cI*$_{857}$*-mKate2 bor::Cm*^{R}	"Unmethylated green phage," *Cm*^{R}	This work
λLZ1379	Fully methylated λ*D-mTurquoise2 cI*$_{857}$*-mKO2 bor::Cm*^{R}	"Fully methylated blue phage," *Cm*^{R}	This work
λLZ1378	Fully methylated λ*D-mNeongreen cI*$_{857}$*-mKate2 bor::Cm*^{R}	"Fully methylated green phage," *Cm*^{R}	This work
-	λ*Dam cI*$_{857}$	Phage with nonsense mutation in *D*	Alan Davidson
λLZ1254	λ*Dam cI*$_{857}$ *bor::Kan*^{R}	Phage with nonsense mutation in *D*, used in recombination to produce phages λLZ1266 & λLZ1369, *Kan*^{R}	This work
λLZ1266	λ*D-mTurquoise2 cI*$_{857}$ *bor::Kan*^{R}	Crossed with phage λLZ1357 to make LZ1367, *Kan*^{R}	This work
λLZ1369	λ*D-mNeongreen2 cI*$_{857}$ *bor::Kan*^{R}	Crossed with phage λLZ1355 to make LZ1373, *Kan*^{R}	This work
-	λ*cI*$^{-}$	λ*cI* point mutant, used in recombination to produce phages λLZ1357 & λLZ1355	Ryland Young
λLZ1357	λ*cI*$_{857}$*-mKO2 bor::Cm*^{R}	Crossed with phage λLZ1266 to make LZ1367, *Cm*^{R}	This work
λLZ1355	λ*cI*$_{857}$*-mKate2 bor::Cm*^{R}	Crossed with phage λLZ1369 to make LZ1373, *Cm*^{R}	This work

Table 2.2 Bacteriophage strains used in this work.

Phages compete via DNA ejection timing and replication

We next wanted to determine how domination is achieved experimentally, as our model suggests that it occurs from phage DNAs being indirectly blocked from replicating due to resource sequestration. It was reported that significant late gene expression from promoter P_R' requires phage DNA replication[157], and impairing phage DNA replication results in phages unable to lyse[158], as in the case of phage DNA replication-deficient mutant λP^-, so any means to inhibit a phage's DNA replication during co-infection could lead to domination. Another potential cause for domination may involve the biochemical kinetics of decision-making, where early commitment by a phage can result in rapid lytic development as to disallow another phage to catch up. Differences in phage DNA ejection timing may vary up to tens of minutes[137], and could facilitate this unsynchronized progression. Phage failure to infect also results in cases of apparent dominant lysis. Thus, to distinguish between infection failure and true domination and to explore the possible mechanisms for domination, we examined specific phage DNA in the cell.

Our strategy to differentially label phage DNA was based on our previous work[135]. SeqA specifically binds fully and hemi-methylated DNA, so *dam*$^-$ (methylation deficient) host strain expressing a SeqA-mKO2 fusion was used to specifically label the initial phage DNA (fully methylated) after infection and the first replicated copy of that phage genome (hemi-methylated), but not label unmethylated phage DNA and host DNA[159] (Fig. 2.13a). For this phage DNA reporter experiment, we used a mixture of unmethylated green phage and fully methylated blue phage to infect the reporter strain to

visualize the fully methylated phage's DNA when it enters the cell, as a SeqA-mKO2-bound fluorescent focus[135]. The unmethylated phage DNA is not seen but inferred based on the cell fate (Fig. 2.12a). In a typical lytic event, the phage DNA focus is visible in the first frame and divides before lytic reporter activity and lysis (Fig. 2.12b). We observed that dominating lysis can be due either to the failure of the labelled phage ejecting its DNA into the cytoplasm (Fig. 2.13b,c), or a successful infection (the appearance of a SeqA-mKO2 focus) lacking typical lytic development (Fig. 2.12c,d). The mixed infected population contains a large amount of pure lysis (78%, 69/88 cells), similar to the WT host infections (Fig. 2.2a). With this DNA reporter system, we are able to divide pure green lysis (56%) into two groups, one resulting from failed infection of the blue phage without SeqA-mKO2 foci (29%) and the other by domination of green phage since the blue phage DNA was successfully ejected with the visible SeqA-mKO2 focus (27%) (Fig. 2.12e).

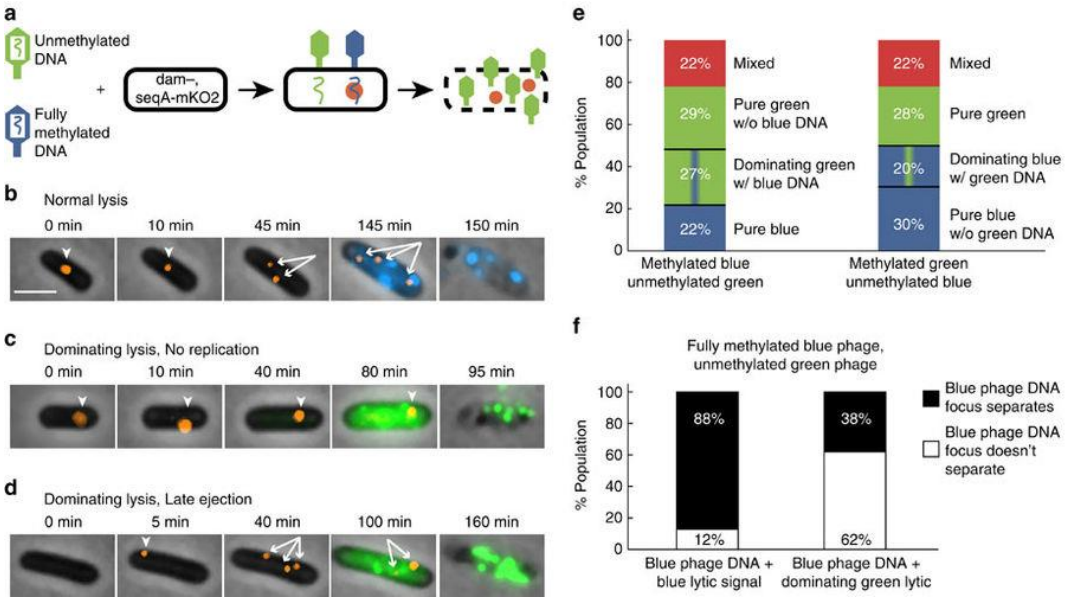

Figure 2.12 Dominating lysis results from phage competition during DNA ejection and replication.

(a) In dam$^-$ seqA-mKO2 cells, the fully methylated phage DNA is bound by SeqA-mKO2 forming a focus. This reporter can show when DNA replicates once, producing two hemi-methylated DNAs bound by SeqA-mKO2. Dominating lysis occurs when unmethylated phage shows pure lysis with intracellular fully methylated phage DNA. (b–d) Overlays showing different lysis types (blue/green phage is fully/unmethylated). Orange foci represent the first cellular DNA observed (arrowheads). After apparent DNA replication, multiple foci appear (branched arrows). (b) Normal lysis. Phage DNA seen at 0 min, two DNA foci at 45 min, then cell develops blue fluorescence and lyses. (c) Dominating lysis. DNA focus seen at 0 min, but the focus does not apparently split, and cell lyses with only green fluorescence. (d) Dominating lysis. DNA focus is absent at 0 min, appears at 5 min. DNA focus divides, but green accumulates, not blue. (e) Different lysis groups in dual-color infection of methylated blue/unmethylated green phages (left, N = 88) and of methylated green/unmethylated blue phages (right, N = 85). Left, when blue phage DNA is labelled, green lysis (56%) is divided into green lacking blue DNA (failed blue infection, 29%), and dominating green with blue DNA (27%). Right, when green phage DNA is labelled, blue lysis (50%) is divided into blue without green DNA (failed green infection, 28%), and dominating blue with green DNA (20%). (f) Lytic cells with a focus (blue phage DNA) in mixed-phage infections (the blue/green phage is fully/un-methylated) are divided: lysis with blue signal (left, N = 91) and dominating green (right, N = 24). Within each lytic group, the frequency of the DNA focus separating into multiple foci is plotted. As lysis requires DNA replication, the 12% non-separating group in the blue lytic group represents basal failure of reporting DNA replication (left). The 62% non-separating group in the dominating green lytic group (right) is higher than basal failure. Of the dominated DNA that does divide, 6/9 showed late ejection. Scale bar, 2 μm.

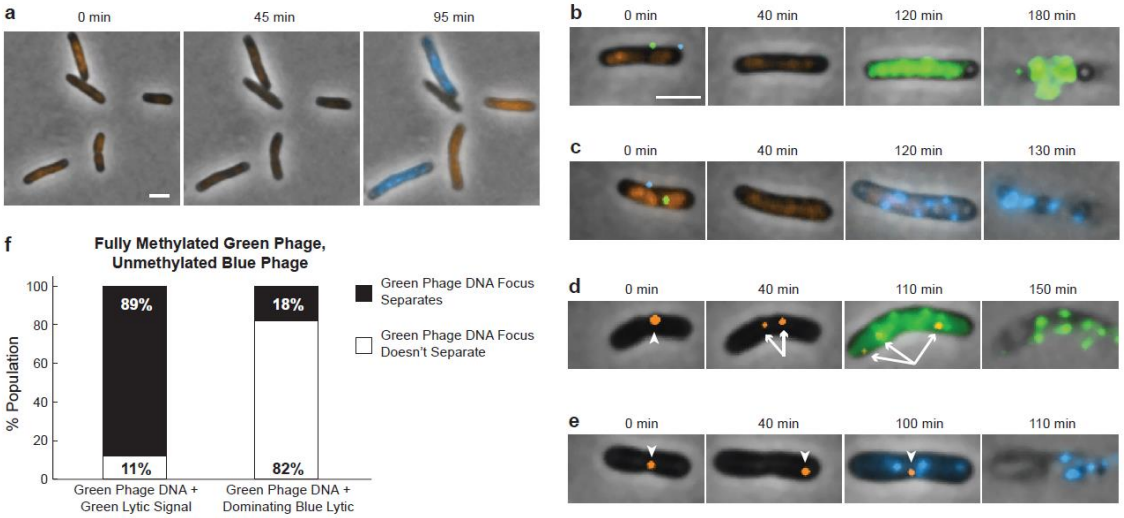

Figure 2.13 DNA reporter cells label green phage DNA and show how DNA is dominated.

(a) Images from infection movie with unmethylated blue phage infecting the reporter cells are shown. No orange foci are observed due to unmethylated phage DNA. At 95 min, the fates of the cells are shown to be lytic (blue cells) and lysogenic (orange cells). (b and c) Overlay fluorescence images of dominating lytic cells due to failed phage DNA ejection for the fully methylated blue (b) and fully methylated green (c) phages (no orange phage DNA foci over time). The cells were lysed by unmethylated green (b) and unmethylated blue (c) phage.

(d and e) The mixed-phage infection of fully methylated green/un-methylated blue phage is similar to that of the reversed methylation state shown in Fig. 5. Arrowheads point to the first appearance of phage DNA (orange dots) and before it divides, and branched arrows point to divided phage DNA. (d) An example of normal lysis: The phage DNA focus is seen at 0 min, and splits into 2 foci at 40 min, then the cell develops green fluorescence and lyses. (e) An example of dominating lysis: The DNA focus (green phage DNA) is present at 0 min, but the DNA focus does not apparently split over time, and the cell lyses with only blue fluorescence.

(f) The lytic cells which have a phage DNA focus (indicating green phage DNA) in mixed-phage infection movies (the green/blue phage is fully/un-methylated) are divided into groups: Lysis with green lytic signal (left, N = 73) and dominating blue lytic (right, N = 17). Within each lytic group, the frequency of the DNA focus separating into multiple foci is plotted, where the lack of separation is in white and observed separation is in black. As phage DNA replication is required for lysis, 11% of the non-separating group in the population with green lytic signal represents the basal level of failure of the reporter to show phage DNA replication (left). However, 82% (14 of 17 cells) of the non-separating group in dominating blue lytic (right) is much higher than the basal level indicating lack of phage DNA replication could be a reason for this phage (green here) being dominated by the blue phage. Of the remaining dominated DNA that does divide, 2/3 showed late ejection into the cell. Scale bars = 2 μm.

We next quantified phage DNA replication in the different lysis groups by tracking the DNA focus, noting whether or not it divides. We found that within the dominating lytic events, the labelled blue phage DNA often does not appear to replicate (Fig. 2.12c), or the DNA apparently appears late (Fig. 2.12d). Although replicated DNAs do not always separate using this reporter system, as lytic cells which must have replicated their DNA, occasionally show non-separating foci (12%, 11/91 lytic cells with blue lytic signal), the frequency of non-separating foci during domination (62%, 15/24 dominated lytic cells with non-separating foci) is much higher, indicative of non-replicated phage DNA (Fig. 2.12f). These findings were reciprocated in experiments with switched phage methylation states (Fig. 2.12e). The data suggest that earlier infection timing provides advantage for phages to compete during the subsequent exponential phage DNA replication, but does not conclude whether these factors are related, as predicted by our modelling.

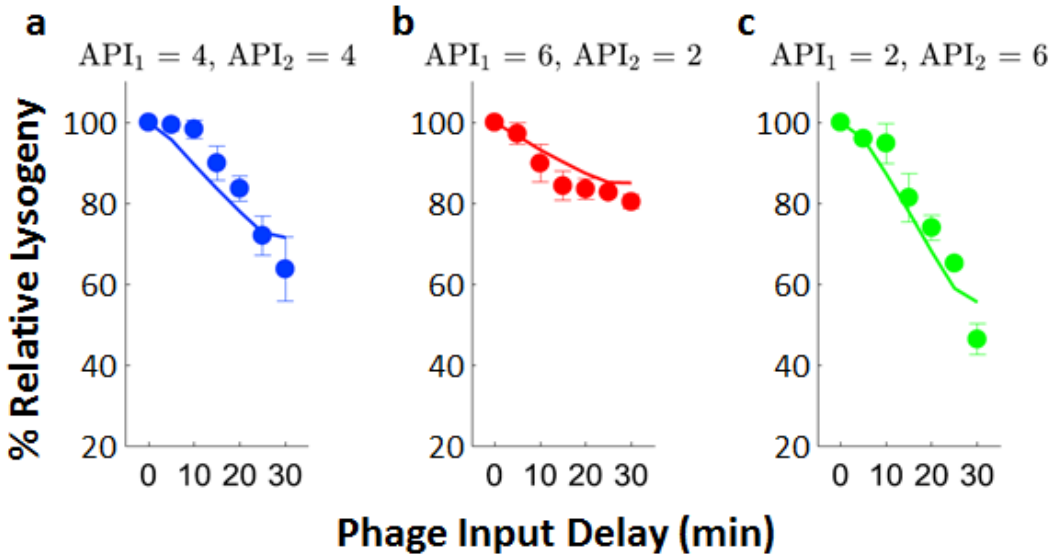

Figure 2.14 Delaying part of the phage infection reduce lysogenization. Infections were performed where a fraction of phages, from a total API, were mixed with phages initially, followed by the input of the remaining phages later (A, 0.5-0.5 split; B 0.75-0.25 split; C, 0.25-0.75 split). The resulting infections were then plated on antibiotic plates to determine lysogenization frequency from prophage-conferred resistance. The data are normalized to the lysogenization frequency of the infection without delay to show how the delays affect lysogenization. The line in each panel represents a computational model prediction of lysogenization frequency considering this time delayed decision-making process.

Time delayed infections reduce lysogeny

We further explored the effect of time on phage infections by characterizing how asynchronous infections affect lysogeny. We infected cells at API = 8 as a reference, using a defined volume and concentration of phages. To test delays, we introduced a fraction of the phages to the cells initially, and delayed the addition of remaining phages for later time points, and quantified the number of lysogens from these experiments (details in Methods). We found that the lysogenization frequency decreased as the delays increased (Fig. 2.14). When we withhold more phages initially, the change in lysogenization frequency is greater, and vice versa. We also constructed a computational model which was able to capture these behaviors well, which suggests that late infecting phages are able to input their gene expression into the overall decision-making circuit, but their effects are diminished as the infection progresses.

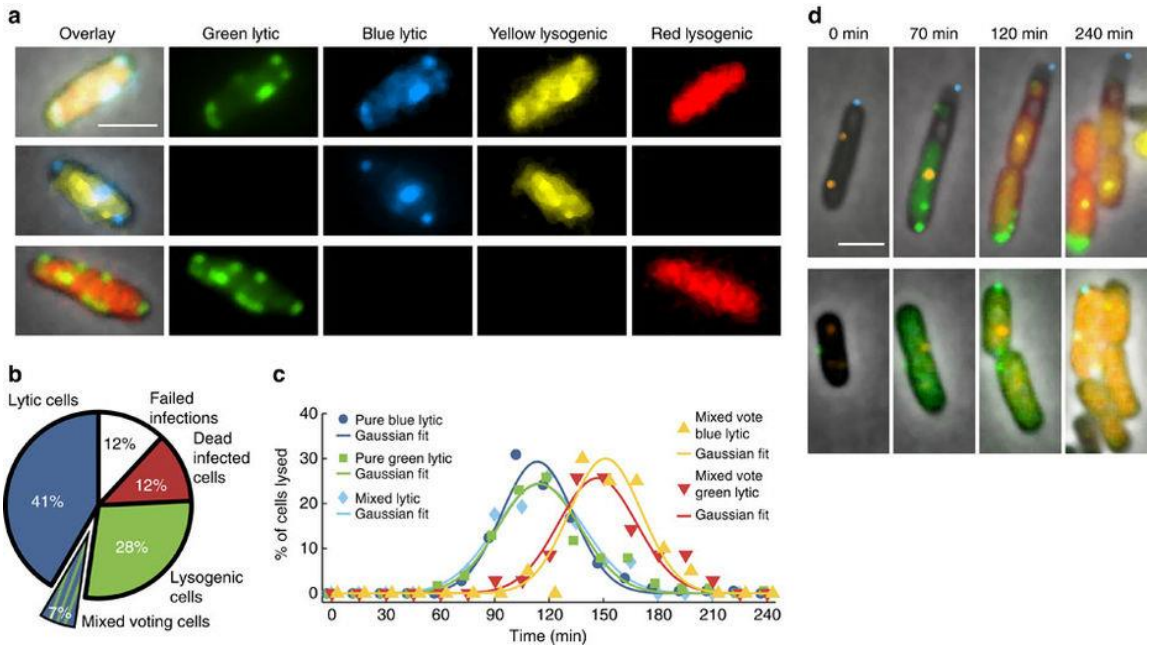

Figure 2.15 Mixed voting for fates occurs between phage DNAs in a cell and delays lytic development.

(a) Examples of three different mixed voting cells including overlay images and their component fluorescence channels. The top row shows a 'cross-phage mixed voting' cell with green and blue lytic signals and with red and yellow lysogenic signals. The middle and bottom rows show examples of 'same-phage type mixed voting', as both lytic and lysogenic reporters can be found on the same phage.

(b) A pie chart is shown comparing the different fates of all cells in this study (1,006 infected cells). Seven percent are mixed voting cells resulting in lysis.

(c) Lytic cells were divided into different groups: pure blue (N = 178) (circles), pure green (N = 179) (squares), mixed lytic (N = 57) (diamonds), mixed voting blue lytic (N = 35) (up triangles) and mixed voting green lytic (N = 20) (down triangles). The number of cells lysed since the previous time point, as a percentage of the total group, is plotted with time. Each group's distribution is well fitted to a Gaussian distribution (lines), with an average lysis time of 114 min (pure blue), 114 min (pure green), 115 min (mixed lytic), 147 min (mixed voting blue) and 151 min (mixed voting green).

(d) Example cells show lytic development yet lysogenic development and cell division using phage DNA reporter cells and fully/unmethylated phages. In the top and bottom rows the green and blue phages are methylated, respectively, with orange foci representing the ejected/replicated DNA. Green lytic signal builds up, but with time, the lysogenic reporter expression occurs (red or orange, the DNA reporter shares the same fluorescent protein as one lysogenic reporter) and the cell divides multiple times during the course of the movie, while the lytic signal ceases to accumulate. Scale bars, 2 μm.

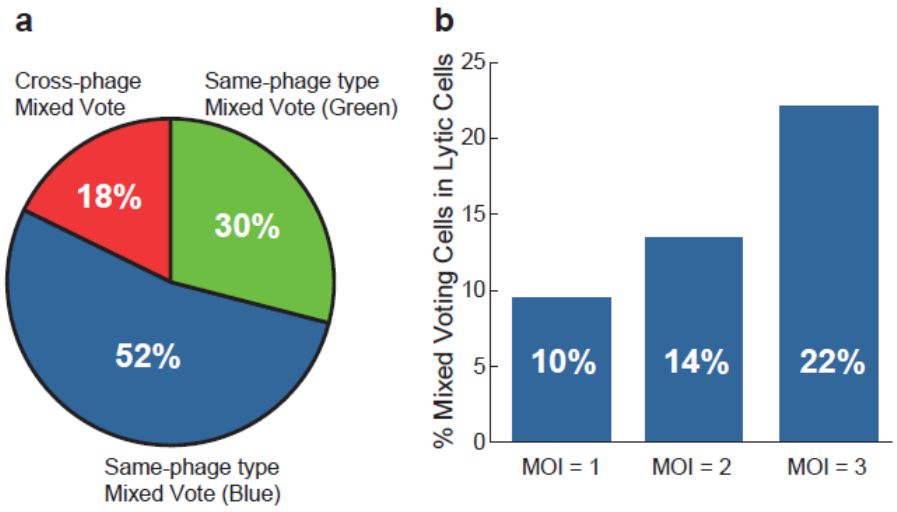

Figure 2.16 Mixed voting cells vary by type and increase with MOI.
(a) Mixed voting cells are grouped into different categories and their frequencies in the mixed voting population are shown (N = 67): cross-phage (lysing with both colors + at least 1 lysogenic color), same-phage type mixed vote blue (blue lytic + yellow lysogenic), and same-phage type mixed vote green (green lytic + red lysogenic).
(b) Mixed voting cells of any category are sorted by their MOI and their frequency is plotted as the percentage population of lytic cells at the given MOIs. The total lytic cells include cells infected with one dark infection. The frequency of mixed voting in lytic cells increases with MOI.

Confusion in mixed voting results in delayed lysis

The different phage interactions in a cell support a prediction from the voting model: mixed lytic and lysogenic phage voting within a cell[133]. We observed these events in our experiments (7%, 67/1,006 infected cells), which were classified in the lytic category (Fig. 2.15a,b). Mixed voting was designated when cells lysing with both phage colors also expressed one or both lysogenic reporters (Fig. 2.15a top row; Fig. 2.16a, denoted cross-phage mixed vote), or cells lysing with one phage color and showing the lysogenic reporter of the same phage (red in green lysis, or yellow in blue lysis) (Fig. 2.15a bottom two rows; Fig. 2.16a, denoted same-phage type mixed vote). Interestingly, same-phage type mixed voting can occur when the cell is apparently only infected by one phage (7/20 mixed vote green, and 12/35 mixed vote blue at MOI=1), suggesting that individual phage DNA, even replicated genomes, can interact with each other and independently commit to either lytic or lysogenic pathways in the same cell. In addition, mixed voting frequency increases with MOI (Fig. 2.16b), similar to lysogenization frequency increasing with MOI[52,133].

Mixed voting occurs regularly in lytic cells (14%, 67/481 lytic cells), so we asked how this interaction affects lytic progression to determine its purpose. Mixed voting cells exhibit lysogenic development, which is expected to inhibit lytic development compared with normal lytic cells, where we used fluorescence as a proxy for lytic development. The average lytic signal for pure lytic cells accumulates, followed by a decrease over time, due to the lysis of infected cells (Fig. 2.5c,d, green squares). Cells classified as mixed voting show lower average level of lytic expression through

100 min after infection, but afterwards show a higher maximum. For mixed voting cells, slower signal accumulation could be due to a lysogenic phage DNA population interfering with lysis, but being unable to repress the entirety of intracellular phage DNA. This would delay the production of lytic signal and cause mixed voting cells to lyse later than normal lytic cells. The average lysis times for each group were quantified from the distribution of lysed cells per time point, where we looked at the mixed voting populations (blue or green dominated), and the non-mixed voting populations (blue or green dominated, and mixed colour lysis) (Fig. 2.15c). The mixed voting cells take longer to complete lysis, suggesting that the confusion between decisions negatively impacts phage propagation. When the mixture of phages infected the WT host, we observed that lytic development inevitably led to lysis, but when the mixture of fully methylated and unmethylated phage infected the DNA reporter host, there were rare cases of mixed voting (<1%, 5/1,371 cells) where lytic development gave way to strong lysogenic expression followed by cell division instead (Fig. 2.15d), exemplifying a possible function of mixed voting.

Discussion

In this work, we developed a 4-colour fluorescence system to study phage decision-making at higher resolution by integrating different reporters into phage genomes, distinguishing between two different phages to determine individual lytic/lysogenic decisions within cells. This system can serve as a platform to explore phage behaviors and interactions under varied growth conditions, host backgrounds, phage mutants, and also using different phages, to characterize variables related to cellular decision-making. The combination of these fluorescent proteins may be used in other systems requiring labelling of multiple pathways, expanding the resolution of study for other models.

We found that phage interactions in the cell are either cooperative or competitive depending on the decision-making of the phages. During lysis, ~100 progeny are assembled and packaged regardless of MOI, due to the timing of cell lysis by holin activity[30], so dominating phages win a larger share of progeny. In lysis, the phage propagates itself rapidly, so competition is beneficial for phages with favorable genetics specifically in conditions promoting lysis. Our model predicts that phage DNA replication is a central point of contention for phage interactions, highlighting the importance of DNA replication in the infection, even though the process is often overlooked. Because phages can replicate their genomes in 2–3 min [25,160], asynchronous DNA ejection timing can account for variation between phages' DNA copy numbers and, therefore, gene expression at given times[161], providing a basis for competition. It is also known that a phage can be starved during an infection, rendering it dormant in a state

called pseudolysogeny[162], which appears similar to a dominated phage's behavior. As lysis requires extensive phage DNA replication, a phage could siphon essential host proteins for phage DNA replication, such as *E. coli* Pol III holoenzymes or DnaB hexamers, both estimated to be low in number[154,163], preventing other phage DNA from developing. Phage genomes were also suggested to inherit replication complexes during replication, thus sequestering replisomes from other DNA[155]. Additionally, the critical late gene regulator, *Q*, was reported to be preferentially *cis*-acting[31,32], which would facilitate competition. For lysogenic cells, cooperation is the typical outcome, reported at the level of transcription and phage integration. This may be attributed to the lower phage DNA copy number requirement for lysogeny, as λP^-, deficient in phage DNA replication, can lysogenize[52]. DNA replication, and thus competition, does normally occur in lysogeny, but lysogenic establishment halts DNA replication, so there is balance in DNA numbers. Our data suggests multiple prophages propagate frequently in lysogens, which would enhance genetic variance, allowing mutants arising from DNA replication as well as co-infecting lysogenization defective mutants to persist in the lysogenic state. The phage interactions and specific gene functions may have evolved to strategically sustain the viral population: when conditions are ripe for propagation, competition ensues, driving the selection of genes favorable for fast reproduction within that environment.

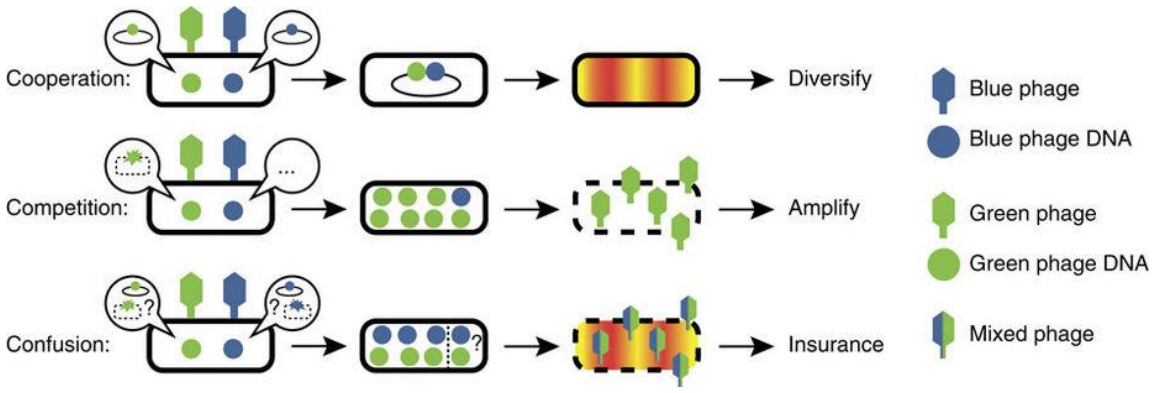

Figure 2.17 Strategic DNA level phage interactions during development increase evolutionary fitness.
Individual phage DNAs make decisions to develop via lytic or lysogenic pathways, and interact with each other based on the decisions. During lysogeny, DNA replication is limited and favors mixed integrations of phage genomes. This cooperation may help diversify lysogens with different phage DNA to produce varied phages when induced later. Varied phages can be beneficial if the cells move to unknown environments. During lysis, extensive DNA replication results in resource competition, which typically favors a single phage type. Competition during lysis allows good genetics to propagate. If conditions favor lysis, dominating phages can spread quicker and more thoroughly. Different phage DNAs may choose different fates, which delays lytic progress. Confusion during development is non-optimal for propagating quickly, but if the delay allows survival in some rare situations, the tradeoff may increase the overall fitness of the phage.

However, when conditions favor lysogenization, typically in poor, host-limited conditions, phages cooperate to integrate their genes as lysogens, and replicate in the absence of selection. The lack of direct selection on phages enables their diversification by genetic drift[164], perhaps aiding subsequent adaptation to new environments (Fig. 2.17). Nevertheless, while selection on phages is absent during lysogenic propagation, selection exists at the host level: dormant lysogens with maladaptive mutations for the host will probably disappear from the population.

Phage voting is independent at the phage DNA level, as studies have observed infected cells concurrently displaying lysogenic and lytic reporter activities, where lysis overcomes lysogeny[133,134]. Our data suggest that during mixed voting, a subpopulation of phage DNA commits to lysogeny, but another subpopulation is unrepressed and commits to lysis. Our work is in agreement with previous work suggesting that steps in lytic development can kill or lyse the cell, overriding lysogeny, such as excessive phage DNA replication[165], or expression of Q-mediated lytic products[166]. That this mixed voting occurs even in MOI=1 infections is evidence that each replicated phage DNA is making decisions and interactions to replicate and sustain itself. By tracking single phage DNAs, we have found that labelled DNAs occasionally move as if they are 'trapped' in the cytoplasm, suggesting that phage genomes may occupy distinct intracellular locations, with potentially different microenvironments favoring different decisions[135]. We observed in *dam*$^{-}$ cells, deficient in DNA repair and thereby prone to mutation[167], using mixed fully methylated and unmethylated phages, that lytic development could be overcome by lysogenic activity, and develop similarly to normal lysogens (Fig. 2.15d),

raising the possibility that mixed voting is a fail-safe against certain host/phage mutations, where lysogeny would be somehow preferable to lysis. The phage DNAs can develop in both pathways, and sometimes commit to different decisions, where specific intracellular conditions determine the final outcome (Fig. 2.17). This scenario has an unknown cause, possibly due to disparate, transient local environments, and may have evolved as an insurance strategy to save some phages from niche situations, with a delayed lysis tradeoff.

The results of this study illustrate how we may discover new details and revisit an established system from a new perspective by expanding the resolution of study. The phage interactions, and the physiologically relevant factors potentially responsible for them, like phage DNA replication and asynchronous infection timing, are crucial aspects to account for when modelling the system. Yet, these factors were not typically considered in previous models. Our approach was to incorporate these new effects into simple models instead of adding them to existing detailed models and increasing their complexity further. The insights we gained demonstrate how improved modelling of natural systems is not always synonymous with increasing the complexity of models. Obtaining new fundamental parameters and including them into simple models can actually facilitate the generation of new insights compared with their incorporation into complex models. Moreover, these simple models of decision-making can also relate the individual phage's behavior to its evolutionary strategy. Technology allows us to push our limits when studying systems to observe the previously unobservable, allowing biological models to be further revisited, improved and understood.

The subject of interactions is of particular interest. Bacteriophage lambda undertakes one of two developmental paths after infecting its host, and although this decision is one of nature's simplest and best characterized, little is known about the specific intracellular events that transpire as cell fates are chosen. To peer into the phage's world, we use fluorescence microscopy to achieve single-virus/viral DNA resolution, distinguishing between two functionally identical phages to track their decision-making. Having previously posited that phages have the agency to 'vote' for cell fates[133], we resolve the viruses as intracellular individuals, finding that at the DNA level, phages compete and cooperate, and that these interactions are tied to different cell fates, lysis and lysogeny, respectively. We used a joint experimental/computational approach to explore the mechanisms behind these behaviors, concluding that earlier infection timing and resource sequestration are means for specific phages to dominate during lytic development. Conversely, lysogenic cells show little sensitivity to these variables and frequently result in mutual phage propagation. Curiously, some infected cells apparently choose both lysis and lysogeny concurrently, even in cells infected by a single phage, implying that as the phage replicates, each DNA becomes a separate individual with the capability to make separate decisions. The varied behaviors occur in a manner that appears to be strategic, as each action may serve a specific role in keeping the viruses fit.

Viruses exist primarily to replicate their genetic material; thus, phages need strategies to efficiently accomplish this function and, ideally, perform better than others within its environment. The lytic pathway is how phage lambda efficiently proliferates in

large numbers, so the phage benefits from dominating this process. The 'living' part of phage lambda, its DNA, is programmed to attempt this domination, being able to commandeer replication complexes from the host, different phages and other lambda phages. This competition encourages the 'self ' to persevere, by ensuring that an advantaged phage begets more of itself on average, maintaining its advantage over time. From the evolutionary perspective, certain genes are readily selected for conditions where lysis is favored, as when host cells are plentiful and healthy. However, for lambda, there is also the option of lysogeny. This alternate mode of reproduction is preferred when hosts are scarce, and, accordingly, is the time for the phages to cooperate. The intracellular phage DNAs produce *trans*-acting repressors during lysogenic establishment to halt the competition occurring during lytic development throughout the cell, which maintains relative parity in DNA numbers between phages. The end result of lysogeny is genomic integration of phage DNA, which commonly involves multiple phage genomes being incorporated into the same cell [8]. This is remarkable as it allows lysogenization-deficient phage mutants, like λ*cII-*, to persist as prophages, provided that those mutants co-infect with non-deficient versions of the phage. Part of the mutant population sacrifices its lytic progeny, or short-term gain, for the privilege of bet hedging against a greater scope of conditions, because the lysogenic bacteria can move to richer environments[168]. In the new, improved environment, the lysogens can be induced to undergo a vegetative cycle and lyse, releasing progeny that has the potential for exponential replication. Cooperation benefits all interacting phages when viewed at the population level, as these phage types propagate in lysogens more frequently following

their interactions. So this paradigm phage system contains a set of interactions that simultaneously expedites selection for favorable genes via competition and stimulates genetic diversity via cooperation, to strategically maintain fitness over space and time, carried out by individual strands of viral DNA encompassed inside tiny bacterial worlds.

Regarding the optimization of fitness across spatial–temporal distances, researchers have recently discovered that phages utilize small-molecule communication. The temperate *Bacillus subtilis* phage, phi3T, takes advantage of the hosts' quorum sensing pathway to release a phage-signaling peptide, which, once imported into new host cells, will promote phi3T lysogeny in subsequent infections in a concentration-dependent manner[127]. This behavior is extraordinary as it opens up the possible existence of many forms of viral small-molecule communication to achieve various ends. Another case of phage communication regarding the outside environment is found in the lytic paradigm phage, T4. New T4 phages that lyse early can proceed to superinfect cells currently undergoing development and interact with the phages inside those cells to delay lysis[169]. This relays information about the excess of phages relative to hosts and enables production of many more progeny per infection, which is a strategy to deal with host shortages by extracting more from existing infections. General recombination represents another means of cooperation common to phages, producing variegated recombinants ambivalently suited to their current environment. These examples highlight how cooperation influences propagation over a timeframe beyond a single lytic cycle, where the phages prepare for unknown conditions. There are also many forms of phage competition characterized[129]. Phages can prevent superinfection of their kind by

blocking their own receptor, such as in phage T5, or inhibiting the translocation of superinfecting phage DNA into the cytoplasm, as proposed in phage P1. Phages also interfere with the replication of other phages, as phage lambda does when activating its RexAB functions to abort phage T4 infections or requisitioning host DnaB from phage phiX174, and when phage P4 commands near-exclusive production of phage progeny from their exploitation of phage P2 lysogens[170]. These examples demonstrate how phages' competitive actions influence their immediate infections, in a departure from the more forward effects of cooperation, but both strategies aim to optimize evolutionary fitness for phages from different aspects.

From this sampling of phage interactions, we hope to show that there is much hidden complexity involved in the propagation of viruses. Not life, but inseparably intertwined with life, viruses too must evolve rapidly, and are equipped with the proper tools through rapid mutagenesis and, importantly, the relevant mechanisms to allow a dominant genotype to prevail in its niche, while also preserving genetic diversity for the unknown of new environments and future times. Phages are the most abundant biological systems on Earth, estimated around 10^{31} in number, and the cooperation and competition between phages will ensure that they readily adapt to changes in their hosts, sustaining the viral population[171]. Future research involving well-characterized DNA phages will focus on revealing more about the mechanisms of cellular fate selection and discovering new forms of communication and interaction between viruses. The largely unexplored field of RNA phages also holds exciting research potential, because a few specimens have been isolated and studied, and must also have their own unique

interactions[172,173]. For instance, one well-studied *Pseudomonas phaseolicola* RNA phage, phi6, was found to have competitive or cooperative interactions to conform to or escape the prisoner's dilemma[76,77]. RNA phages may also have closer ties to some eukaryotic viruses, so their studies could prove valuable to treating certain viral conditions, for example, different hepatitis viruses interact, thereby exacerbating infection severity[174]. The viruses inhabiting and interacting in their world mirror us in ours, so cultivating these models to better understand their behaviors will help generate insights into the cellular decision-making, disease and evolutionary aspects of life sciences.

Plasmids		
pBR322-*D-mTurquoise2-E*	Crossed with phage λLZ1254 to produce phage λLZ1266, Amp^R	This work
pBR322-*D-mNeongreen-E*	Crossed with phage λLZ1254 to produce phage λLZ1369, Amp^R	This work
pBR322-cI_{857}-*mKO2-partRexB*	Crossed with phage λcI to produce phage λLZ1357, Amp^R	This work
pBR322-cI_{857}-*mKate2-partRexB*	Crossed with phage λcI to produce phage λLZ1355, Amp^R	This work
pBR322-PLate**D*	Expresses wild type gpD for phage stability, Amp^R	This work
pACYC177-PLate**D*	Expresses wild type gpD for phage stability, lower expression than pBR322-PLate*D , Amp^R	This work
pZA3-*R-Cam-cos*	Plasmid for recombination, $bor::Cm^R$	Ryland Young
pER157	Plasmid for recombination, $bor::Kan^R$	Ryland Young
pKD46	Arabinose-induced λ red recombination, Amp^R	Ryland Young

Table 2.3 Plasmids used in this work.

Strain #	Bacterial Strains	Comments	Source
-	MG1655	Wild type *E. coli*	Lab stock
-	LE392	sup^E and sup^F host	Lab stock
LZ1007	MG1655[pBR322-PLate**D*]	Host expressing gpD for titering all λ*D-mNeongreen* phages, Amp^R	This work
LZ1386	MG1655 *seqA-mKO2 Δdam::*Kan^R Cm^R	For methylated phage DNA labeling, Kan^R Cm^R	This work
LZ1387	MG1655 *seqA-mKate2 Δdam::*Kan^R Cm^R	Same as LZ1386, seqA fusion variant, Kan^R Cm^R	This work
LZ1367	MG1655 (λ*D-mTurquoise2* cI_{857}*-mKO2 bor::*Cm^R)[pACYC177-PLate**D*]	Lysogen, induced to produce phage λLZ1367, Cm^R Amp^R	This work
LZ1373	MG1655 (λ*D-mNeongreen* cI_{857}*-mKate2 bor::*Cm^R)[pACYC177-PLate**D*]	Lysogen, induced to produce phage λLZ1373, Cm^R Amp^R	This work
LZ1379	MG1655 (λ*D-mTurquoise2* cI_{857}*-mKO2 bor::*Cm^R)[pACYC177-PLate**D*][pGG503]	Lysogen, induced to produce phage λLZ1379, Cm^R Amp^R Tet^R	This work
LZ1378	MG1655 (λ*D-mNeongreen* cI_{857}*-mKate2 bor::*Cm^R)[pACYC177-PLate**D*][pGG503]	Lysogen, induced to produce phage λLZ1378, Cm^R Amp^R Tet^R	This work
LZ1381	MG1655 dam^- (λ*D-mTurquoise2* cI_{857}*-mKO2 bor::*Cm^R)[pACYC177-PLate**D*]	Lysogen, induced to produce phage λLZ1381, Cm^R Amp^R	This work
LZ1380	MG1655 dam^- (λ*D-mNeongreen* cI_{857}*-mKate2 bor::*Cm^R)[pACYC177-PLate**D*]	Lysogen, induced to produce phage λLZ1380, Cm^R Amp^R	This work
-	LE392[pZA3-*R-Cam-cos*]	Used to make phages with *bor::*Cm^R via recombination, Cm^R Kan^R	Ryland Young
-	LE392[pER157]	Used to make phages with *bor::*Kan^R via recombination, Kan^R Amp^R	Ryland Young

Table 2.4 Bacterial strains used in this work.

Methods

Strains and plasmids

The host strain for normal phage movies is MG1655. The host for phage DNA tracking movies, MG1655 *seqA-mKO2/mKate2* Cm^R Δ*dam::*Kan^R strain was produced by recombineering the fluorescent fusion protein with the chloramphenicol resistance cassette fused to the native *seqA* gene using the λ red system[175] into MG1655, and then the same system was used on the resulting cell to replace the *dam* gene with the kanamycin resistance cassette. For antibiotic selection, 10 μg ml^{-1} of *Cm*, 50 μg ml^{-1} of *Kan*, 100 μg ml^{-1} of *Amp* and 10 μg ml^{-1} of *Tet* were used as appropriate.

New reporter phages are λ*D-mTurquoise2* cI_{857}*-mKO2* *bor::*Cm^R and λ*D-mNeongreen* cI_{857}*-mKate2* *bor::*Cm^R (blue and green phages, respectively). With the exception of the λcI^- phage, all of the phages and their lysogens have the cI_{857} allele[176], which does not undergo auto-cleavage by the host SOS system[177] and is temperature sensitive (lysogeny is non-permissive at 37 °C).

All phages with *bor::*Kan^R were produced through recombination by titering onto cells with plasmid pER157 (gift of Ryland Young) , and phages with *bor::*Cm^R were produced through recombination by titering onto cells with plasmid pZA3-*R-Cam-cos*[178].

All bacterial strains used are listed in Table 2.4, plasmids in Table 2.3 and phages in Table 2.2.

Phage strain construction

The fluorescent proteins in the recombination plasmids, pBR322-*D-mTurquoise2/mNeongreen-E* and pBR322-cI_{857}*-mKO2/mKate2-partRexB,* were cloned

from plasmids with each individual gene: *mTurquoise2* (received from Stanislav Vitha as a gift from Theodorus W. J. Gadella), *mNeongreen* (from Allele Biotechnology), *mKO2* (received as a gift from Michael Davidson (Addgene plasmid # 54625)) and *mKate2*(received as a gift from Anna Planas and Tomas Santalucia (Addgene plasmid # 48345)). WT lambda phages were recombineered into the green and blue reporter phages via infecting host cells bearing the recombination plasmids.

First, *λD-mTurquoise2/mNeongreen* cI_{857} *bor::KanR* phages were produced by infecting *λDam* cI_{857} *bor::Kan*^{R} phages on LE392 (permissive host) bearing plasmids pBR322-*λD-mTurquoise2/mNeongreen-E* for recombination. The resulting lysate contained the phage of interest, and was titered on a non-permissive MG1655 to select for recombinants, and the resulting plaques were screened with a fluorescence dissecting microscope to pick fluorescent plaques, yielding *λD-mTurquoise2/mNeongreen* cI_{857} *bor::Kan*^{R} phages which were amplified and lysogenized into MG1655. Separately, *λ*cI_{857}*-mKO2/mKate2 bor::Cm*^{R} phages were produced by infecting *λcI⁻* phages onto MG1655 bearing plasmids with *λ*cI_{857}*-mKO2/mKate2* for recombination at 42 ^oC to ensure that the temperature-sensitive CI_{857} from the plasmid was inactivated. The resulting lysate contained the phage of interest and was titered on MG1655 at 30 ^oC, a temperature permissive for lysogenization, and recombinant phages were screened by picking turbid plaques, yielding *λ*cI_{857}*-mKO2/mKate2* phages. The phages were then crossed with plasmid pZA3-*R-Cam-cos* (gift of Ryland Young) to replace *bor* with the antibiotic resistance cassette through recombination, yielding *λ*cI_{857}*-mKO2/mKate2 bor::Cm*^{R} phages. Then co-infection of pairs of phages, *λD-mTurquoise2* cI_{857}

bor::Kan^R/*λcI*$_{857}$*-mKO2 bor::Cm*^{R} and *λD-mNeongreen cI*$_{857}$ *bor::Kan*^{R}/*λcI*$_{857}$*-mKate2 bor::Cm*^{R}, was done for recombination to generate the final strains for the experiments, *λD-mTurquoise2 cI*$_{857}$*-mKO2 bor::Cm*^{R} and *λD-mNeongreen cI*$_{857}$*-mKate2 bor::Cm*^{R}. Screening was done by titering the lysate from the crossing infection at 30 ^{o}C to produce turbid plaques, and then small turbid plaques, which are likely fluorescent phages, were selected for Cm resistance, indicating a cross had occurred. The strains were confirmed through PCR and microscopy to be single integration lysogens with the correct fluorescence combinations. The lysogens were transformed with the plasmid pACYC177-PLate**D* to produce mosaic WT and fluorescent gpD progeny phages upon induction. Phages with *λD-mNeongreen* were titered on MG1655[pBR322-PLate**D*] to generate stable phages to make plaques. The phage lysogens were then transformed with the pACYC177-PLate**D* plasmid in order to generate stable fluorescent phages. The unmethylated version of these phages were produced by infecting *dam*$^-$ cells with these phages and then transforming those verified single integration lysogens with the pACYC177-PLate**D* plasmid (generating LZ1380 and LZ1381). The fully methylated version of these phages was produced by transforming pGG503 plasmid[179] into the lysogens already bearing pACYC177-PLate**D* plasmid (transformed LZ1367 and LZ1373 to generate LZ1379 and LZ1378 respectively), followed by heat induction of the lysogens.

Phage purification by ultracentrifugation

The purification steps were as described[180]. Briefly, a single colony of the lysogens of the desired phages was first grown in 5 ml of LB+10 mM $MgSO_4$ (LBM)

with appropriate antibiotics at 30 ^{o}C overnight. The overnight culture was then diluted 1:100 into 500 ml of fresh LBM with appropriate antibiotics and grown at 30 ^{o}C until OD_{600} ~ 0.4, then moved to 42 ^{o}C for 20 min, then moved to 37 ^{o}C until lysis occurred. 2% volume of chloroform was then added, and left to shake gently on an orbital shaker at room temperature for 15 min, then the lysate excluding the chloroform was centrifuged at 10,000 x g for 20 min, the resulting supernatant was then centrifuged again under the same conditions. The new supernatant was then treated with DNase I (Sigma) and RNase A (Sigma) with a concentration of 1 μg/ml each at room temperature for 1 hour, and then NaCl was added to reach a concentration of 1 M, and incubated on ice for ~3 hours. The mixture was then centrifuged as before and PEG8000 (Fisher Scientific) was added to reach 10% w/v, and the mixture was left at 4 ^{o}C with gentle shaking overnight, ~16 hours. The next day, the mixture was centrifuged at 3000 x g and the supernatant was discarded. The pellet was soaked in a total of 8 ml of cold SM buffer and incubated at 4 ^{o}C overnight, ~16 hours. The resuspended pellet was removed and the centrifugation bottles were rinsed with 1-2 ml of SM buffer and combined, then the SM suspension was mixed gently with an equal volume of chloroform and centrifuged at ~3700 x g for 15 min at 4 ^{o}C. The supernatant was removed to exclude the PEG pellet, and the process starting from the chloroform mixing was done 2 more times, to finally yield a clear supernatant containing the phage. A step gradient was made for each desired phage using 1.5 ml each of 1.3, 1.5, and 1.7 g/ml CsCl (Sigma) + SM buffer solutions, and the phage (~ 8 ml) was layered on top in a 13.2 ml ultra-clear tube (Beckman Coulter), then ultracentrifuged in a Beckman SW 41Ti rotor at 24,000 rpm for

6-8 hours at 4 ^{o}C . The phage migrates to a band and is then extracted using a 3 ml syringe (Becton Dickinson) and 20 gauge needle (Becton Dickinson) from the side wall of the tube. This phage extraction was then loaded a 5 ml ultraclear tube (Beckman Coulter) and then filled by a 1.5 g/ml CsCl+SM buffer and ultracentrifuged in a Beckman SW50 rotor at 35,000 rpm for 24 hours at 4 ^{o}C, and then was extracted in the same manner. This new phage extraction was then loaded into a dialysis cassette and dialyzed 1:1000 against SM buffer in three steps for a total of ~24 hours. This phage solution was then extracted and stored away from light and at 4 ^{o}C to be used in the experiments. DAPI (Sigma) staining was done to verify that the phages have DNA.

Single-cell infection assay

Both phages (λLZ1367 and λLZ1373) were purified then diluted to the same titer and mixed together at a 1:1 ratio to generate the phage mixture for infection. Infection was done as previously described[133], using M9 minimal medium as the growth medium in order to have optimal fluorescence signals. The phages used for infection were gpD-mosaic with a mixture of WT gpD and gpD fluorescent fusions, to avoid capsid instability due to assembly of too many copies of the gpD fluorescent fusion proteins.

Briefly, a 1 ml overnight culture of host MG1655, grown at 37 °C (265 r.p.m. shaking) in M9 + 0.4% maltose (M9M), was diluted 1:100 into M9M (50 μl of overnight culture into 5 ml of M9M), and grown at 37 °C (265 r.p.m. shaking) until OD_{600} ~ 0.4. Once grown, 1 ml of the culture was centrifuged (4 °C, 2,000*g*, 4 min), supernatant was discarded, and cells were resuspended in 150 μl of cold M9M. Twenty microliters of the phage mixture was then mixed with 20 μl of the resuspended MG1655 culture to infect.

The infection mixture was left on ice for 30 min, then 80 μl of cold M9M was added to dilute the infection mixture (pipette tips cut for wider opening), and gently mixed by tapping, then moved to a 35 °C water bath for 5 min, then 1 μl of the mixture was placed (pipette tips cut for wider opening) onto a 1.5% agarose pad of M9M (prepared by microwaving 0.09 g of agarose (Fisher Scientific) with 6 ml of M9 media, then adding 120 μl of 20% maltose to the molten agarose) resting on a small No.1 coverslip (18 × 18 mm, Fisher Scientific) until visibly dry (~1 min), then covered by a large No. 1 coverslip (24 × 50 mm, Fisher Scientific), and then moved to the microscope for time-lapse imaging, where the time=0 is set to the first time-lapse image taken, which typically will be ~15–20 min after cells are initially placed in the 35 °C water bath.

For the phage DNA reporter movies the same conditions were used but with the reporter host strain (MG1655 *seqA-mKO2 Δdam::Kan*^{R}) infected with a 1:1 mixture of mixed methylation blue/green phages (λLZ1379+λLZ1380 or λLZ1378+λLZ1381). Similarly, for pure infection movies, a single purified phage is used instead of a mixture.

Microscopy imaging

Imaging was performed on a Nikon Eclipse Ti inverted epifluorescence microscope using a 100 × objective (Plan Fluo, NA 1.40, oil immersion) with a 2.5 × TV relay lens, using a mercury lamp as the light source (X-Cite 200DC, Excelitas Technologies), within a cage incubator (InVivo Scientific) at 30 °C, and acquired using a cooled EMCCD (electron multiplying charge-coupled device) camera (iXon3 897, Andor, Belfast, United Kingdom). For a typical movie, 8 or 16 stages were selected where cells were well separated but plentiful. The software images each stage through

each filter sequentially for each time point before moving to the next stage. The cells were imaged under the phase-contrast and four fluorescent filter cubes. The fluorescent filters used in the study were as follows (Xnm;Yex [bandwidth] excitation filter/dichroic beamsplitter wavelength/Xnm;Yem [bandwidth] emission filter-company, product #): blue (436 nm;20ex /455 nm/ 480 nm;40em-Nikon, 96,361), green (490 nm;20ex /505 nm/ 525 nm;30em-Chroma, custom 49,308), yellow (539 nm;21ex /556 nm/ 576 nm; 31em-Chroma, 49,309) and red (592 nm;21ex /610 nm/ 630 nm;30em-Chroma, 49,310). The first frame of the movie imaged cells with z-stacks of ±1.2 μm, 0.3 μm each step, under the blue and green filters, to visualize infecting phages surrounding the cells. For this first frame, the images are acquired in this order (with exposures): phase-contrast (100 ms), red (200 ms), yellow (100 ms), blue (200 ms) and green (200 ms), and the phase-contrast, red and yellow channels are only taken at the focal plane. The time-lapse movies were then taken every 5 min without z-stacks for ~4 h after all cell decisions were resolved. For the time-lapse portion, the images are acquired in this order (with exposures): phase-contrast (100 ms), red (1 s), yellow (100 ms), blue (40 ms) and green (40 ms).

For the DNA reporter movies, z-stacks (focal plane and +0.4 μm) are taken in the DNA reporter channel throughout the whole movie to track the DNA focus. The first frame of the movie imaged cells with nine z-stacks of ±1.2 μm, 0.3 μm each, under the blue and green filters, to visualize infecting phages surrounding the cells. For the first frame, the images are acquired in this order (with exposures): phase-contrast (100 ms), red (200 s), yellow (200 ms), blue (200 ms) and green (200 ms). For time-lapse portion,

the images are acquired in this order (with exposures): phase-contrast (100 ms), red (1 s), yellow (200 ms), blue (40 ms) and green (40 ms).

When presenting microscopy images in our figures and movies, uniform contrast settings are applied for each separate channel throughout the entire figure subpanel or movie.

Analysis of time-lapse movies

Movie images were analyzed using the cell recognition program Schnitzcell (gift of Michael Elowitz, California Institute of Technology) and homemade script in Matlab. Cell lineages were determined from the phase-contrast images. The fluorescent signal was normalized to the background, corrected by the crosstalk and then scaled for further analysis.

Frequencies of failed, dark and dead infection

For failed infection frequencies, those cells observed to be infected with a single blue/green phage were selected from the mixed-phage infection movies (MOI = 1 infections). If a cell showed no fluorescence development and grew and divided over the movie, it was marked as a failed infection. The failed infection frequency is the number of failed infections over the total number of MOI = 1 infections for the respective phage.

For dark infection frequencies, those cells with no phage attached in the first frame were selected from the mixed-phage infection movies (MOI = 0 infections). If a cell showed a pure fate (pure blue/green lysis or pure red/yellow lysogenic) or same-phage mixed voting (blue with yellow or green with red development), it was marked as

a dark infection. The dark infection frequency is the number of dark infections over the total number of MOI = 1 infections plus the number of dark infections.

For dead cell infection frequencies, those cells observed to be infected with a single blue/green phage were selected from the mixed-phage infection movies (MOI = 1 infections). If a cell did not grow and divide over the movie (regardless of lysogenic fluorescence), lysed without lytic fluorescence, or filamented without any fluorescence, it was marked as a dead cell infection. The dead cell infection frequency is the number of dead cell infections over the total number of MOI = 1 infections for the respective phage.

Bulk lysogenization assay

The reporter phages, λ*D-mTurquoise2 cI*$_{857}$*-mKO2 bor::Cm*^{R} (blue phage) and λ*D-mNeongreen cI*$_{857}$*-mKate2 bor::Cm*^{R} (green phage), and WT phage, λ*cI*$_{857}$ *bor::Cm*^{R} (λWT-*Cm*), were diluted using SM buffer to an approximate API of ~10 based on previously known titers. Two-fold dilutions done in duplicate were then made to reach a final concentration of 2^{-6} and the seven samples for each phage were kept on ice until infection. Host *E. coli* MG1655 from an overnight culture was diluted 1:1,000 into LB + 0.2% maltose + 10 mM $MgSO_4$ (LBMM) (10 µl of overnight into 10 ml LBMM) and grown at 37 °C, 265 r.p.m. until an OD_{600} of ~0.4, where it was then concentrated through centrifugation (4 °C, 10 min, 2,000*g*), then resuspended in fresh LB + 10 mM $MgSO_4$ (LBM) using one-tenth of the original volume (cells concentrated 10 ×). Twenty microliters of the cell suspension and 20 µl of each phage dilution were mixed to make an infection mixture, and the infection mixtures were kept on ice for

30 min. The infection mixtures were then transferred to a 35 °C water bath for 5 min, and then 10 µl of each infection mixture was diluted separately into 1 ml of pre-warmed LB + 0.2% glucose +10 mM $MgSO_4$ (LBGM) in a 30 °C, 265 r.p.m. water shaker for 45 min. The new infection mixture was then transferred to ice and diluted with cold PBS (Lonza) appropriately to allow ~100–500 colonies to grow, and then 100 µl of each dilution was spread onto LB+*Cm* plates and incubated overnight at 30 °C to select for lysogens. Lysogen counts were determined by counting the number of Cm^R colonies. Pre-infection phage and bacteria concentrations were measured using standard plate assays, titer using LE392 as the indicator strain for phage and plating on LB for bacteria. The lysogenization probability was plotted as a function of API on a log-log scale (Fig. 2.2a). It was found that the reporter phages exhibit the same API-dependent lysogenization response as wild type.

Different types of phage integrations were determined using the same protocol as above with different phage solutions. A 1:1 mixture of WT phages bearing a Kan^R marker and WT phages bearing a Cm^R marker (λWT-*Kan* + λWT-*Cm*) was diluted with SM buffer to API ~10, then duplicate twofold serial dilutions using SM were done to reach API ~1. In the final plating step, for each lysogen culture, 100 µl was plated on LB+*Kan*, LB+*Cm* and LB+*Kan*+*Cm* plates, and the plates were incubated at 30 °C overnight to form lysogen colonies. After lysogenic growth, colonies were counted to determine pure and mixed integrations. This assay to determine integrations was done in both LB and M9 media, where the M9 experiment differs from the LB

method by using M9M in place of LBMM, and M9 + 0.4% glucose (M9G) in the place of LBM and LBGM when using liquid media. Plating is done on LB agar plates.

Mixed integrations are defined as lysogens that grew on the LB+*Kan*+*Cm* plates:

$$MixedIntegrations = Lysogens_{Kan+Cm}$$

Pure Kan^R integrations are defined as:

$$PureIntegrations_{Kan} = Lysogens_{Kan} - Lysogens_{Kan+Cm}$$

Which are the lysogens growing on the LB+*Kan* plates subtracted by the mixed integrations, and pure Cm^R integrations are defined in the same manner but using the LB+*Cm* plates:

$$PureIntegrations_{Cm} = Integrations_{Cm} - Integrations_{Kan+Cm}$$

The total lysogens are defined as the sum of the mixed integrations and both pure integrations. The frequencies were shown in Fig. 2.11a.

Similarly for the complementation lysogenization assay, a 1:1 mixture of WT phages bearing a Cm^R marker and mutant phages (λcII^- or λP^-) bearing a Kan^R marker (λWT-*Cm* + λ cII^--*Kan* or λ P^--*Kan*) was used for the infection. The plating step was as described above on different antibiotic plates. The total WT integrations for mixed-phage infections are defined as the sum of the mixed integrations and pure WT integrations (mixed integrations + pure $integrations_{Cm}$ as calculated above) and the total mutant integrations for mixed-phage infections is calculated in a similar manner (mixed integrations + pure $integrations_{Kan}$ as calculated above). Also, for the double mutant complementation, the λ cII^- phage with a Kan^R marker was mixed 1:1 with the

λ*P*⁻ phage with the *Cm*^{R} marker (λ*cII*⁻-*Cm* + λ*P*⁻-*Kan*). The total integrations for each mutant are calculated in the same manner as the WT and mutant above.

Bulk mixed lysis assay and calculations

Host cells MG1655[pBR322-PLate***D*] were grown in the same manner as described for movies (in M9M + *Amp*). One-hundred fifty microliters of the same phage mixture as used for the movies was mixed with 150 µl of the resuspended host cells and kept on ice for 30 min. The infection mixture was then moved to a 42 °C water bath for 5 min, then the mixture was diluted into 3 ml of fresh M9G, and moved back to the 42 °C water bath for 10 min, then moved to a 37 °C shaking water bath until visible lysis occurred. This procedure ensures that all infected cells lyse to produce more phages for analysis. Following lysis, the lysate was moved to a tube and chloroform (Fisher Scientific) was added to reach 5% volume of the mixture and mixed with a tube shaker (Fisher Scientific) for 10 min, then centrifuged (4 °C, ~4,800*g*) to pellet debris, and the supernatant was transferred to a new tube. This chloroform and pelleting process was repeated twice more. The lysate was imaged under the microscope using the lytic reporter channels to determine pure blue, pure green and mixed phage progeny. This mixed lysis experiment was done in both M9 and LB media, where the LB version differs from the M9 method by replacing M9M with LBMM, and replacing M9G with LBM.

The same phage mixture as in the movie was used (API ~2) to infect cells with the pBR322-PLate***D* plasmid to help generate stable phage progeny, and the predicted values are based on that API. The prediction is based on the assumption that phage

adsorption follows the Poisson distribution[49], the different phages adsorb in an unbiased manner (the mixture of phages behaves uniformly, so dual-color infections follow the binomial distribution), and that mixed lytic infections result in mixed phage progeny. The lysate was examined under the microscope for phage foci of one (pure, blue or green) or both (mixed, blue and green) colors.

At a given API, the distribution of different phage MOIs can be determined using the Poisson distribution,

$$P(M,\lambda) = \frac{\lambda^M e^{-\lambda}}{M!}$$

Where M=MOI and λ=API, giving the population fraction of individual MOIs. Since the phage mixture is a 1:1 mixture of blue and green phages, the fraction of mixed infected cells with one or more of each phage can be determined for different MOIs using the binomial distribution, where M=MOI. By combining the equations we obtain,

$$G(M) = 1 - 2 * (\frac{1}{2})^M$$

$$V(\lambda) = \sum_{M=1}^{\infty} P(M,\lambda)G(M)$$

Which gives the fraction of mixed infected cells as a function of the API. For API=2, 40% of cells are expected to be mixed infected, and, therefore, ~40% of the fluorescent phage foci would be expected to have both colors, assuming that phages do not interfere with each other's lytic development.

Computational methods

We formulated two separate simple biochemical reaction models, one for the lytic fate and one for the lysogenic fate. These were both simulated using a stochastic simulation, the tau-leap[181], an offspring of the Gillespie stochastic simulation algorithm[48].

In both, we assumed that the starting point was upon entry of the first of two phage DNAs into the host cell. The biochemicals involved in the models are viral DNA (lytic DNA *V*, unreplicated pre-lysogenic DNA *N*, replicated pre-lysogenic DNA *P*, and lysogens *L*), an unspecified resource that we assumed to be host replisomes/replisome component (R), DNA-replisome complexes (CV, CN, and CP), and fluorescent reporters (D and E).

The goal of the models was to examine the interactions between two individual phages and the resource, so there were two sets of each biochemical species: one to represent the blue and one for the green phage, and copies of their DNA and proteins. The model consisted of the following reactions:

Lytic model:

1. $V_1 + R \xrightarrow{k1} C_{V1}$	Viral replication: phage DNA binds DNA pol/replisome
2. $V_2 + R \xrightarrow{k1} C_{V2}$	
3. $C_{V1} \xrightarrow{k2} C_{V1} + V_1$	Viral replication: DNA production
4. $C_{V2} \xrightarrow{k2} C_{V2} + V_2$	
5. $C_{V1} \xrightarrow{k3} V_1 + R$	Replisome unbinds from DNA
6. $C_{V2} \xrightarrow{k3} V_2 + R$	
7. $V_1 \xrightarrow{k4} V_1 + D_1$	Lytic reporter protein production
8. $V_2 \xrightarrow{k4} V_2 + D_2$	

Lysogenic model:

9. $N_1 + R \xrightarrow{k\prime1} C_{N1}$	Viral replication: unreplicated DNA binds DNA pol/replisome
10. $N_2 + R \xrightarrow{k\prime1} C_{N2}$	
11. $P_1 + R \xrightarrow{k\prime1} C_{P1}$	Viral replication: replicated DNA binds DNA pol/replisome
12. $P_2 + R \xrightarrow{k\prime1} C_{P2}$	
13. $C_{N1} \xrightarrow{k\prime2} C_{P1} + P_1$	Viral replication: unreplicated DNA becoming replicated DNA/complex

14. $C_{N2} \xrightarrow{k'2} C_{P2} + P_2$	
15. $C_{P1} \xrightarrow{k'2} C_{P1} + P_1$	Viral replication: replicated DNA complex producing replicated DNA
16. $C_{P2} \xrightarrow{k'2} C_{P2} + P_2$	
17. $C_{N1} \xrightarrow{k'3} N_1 + R$	Replisome unbinds replicated DNA
18. $C_{N2} \xrightarrow{k'3} N_2 + R$	
19. $C_{P1} \xrightarrow{k'3} P_1 + R$	Replisome unbinds replicated DNA
20. $C_{P1} \xrightarrow{k'3} P_2 + R$	
21. $L_1 \xrightarrow{k'4} L_1 + E_1$	Lysogenic reporter production
22. $L_2 \xrightarrow{k'4} L_2 + E_2$	
23. $P_1 \xrightarrow{k'5} L_1$	Replicated DNA switch to lysogen
24. $P_2 \xrightarrow{k'5} L_2$	
25. $C_{P1} \xrightarrow{k'5} L_1$	Replicated DNA complex switch to lysogen
26. $C_{P2} \xrightarrow{k'5} L_2$	
27. $N_1 + L_2 \xrightarrow{k'6} L_1 + L_2$	Forced lysogenization of naive DNA by lysogen
28. $N_2 + L_1 \xrightarrow{k'6} L_1 + L_2$	
29. $C_{N1} + L_2 \xrightarrow{k'6} L_1 + L_2$	Forced lysogenization of unreplicated complex DNA by lysogen
30. $C_{N2} + L_1 \xrightarrow{k'6} L_1 + L_2$	
31. $P_1 + L_2 \xrightarrow{k'6} L_1 + L_2$	Forced lysogenization of replicated DNA by lysogen
32. $P_2 + L_1 \xrightarrow{k'6} L_1 + L_2$	
33. $P_1 + L_1 \xrightarrow{k'6} 2L_1$	
34. $P_2 + L_2 \xrightarrow{k'6} 2L_2$	
35. $C_{P1} + L_2 \xrightarrow{k'6} L_1 + L_2$	Forced lysogenization of replicated DNA complex by lysogen
36. $C_{P2} + L_1 \xrightarrow{k'6} L_1 + L_2$	
37. $C_{P1} + L_1 \xrightarrow{k'6} 2L_1$	
38. $C_{P2} + L_2 \xrightarrow{k'6} 2L_2$	

The two main premises of the lytic model are that the phage DNA replicates, and that in order to replicate it must temporarily use up a resource, which it releases some time later. The resource may be a host replisome or replisome component such as

polymerase, which binds to DNA and allows it to replicate[182]. The resource is kept bound after replication, as DNA replication complexes are thought to be inherited following replication[183]. We hypothesized that these replisomes were the limiting factor in the phage competition, since it is known that there are very few of them in an *E. coli* cell[184,185].

The lysogenic model is simply an expanded model of the lytic one, with the difference that DNA initially starts off as 'naïve' DNA, which must then convert into lysogen by integrating into the host genome. We added a further layer of complexity by forcing the naïve DNA to replicate at least once before becoming a lysogen, as phage lambda requires DNA replication to efficiently lysogenize. In addition, we allowed lysogens to force naïve and replicated DNA to themselves turn into lysogens, to account for the action of CI protein. These lytic and lysogenic models were both simulated using the tau-leap stochastic simulation method developed by Daniel T. Gillespie as an offspring of his original stochastic simulation algorithm. This is an approximate but fast simulation method that samples the biochemical system at various time points (the frequency of which can be influenced by an error parameter, which controls the trade-off between accuracy and speed; we set his as 0.1). It is ideal for quickly simulating biochemical systems that may have reactions with disparate propensities (frequent and rare reactions). Such stochastic methods take into account the randomness of biochemical reactions within the cell, which can become important at low copy numbers, e.g. of genes.

These models assume an MOI = 2 and the key parameters that are varied are the second phage arrival delay and the initial resource level. The simulation also ends after a variable time, with the exact end time for each simulation being chosen from a normal distribution. For the lytic simulations, we ran the simulation for 6,600 ± 1200 seconds, which is roughly the average lysis time and standard deviation of the experimental data for normal lytic cells (Fig. 6c). The lysogenic model ends after 13,500 ± 60 seconds, which roughly corresponds to the time point that the experimental lysogenic data was taken, and the standard deviation is based on the fact that the images at different stages for each time point are taken up to a few minutes apart due the automatic image capturing. We ran 1000 simulations for each set of conditions. We simulated these systems of equations for resource levels of 1, 2, 3, 5, 10, 50, 100, 500, 1000, and 5000. These models assume an MOI = 2. In each of simulation, we also varied the mean arrival delay of the second phage, defined in units of number of replication cycles (1 cycle = 100 seconds), in order to more intuitively link it to biological considerations. The values we tested were 0, 0.2, 0.5, 1, 1.5, 2, 3, 5, 10, 20, and 50 replication cycles. When we tested the effect of varying the arrival delays or resource levels we set the other variable to that of our representative parameter set. The actual arrival delay for both phages in each simulation was drawn from an exponential distribution with a mean of the arrival delay we chose. These arrival times were both then normalized so the first phage arrived at $t = 0$. In addition, the simulation runtimes were also stochastic, sampled from a normal distribution with the same mean and standard deviation as our experimental data. In the rare cases that the arrival time of the second phage exceeded the simulation time, the

runtime was re-sampled. Starting out with the lytic model, we performed a brief parameter scan to find the optimal regime that best resembled the experimental data. We found two sets of parameters that both had reasonable behavior, in terms of the % pure and mixed reporter signals and the actual numbers of phage DNA, lysogens and reporters. The first one, which we call replication-limited, had $k1 > k2$, and vice versa for the second one, which we call binding-limited. The main difference between the two was usage of the resource: in the replication-limited schema, binding of phage DNA to resource was fast, and so all DNA quickly formed complexes that began to replicate. In the binding-limited schema, binding was much slower; because of this there was a reversal of the expected order, and in simulations with high resources, they were bound faster than in those with low resources. We chose to work with the replication limited schema, as this was more biologically realistic in terms of both the likely reaction rates of the processes, as well as the resource usage dynamics. As constraints, we were able to use lytic DNA, lysogen and reporter numbers, which are roughly known in the literature (Table 2.1). Once we had chosen the parameters for the lytic model, we based the lysogenic model on these and set $k'1 = k1$, $k'2 = k2$, and $k'3 = k3$. However, we chose a different reporter protein production rate in order for the model to match known stable numbers of CI protein, and it is known that CI regulates itself to a low level with slower production. To find $k'5$ and $k'6$, we ran another parameter scan, picked the parameter region that most resembled the data, then manually fine-tuned these parameters.

We normalized the fluorescent reporter signals, in order to compare to experimental results, as:

$$Normalized\ data = \frac{data - \min(data)}{\max(data) - \min(data)}$$

To create bivariate histograms, these normalized data were then binned into bins of width 5%, in both their blue and green lytic fluorescence signals (or red and yellow lysogenic signals). Percent mixed signals were calculated by setting a threshold of 5%; if both lytic/lysogenic fluorescence signals were above this value the simulated cell was labeled as mixed; of one signal was > 5% but the other was < 5%, it was labelled as pure. When both signals were < 5%, those results were labelled as dead cells and discard. The frequency of these was < 0.3% for all conditions. From here, the number of pure and mixed infections divided by the total simulation number yielded the prevalence of each infection fate. For our representative simulations (n = 71 and n = 49 for lytic and lysogenic, respectively), we used a resource level of 3 and average delay of 3 cycles (about 5 minutes), as under these conditions, the simulations resemble our experimental data, and are biologically realistic.

Asynchronous lysogenization experiment

Phage solution (λcI_{857} bor::Kan^R) was diluted with SM buffer to API = 8, 6, 4, 3, 2, and 1, calculated as phage concentration/host cell concentration (~$1x10^9$ cfu/mL). Host *E. coli* MG1655 from an overnight culture was diluted 1:1000 into lysogeny broth (LB) + 0.2% maltose + 10 mM $MgSO_4$ and grown at 37°C with shaking at 265 rpm, until an OD600 ~ 0.4. The culture was then centrifuged (4°C, 2000 x g, 10 min) and the pellet was resuspended in one-tenth of the original volume in fresh LB + 10 mM $MgSO_4$ (LBM) to concentrate the cells. There were three groups of infections in each experiment: time delay, mixing control, and unmixed control groups. 20 µl of host cells were added

to 16 microcentrifuge tubes on ice (seven each for time-delay and mixing-control groups, and two for the unmixed control group). In the first step, for the time-delay group, 10 μl of the ‘‘API_1’’ phage solution was mixed with the cells; for the mixing-control group, 10 μl of the API = 8 phage solution was mixed with the cells; and for the unmixed control group, 20 μl of the API = 4 for one tube and 20 μl of the phage solution that is one-half the API of the API_1 solution for the second tube were mixed with the cells. The mixtures were placed on ice while the samples were being prepared. In the next step, all tubes were placed in a 35 ^{o}C water bath and every 5 min (through 30 min), 10 μl of the ‘‘API_2’’ phage solution was added to the time-delay group; 10 μl of SM buffer was added to the mixing control group (time = 0 is as soon as the cells are placed in the water bath); and the unmixed control group was not handled. The temperature and times were chosen because adsorption is faster at higher temperatures and 35 ^{o}C is still permissive for the function the of cI_{857} temperature-sensitive allele[186]. At 30 min, immediately after the final time point, the tubes were removed from the water bath and 10 μl of each infection mixture was diluted into 1 mL of prewarmed LB + 0.2% glucose + 10 mM $MgSO_4$ (LBGM) and transferred to a 30 ^{o}C water shaker at 265 rpm for 30 min. Next, the infection mixtures were diluted appropriately with a common dilution factor, on ice using cold phosphate-buffered saline (PBS), and 100 mL of each dilution was spread onto LB + Kan plates and placed in a 30 ^{o}C incubator overnight for lysogen selection. Colony counts were compared to determine the effect of the time delays. Host cells were diluted using PBS and 100 μl of this dilution was plated on LB and grown in a 30 ^{o}C incubator overnight for the host colony counts. There were three sets of experiments

with different mixing ratios for the API_1 and API_2 phage solutions (1:1, 3:1, and 1:3). In the 1:1 experiment, both API_1 and API_2 = 4 (second unmixed control tube uses API = 2). In the 3:1 experiment, API_1 = 6 and API_2 = 2 (second unmixed control tube uses API = 3). In the 1:3 experiment, API_1 = 2 and API_2 = 6 (second unmixed control tube uses API = 1). The data for each time point were normalized to the mixing control data of its corresponding time point to account for the effects of diluting the infection mixture at different times. For each experiment, the normalized data points were again normalized to the first time point to visualize how the lysogen counts change with delayed phage inputs.

CHAPTER III

BACTERIAL VIRUSES ORGANIZE SUBCELLULAR ENVIRONMENTS TO MEDIATE HETEROGENEOUS DEVELOPMENT

Introduction

Organization is a fundamental part of life. For complex organisms, the spatial development of body parts must be controlled for proper function[187]. In the cells comprising these organisms, we find that organelles with different functions are organized by membranes[188]. Simpler bacterial cells use proteins to localize certain processes in lieu of intracellular membrane compartments[92], and furthermore, the natural heterogeneity of the bacterial cytoplasm might favor the segregation of different components for different processes[101]. Viruses are similar to these other forms of life, as they too have been reported to organize their development.

Bacteriophages, viruses of bacteria, are among the simplest biological systems, and they serve as model systems for advanced cellular processes. Phage lambda infects *Escherichia coli* and chooses between the lytic and lysogenic pathways as means of propagation. This subcellular choice serves as a paradigm of cellular decision-making. Recent efforts to probe this classical system with an expanded resolution of study have uncovered a range of interesting phenomena. Subcellular interrogation of lambda infections yields somewhat paradoxical conclusions, where co-infecting viruses display both individuality as well as mutual interplay when choosing cell-fate outcomes. Individual phage DNAs appear capable of committing to separate decisions in single

cells, yet also interact during development to make decisions at the whole-cell level. These observations raise fundamental questions about how intracellular genetic circuits remain semi-autonomous while also engaging with each other to mediate decision-making and heterogeneous development. Such questions may be addressed by focusing on how multiple components of phage development are spatially organized.

In this study, we utilize multiple fluorescence reporters to target phage lambda DNA, phage transcription, phage assembly, and essential host replication resources to study how lambda organizes its subcellular environment during infection. We use live-cell single-DNA molecule reporters in conjunction with additional phage DNA labeling to characterize how DNA replicates over time in cellular space. We also label and track *E. coli* DnaB, an essential DNA replication resource, to determine how phages manipulate host resources during infection. Additionally, we label the decision-outcome pathways to correlate the final cell fates with the preceding viral development. We complement this live-cell imaging with *in-situ* techniques to visualize phage mRNA and DNA, to correlate how phage transcription and DNA replication are organized from a different perspective. We focus our analyses on determining how these components are spatially oriented during infection to understand how phage lambda organizes distinct microenvironments in the cell. The organization of key decision-determining processes may be an important "hidden" variable contributing to noisy cell-fate decisions.

Results

Infecting phage DNA recruits host DnaB to its location

To visualize the entire phage infection cycle, we use fluorescence reporters to capture some essential processes including initial phage DNA translocation, phage DNA replication, gene expression, and the ultimate cell fates. We first visualized the events that occur early after the initial phage DNA enters the host cytoplasm (Fig. 3.1a). As the interplay between this infecting DNA and the host's DNA replication resources is crucial for downstream viral development, we fluorescently tagged the *E. coli* helicase, DnaB[24], with mTurquoise2 (mTurquoise2 signal is hereafter referred to as "blue") by replacing the native *dnaB* gene with a *dnaB-mTurquoise2* translational fusion gene on the *E. coli* chromosome (Fig. 3.1c). This was an attractive target because it directly interacts with phage lambda P protein[189], the analog of the host DnaC protein[190]. DnaB is essential for host and phage DNA replication and is a functional hexamer, which is predicted to exist in low levels in the cell. We visualized the initial infecting phage DNA using our previously developed system[135]. Briefly, we infected a *dam*$^{-}$ *seqA-mKO2* (mKO2 signal is hereafter referred to as "yellow") host cell with a natively methylated phage[135]. The SeqA-mKO2 fusion protein will bind exclusively to the methylated phage DNA to label it and its first replicated hemi-methylated copy (Fig. 3.1d). We used P1 transduction[191] to combine the modified *dnaB*, *seqA*, and *dam* alleles into a MG1655 host strain for our experiments.

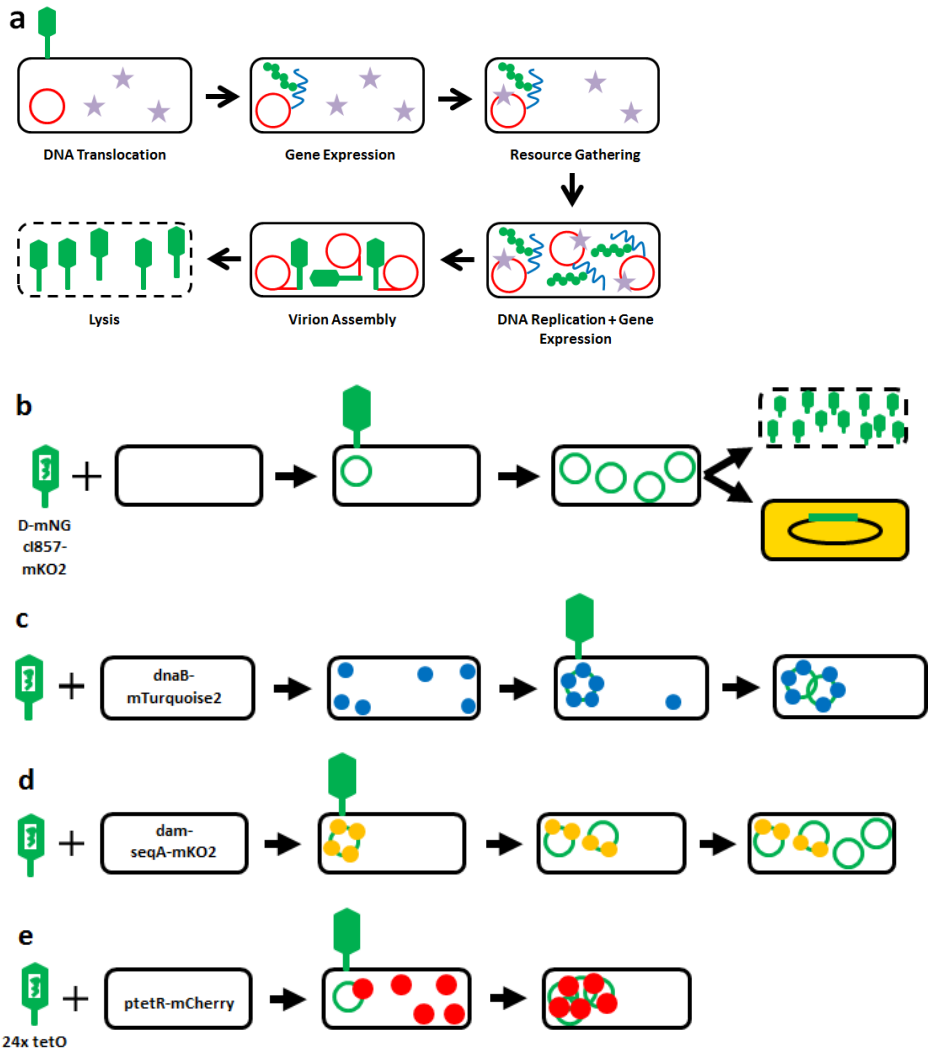

Figure 3.1 Reporters for the phage processes occurring during infection.
(a) Phages undergo many steps during infection. After phage DNA enters the cell, phage gene expression occurs. Phage DNA needs to collect resources (purple stars) to replicate, and continue gene expression. During lytic development, progeny phages are assembled and the cell bursts.
(b-e) Different live-cell reporters target different phage processes. (b) Phage D fusions allow visualization of lytic development, including progeny assembly. CI fusions show lysogenic development. (c) DnaB is the essential helicase that acts on phage DNA, and represents the resource for phage DNA replication. DnaB fusions allow visualization of how cellular resources behave in phage development. (d) SeqA fusion binds to methylated DNA, and infecting phage DNA is methylated, dam^- host DNA is not. This reporter has single-DNA molecule sensitivity for phage DNA, but only for first infecting copy and first replicated copy. (e) TetR fusion binds to phage genome modified with tetO binding sites. All phage DNAs will be labeled during phage replication.

To study how the phage collects resources for DNA replication, we infected our reporter strain with a phage carrying a genomic fluorescent capsid fusion[132]. Briefly, the phage has a fluorescent genomic *D* gene fusion, so virions of this phage strain are fluorescent. This reports the location of the infecting phage particle on the cell surface, and acts as the lytic reporter by labeling the expression of gpD protein during lytic growth (Fig. 3.1b). We observed that in the absence of phage infection, the cells displayed a diffuse expression pattern of blue and yellow fluorescence over time, indicating that DnaB and SeqA proteins do not localize specifically under our experimental conditions (Fig. 3.2a). When we infected these cells with phages, we observed the formation of yellow foci within the cells, indicating that phage DNA has entered the cell (Fig. 3.2b). As we continued imaging over time, we then observed that blue (DnaB) foci form in the cells, typically co-localized with the yellow foci. This indicates that the natural diffusive behavior of DnaB is altered by the presence of the phage, and many copies of DnaB become bound to the phage DNA. In many cells, both yellow and blue foci were stable over long periods of time, suggesting that a stable interaction is made. This interaction is likely for phage DNA replication mediated by the O protein of lambda (the *E. coli* DnaA analog of lambda) which binds to the phage origin of replication and the P protein of lambda[23,192].

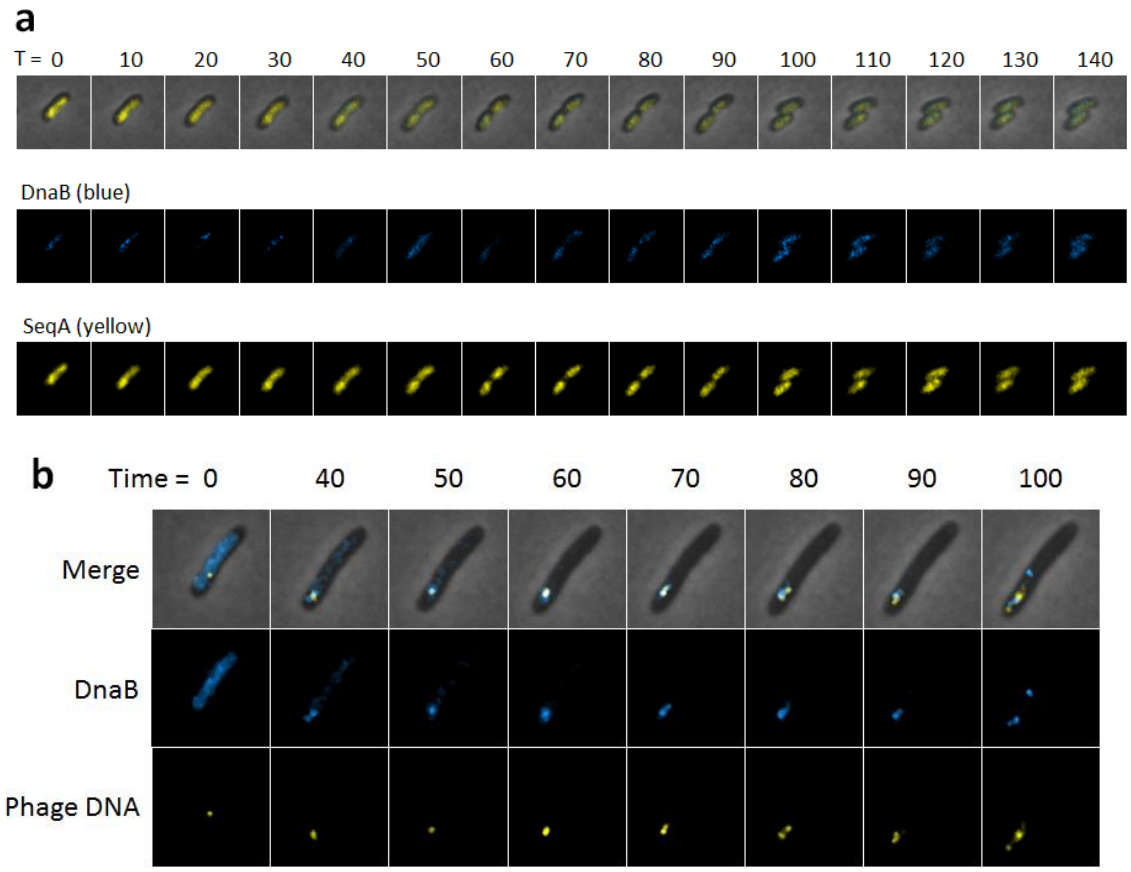

Figure 3.2 Phage DNA causes organization of cellular DnaB.
(a) A representative cell in the absence of phage infection is shown. In the uninfected cell, DnaB-mTurquoise2 and SeqA-mKO2 do not localize in the cell for periods of time. (b) A representative phage-infected cell is shown. During phage infection SeqA-mKO2 binds to single methylated phage DNA, forming a yellow focus. Afterwards, DnaB localizes in the same area as SeqA, phage DNA. This localization is stable over time.

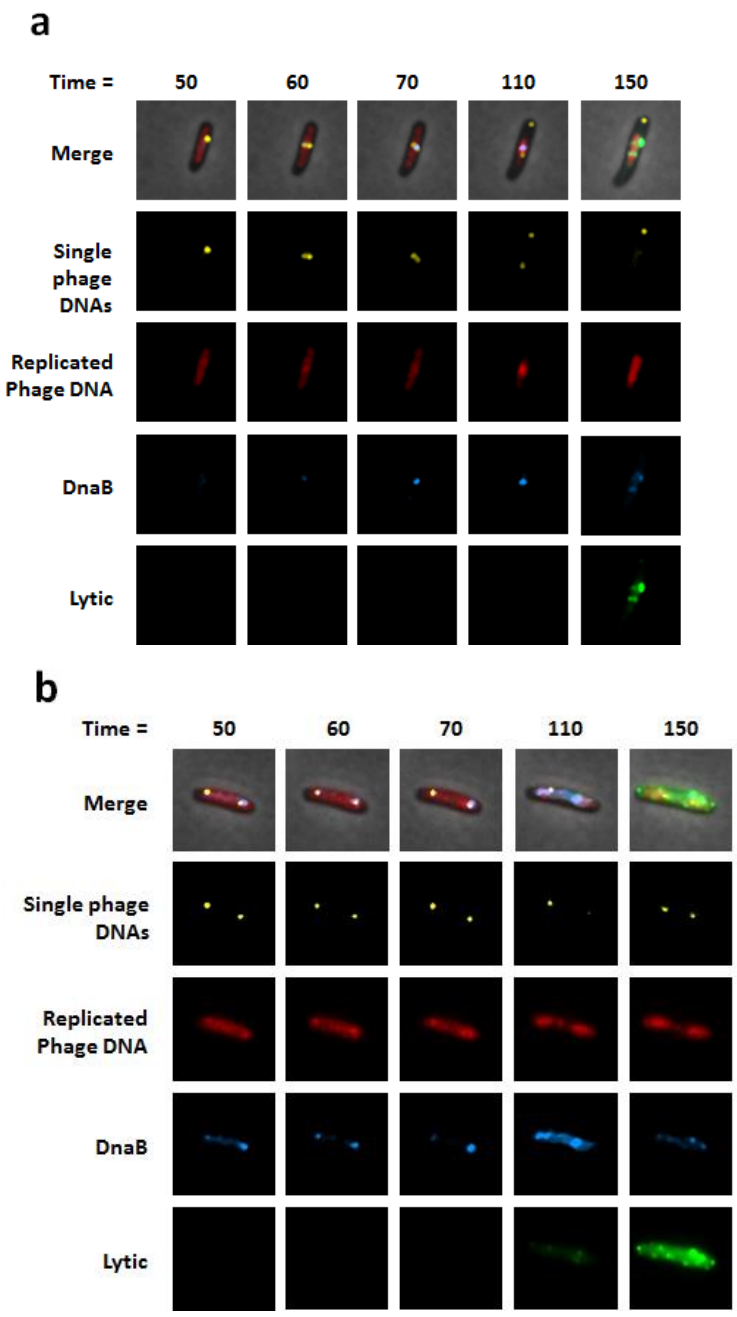

Figure 3.3 Live-cell spatial organization of phage DNA, DnaB, and assembly.
(a) A representative cell with one phactory is shown. A single phage DNA (yellow focus) sequesters host DnaB (blue focus) to itself. Phage DNA replication occurs in the same area, and replicated phage DNAs (red) remain spatially isolated. Phage capsids (green) form during virion assembly and cluster near the replicated phage DNA. These are termed as phage factories (phactories).
(b) A representative cell with two phactories is shown. When multiple DNAs infect the cell in different areas, each is capable of organizing its own phactory).

Phage DNAs replicate and develop in separate intracellular microenvironments

The initial phage DNA replicates over the course of infection irrespective of lytic or lysogenic cycle. So, we next focused on tracking the full process of phage DNA replication within the cell. We first focused on lytic cells, because they require extensive DNA replication to complete the infection cycle, whereas lysogenic cells do not. Our SeqA-based reporter is sensitive to single molecules of phage DNA, but it cannot reliably capture the full process of DNA replication because it only labels two copies of DNA[134,135]. To fully track phage DNA replication, we constructed a reporter that fluorescently labels all phage DNA copies. This labeling, however, lacks single-molecule sensitivity under our imaging conditions. We recombineered an array of a 24x *tetO* tandem array into our fluorescent phage. When this phage infects a cell bearing a plasmid constitutively expressing a TetR-mCherry (mCherry signal is hereafter referred to as "red") fusion, the phage DNAs will be bound at the *tetO* sites by TetR and be labeled (Fig. 3.1e). During infections with this system in conjunction with the SeqA labeling, the behavior of the first phage DNA and DnaB were similar to before. Over time, we observed that some cells have a cluster of red fluorescence that grows over time, likely corresponding to multiple replicated phage DNAs (Fig. 3.3a). We found that the size of each DNA cluster varied from cell to cell, which suggests that the amount of phage DNA varied for different cells (Fig. 3.4). The first phage DNA copy and the DnaB foci also resided near these clusters. At later time points, we observed accumulation of our lytic reporter, gpD-mNeongreen for this infection (mNeongreen signal is hereafter referred to as "green"), which forms foci and clusters likely corresponding to assembled,

DNA-filled phage capsids (Fig. 3.3a). We observed that the green foci first appear nearby the red phage DNA clusters, and over time, the green signal remains localized to the red signals, indicating that that phage assembly is coordinated to the areas of phage DNA (Fig. 3.3a). Our data suggest that phage lambda DNA replication is spatially organized by the first infecting DNA, which gathers the resources necessary for replication; these processes organize phage assembly later during infection. If a single infecting phage DNA can organize its development, then we predict that multiple co-infecting phages would be able to form separately organized areas. In the cases where multiple phages infect a cell, we observed single phage DNAs in different intracellular locations (Fig. 3.3b). However, this was not always the situation, because multiple infecting phages may enter the cell and remain in close proximity which may appear as a single focus instead of punctuate foci. For the separated single DNAs, each collected their own spatially segregated cache of DnaB, and then multiple red clusters appeared and grew inside the cell. Finally, green foci grew into clusters nearby the separate DNA clusters, suggesting that different zones of phage development occur within single cells. Because developmental variation occurred in different cells with areas of development, it is likely that separate areas within single cells also display varying levels of DNA and lytic signals. Indeed, we found that there are subcellular differences in the DNA and lytic reporter levels, which we refer to as subcellular heterogeneity for different developing phages. We note that the separated zones do not always arise from different single DNA foci, suggesting that the replicated phage DNA might diffuse away from its sisters to establish a separate replicating cluster, for example, in some cells infected by a

single phage (Fig. 3.5). This observation supports previous conclusions that replicated DNAs may be able to retain individuality during phage infection.

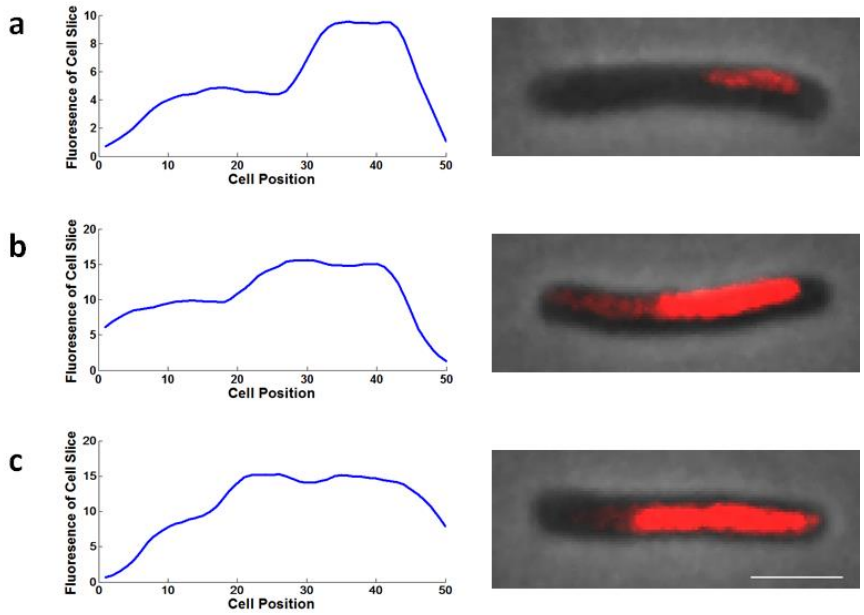

Figure 3.4 Phage development varies from cell-to-cell.
Examples of different cells imaged at the same time point are shown. The amount of phage DNA in the cell varies in the different cells (least to most DNA, a-c). The intensity of the fluorescence is plotted against the cell position to show that the spatial profile of phage DNA varies in different cells.

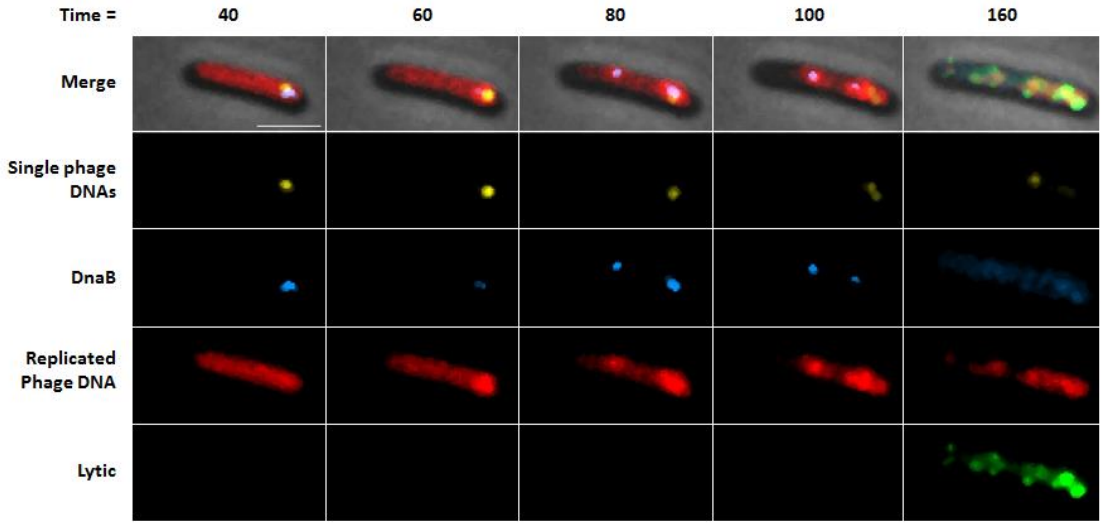

Figure 3.5 Replicated intracellular phage DNAs can establish microenvironments. Images show a representative cell that is infected with a single phage DNA focus (yellow) which sequesters its resources (blue) and replicates itself in a space in the cell (red, 60 min). A second zone of phage DNA replication forms with its own resources, without a corresponding yellow DNA focus. Replicated DNAs may move to different areas of the cell to establish microenvironments. Phage capsid (green) accumulates in the different phactories.

Lysogenic cells have limited DNA replication

Having focused mainly on lytic development, we then moved to explore how lysogeny differs. Lysogeny does not depend as strongly on DNA replication to succeed, as even mutants lacking phage DNA replication are able to lysogenize, albeit in a compromised manner. Previous work has shown that phages display the ability to individually commit, or vote for decisions in the cells, but when lytic and lysogenic decision conflict, the lytic vote wins an overwhelming amount of the time[133]. This suggests that some element of lytic progression is antithetical to lysogeny. One possibility is that the numerous replicating phage genomes overwhelm the capacity of the few CI-producing, lysogenic-voting genomes to repress lytic gene expression, as lysogenic cells typically have fewer phage DNAs. To explore this, we inserted a transcriptional lysogenic reporter, *cI-mKO2*, into our phage. Briefly, lysogenic cells will express yellow fluorescence over time and not lyse (Fig. 3.1b). The fluorescent protein is shared with the SeqA reporter, but lysogeny occurs fairly late, so we are able to observe the initial infecting DNA and the lysogenic outcome without conflict. We found that for cells which become lysogenic, it is more difficult to observe the DnaB foci with the SeqA DNA foci, and even when it is observed, the DnaB dissipates quickly compared to lytic cells (Fig. 3.6), where DnaB foci remain on an hourly timescale (Fig. 3.3c). Lysogenic cells typically do not display any red replicated DNA clusters either, although DNA replication should be occurring, suggesting that the levels of DNA replication for lysogenic cells are below our detection sensitivity. Altogether, the data support previous conclusions that DNA replication is limited for lysogenic cells, in contrast to lytic cells.

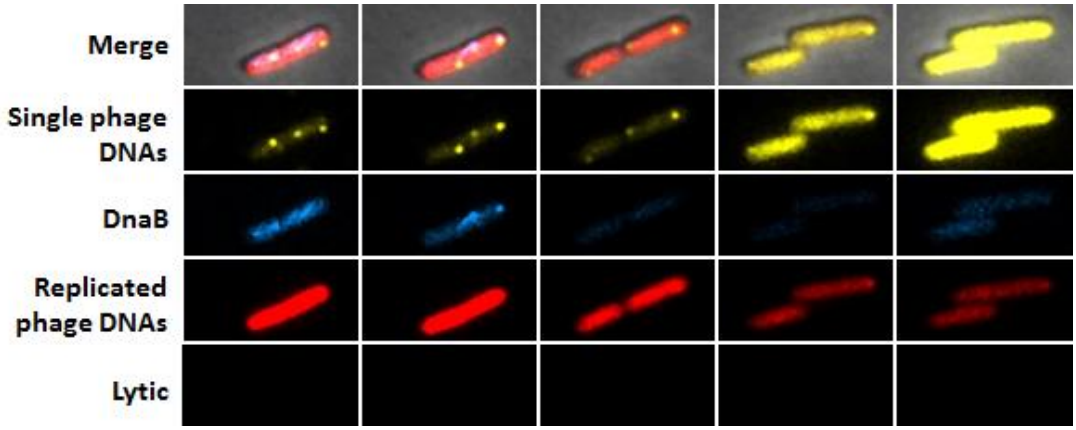

Figure 3.6 Lack of DNA replication and limited organization in lysogeny.
A representative lysogenic cell is shown. Lysogenic development behaves differently than lytic development. Imaging shows that phage DNAs do not keep DnaB sequestered for long periods during lysogeny. Some phage DNAs do not appear to have DnaB foci at all. Replication is shown to be limited from the TetR reporter during lysogeny. There is a lack of noticeable red signal accumulation. At later time points, the lysogenic reporter (yellow) accumulates throughout the cell, making the single DNA reporter not detectable. Lysogenic cells may divide after enough time has passed. Any DnaB foci in the cell become dispersed, and there is no lytic signal development

Phage transcription is spatially organized near infecting phage DNA

To rule out any artifact introduced by our live-cell fluorescence imaging, we set out to use phages and cells without any reporter systems to examine phage development using alternate techniques. We used single-molecule fluorescence *in-situ* hybridization (smFISH) to characterize phage transcription and to track phage DNA replication.

We performed smFISH for phage DNA during phage infection. At early time points, we observed phage DNA as single foci in cells, which likely correspond to single phage DNAs (Fig. 3.7a). The localization of these foci bears similarity to the localization of the yellow foci using our SeqA system in live cells (Figs. 3.8 and 3.9). At later time points, we found that the DNA signal increased with time, and appeared as larger clusters taking up part of the cell area, which is also in accordance with the live-cell replicated DNA reporter (Fig. 3.7b). Notably, we also observed multiple clusters of phage DNA signal in the cells. The amount of DNA per cell and intracellular clusters are variable, similar to the variation in size of the live-cell DNA clusters. These data mirror our live-cell data suggesting that phage DNA localizes during infection, where separate development is possible.

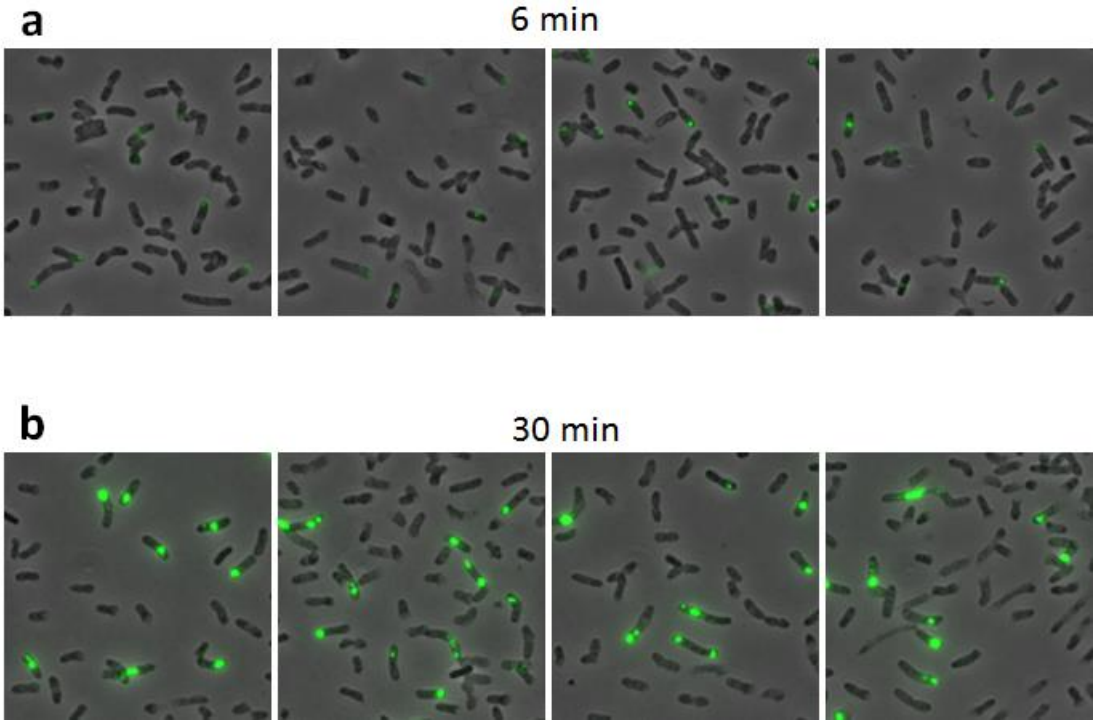

Figure 3.7 Phage DNA replication is localized from DNA FISH.
DNA FISH was performed on cells to examine phage lambda DNA. Cells were grown in LB and samples were taken at given time points. Lambda DNA is visualized in green. At an early time point (a), foci are found in the cell, commonly at the poles or mid-cells. At a later time point (b), the foci are larger, brighter clusters.

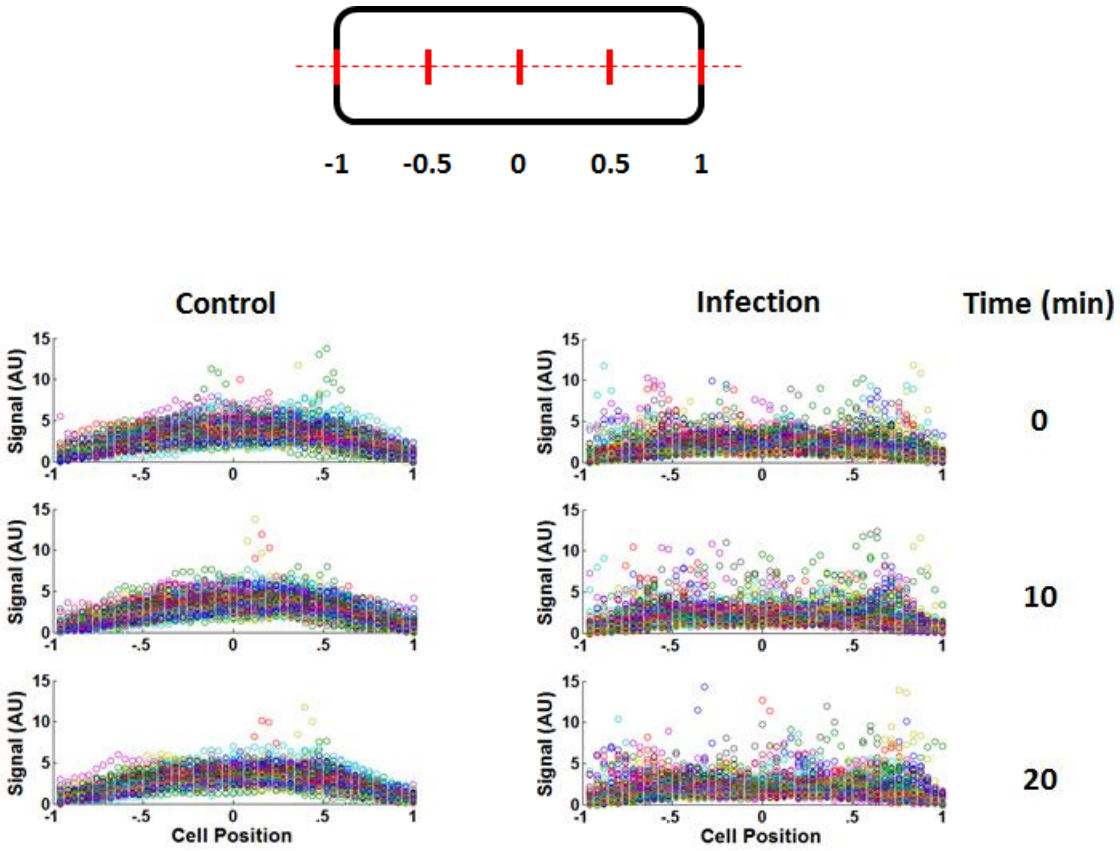

Figure 3.8 Phage DNA has location preference during live-cell infection.
The SeqA-mKO2 signal for lytic and lysogenic cells (N = 139) is plotted based on its position along the cell for non-infected control cells, and infected cells for given time points. The higher signals, which are outliers from the bulk of the signal, represent the locations of SeqA-mKO2 foci. Infected cells show increased SeqA signals in certain locations of the cell throughout the time points.

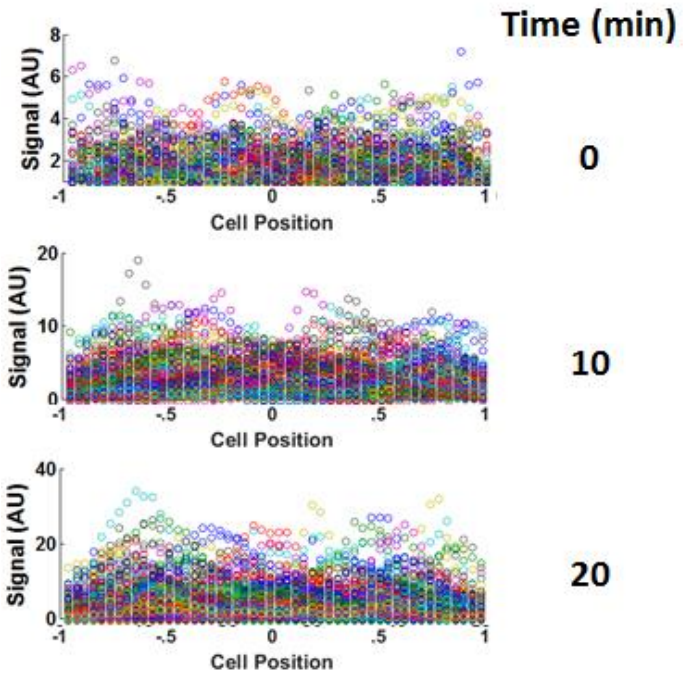

Figure 3.9 Phage DNA has location preference in fixed cells.
The fluorescent signal of DNA FISH probes targeting lambda is plotted based on its cellular position for infected cells at 0, 10 and 20 min (N = 330, 235, 384 respectively). Higher signal preferentially locate to certain positions. Localization remains at later time points, and the signals increase.

Transcription is an important process for phage gene expression, and we use RNA smFISH to characterize it here. We first targeted the pR transcript, a constitutive early phage gene transcription unit. This operon contains important genes for decision-making and phage DNA replication, so its localization might be important for lambda development. We observed that the pR transcripts appear as foci, and that these foci localize to similar locations as the phage DNA reported by DNA smFISH and the SeqA system (Fig. 3.10a). In our RNA smFISH protocol, we also treated our cells with DAPI to stain the DNA. We observed that the nucleoid of the cell locates at specific areas, and that there were distinct nucleoid-free zones. The phage pR transcript signals were generally anti-correlated with the DAPI signals at 15 min after infection, suggesting that the phage mRNA resides in where the nucleoid does not (Fig. 3.11). However, DAPI staining during DNA smFISH does not show the same localization, perhaps owing to the differences in protocols. When we examined pR at later time points, we found that there were generally more pR transcripts in larger clusters, but they still retained their localization in parts of the cell (Fig. 3.10a). We note that at later time points, pR signals and DAPI signals overlap, which may be due to phage DNA replication resulting in DAPI staining phage DNAs. When we quantified pR clusters in different areas of the cell, we found that like phage DNA, phage mRNA levels can differ intracellularly.

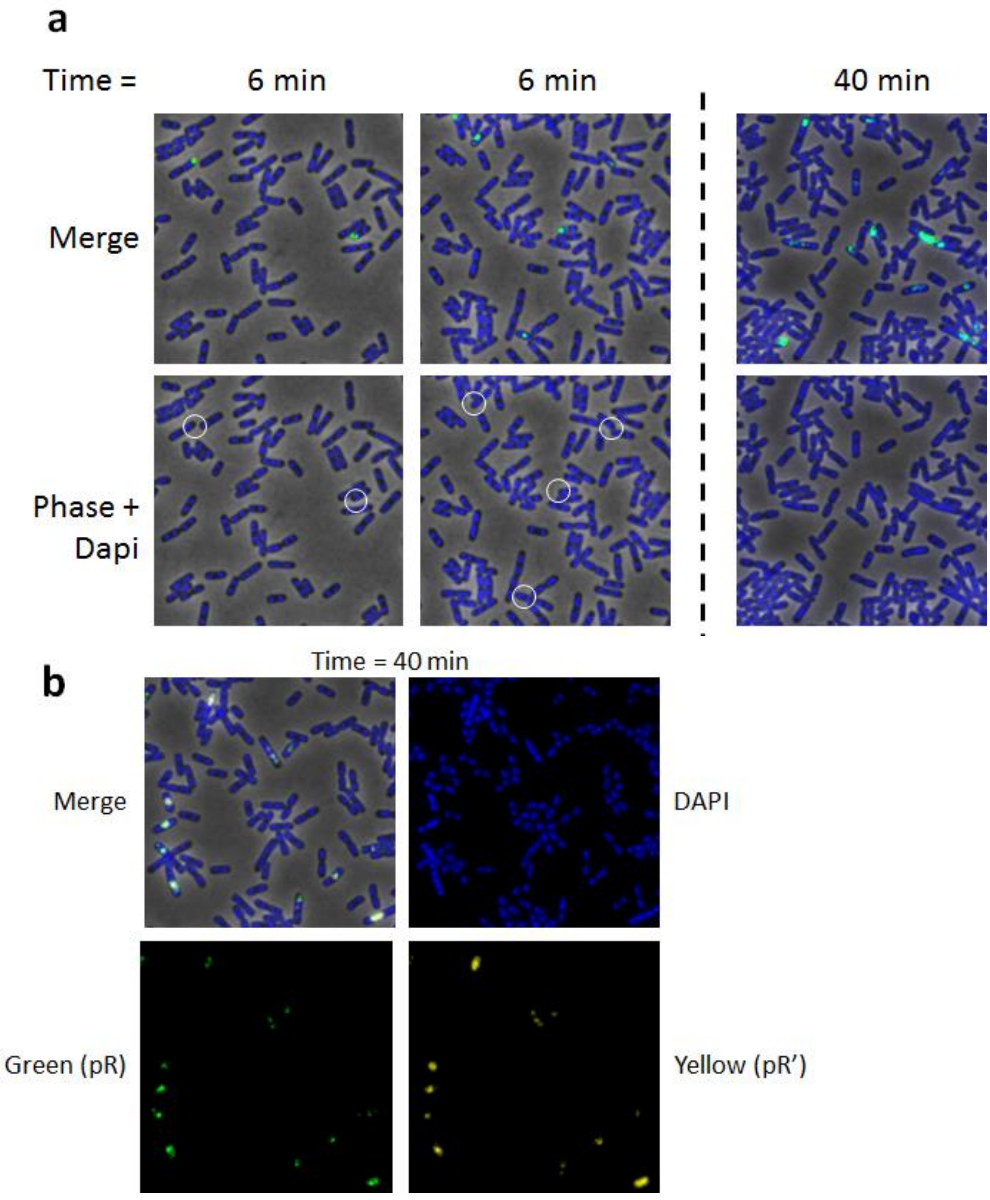

Figure 3.10 Phage lambda transcription is organized in the cell.
(a) RNA FISH was performed on cells after lambda infection targeting the pR transcript. The pR transcripts are visualized as green signal. At 6 min, early in the infection, pR is localized preferentially near the cell poles and mid-cells. These samples were also stained with DAPI to visualize DNA in the cell. At 6 min, pR foci are located in areas lacking DAPI signal, suggesting that phage transcripts accumulate away from host DNA.

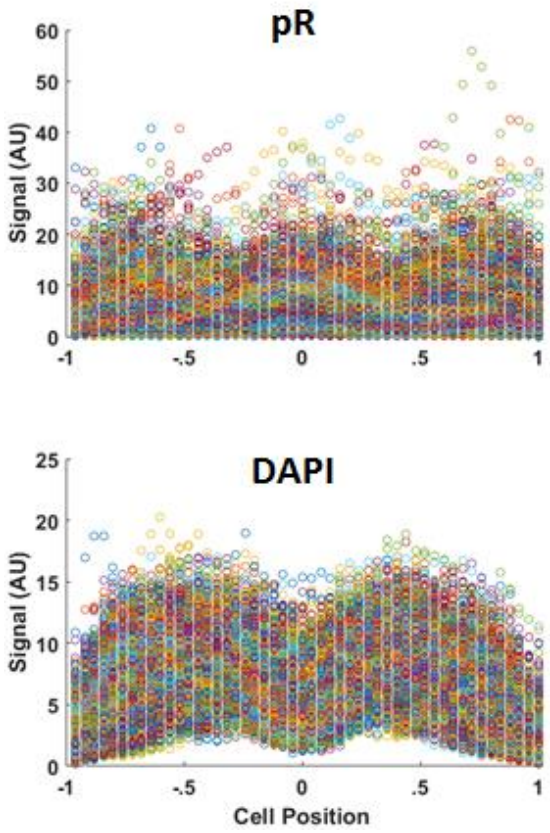

Figure 3.11 Lambda pR mRNA and *E. coli* DNA have different localization patterns.
The pR transcript signals, labeled with RNA FISH, of phage-infected cells (N=1565) at 15 min after infection are plotted based on their positions in the cell. Higher signals correspond to foci and localize to certain areas of the cell (a). The DAPI signals from the same cells are plotted based on their positions in the cell. The location preference of DAPI signals is different than that of the pR transcript.

Phage lambda gene expression is segregated by time, where the accumulation of the early gene products results in decisions carried out by late genes. We then targeted the late pR′ transcript, which is the operon encoding the lysis and morphogenesis genes late in infection, simultaneously with the pR transcript. We found at later time points, both the pR and pR′ transcripts shared similar localization, suggesting that the phage DNAs in this area are transcribing both sets of genes (Fig. 3.10b). These data indicate that certain phage transcripts are maintained in close proximity to its cognate DNA, which is specifically localized in consistent with the organization we found from live-cell imaging. The transcripts we targeted were relatively long transcripts, ~7kbp for pR and >20kbp for pR′, which would be expected to remain attached to its template DNA for a period of time, not to be released until transcription termination. Even at maximal transcription speed, the pR transcript completes in about 90 seconds, and the half-lives of bacterial mRNAs have been reported to be 1-2 minutes[193]. This organization might help establish a local concentration of phage gene transcripts followed by translation in these regions. The observed locations of phage DNA and transcripts correspond to where *E. coli* ribosomes are enriched[114], which would favor expedient gene expression if the genes were retained nearby.

To observe phage DNA and mRNA concurrently, we combined our SeqA DNA-labeling system with RNA smFISH. We infected cells with the SeqA DNA reporter with WT phages and treated the cells for RNA smFISH. We found that the SeqA reporter is apparently functional, forming punctate foci in infected cells (Fig. 3.12). The pR transcript using smFISH are co-localized with phage DNA SeqA foci, suggesting that pR

does localize with its cognate DNA. We also observed that some SeqA foci do not have pR transcripts, possibly due to stochastic gene transcription, or some pR transcripts without an apparent nearby phage DNA. This inconsistency may be due to replicated phage DNAs without the SeqA label or the malfunctioning of the SeqA system after fixing the cells.

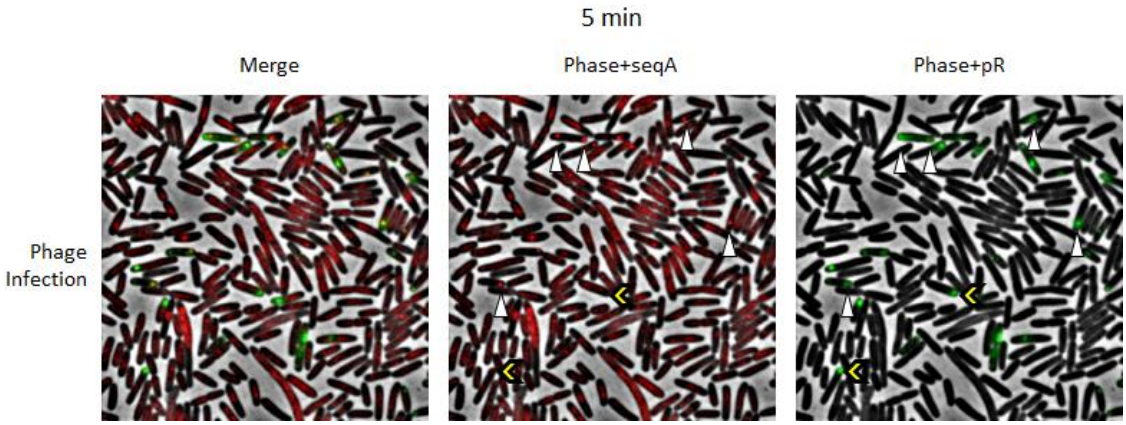

Figure 3.12 Phage DNAs and mRNAs co-localize.
RNA FISH was performed on dam⁻ SeqA-ECFP cells infected by methylated phages targeting the pR transcript. Phage DNAs are visualized as red foci and pR transcripts as green foci. Examples of co-localization of phage DNA and transcripts are marked by white arrowheads. Examples of pR mRNA without phage DNA are marked by yellow carats.

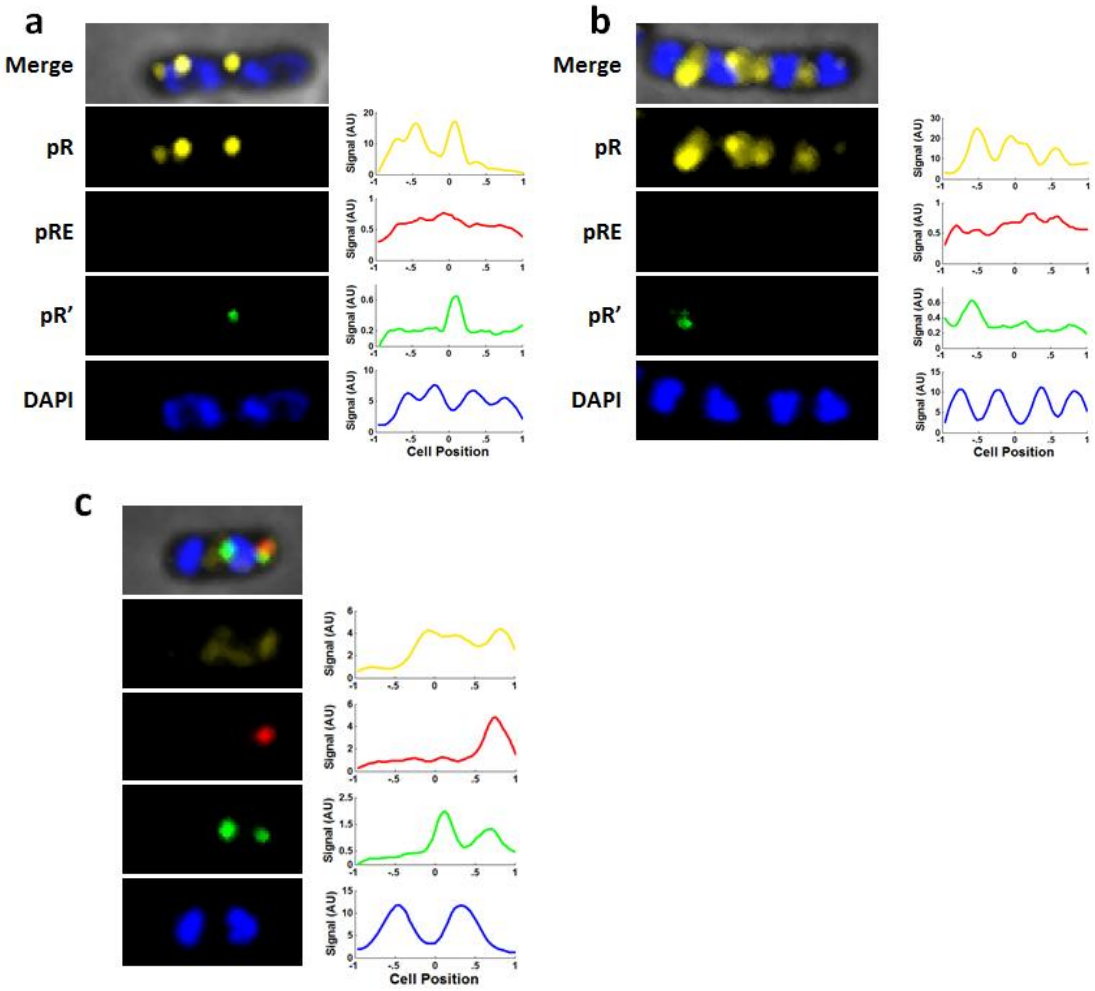

Figure 3.13 Separate microenvironments in the cell undergo different transcription. RNA FISH was performed on cells infected by phage lambda targeting the pR, pR′, and pRE transcripts, and the cells were DAPI-stained. The pR′ and pRE transcripts are from lytic and lysogenic programs respectively. These cells were fixed 15 min after infection. (a and b) Cells show multiple distinct areas of localized pR transcripts (yellow) in DAPI-free zones of cells. The locations of the fluorescent signals are shown in colored traces next to the microscopy images. pR peaks are generally offset from DAPI peaks. These cells also have pR′ transcripts (green) corresponding to a single pR cluster, not in the other clusters, which is also shown in the traces. Some cells show combinations of pR, pR′, and pRE transcripts (red) in different areas of the cell (c), where pRE clusters reside in one area of the cell but not others.

Phages organize separate subcellular microenvironments for development

Our experimental results converged, indicating that infecting phages generate microenvironments consisting of phage DNA, phage mRNA, *E. coli* DnaB, and phage assemblies, where each could be considered as a phage factory (shortened as "phactory"). Furthermore, different co-infecting or replicated phages were capable of generating quantitatively distinct phactories within single cells. If this is true, then this subcellular organization may underlie the viral behaviors intimating individuality. These subcellular differences should manifest themselves in differential decision-making, or mixed-voting as we have previously termed. From our RNA smFISH experiments, we have established that multiple pR transcript clusters appear in single cells, and have shown that different clusters appear adjacent to different phage DNAs or in different nucleoid-free zones in cells where phage DNAs prefer to reside. From our smFISH experiments, at 15 min, we noticed cells with multiple pR foci, but only a single pR′ focus, which might be the commitment of an individual phactory towards lysis (Fig. 3.13 a and b). Furthermore, when we also targeted the pRE transcript, the lysogenic decision transcript, we observed some cells with multiple pR/pR′ foci but varying numbers of pRE foci (Fig. 3.13c). Cells such as these might develop into the mixed-voting population that we characterized earlier. At relatively early time points after infection, phages may be initiating commitment to decisions. The different transcripts within single cells, in different locations, suggest a degree of independence in decision-making for phage infections. These individual decisions might only occur transiently, as over time, multiple pRE/pRM promoters will be activated throughout the cell to establish lysogeny

or different phactories will commit to making proteins to package progeny phages, but nonetheless, this provides evidence that development is variegated for different viruses within cells. This type of spatial development also helps reconcile the apparent incompatibility between independence and interaction because while DNA replication and transcription are spatially confined, the resulting proteins are able to be shared, as demonstrated from mutant complementation[156].

Organization during prophage induction differs from infection

To further test that multiple phage DNAs can develop separately in cells, we tested our live-cell reporter systems during prophage induction. Following induction, the lambda prophage will undergo development very similar to a lytic infection, requiring DNA replication and late gene expression. For an infection experiment, to achieve spatially separated co-infections, we require a high API (average phage input) to probabilistically result in cells with a high MOI (multiplicity of infection), and the infecting phages must infect in separate areas of the cell. Whereas, induction only requires bacterial growth to achieve multiple, spatially separated phages per cell. During exponential growth of the lysogen, there are as many copies of the prophage as *E. coli* chromosomes, which are numerous during growth in rich medium, and the prophages are separated due to nucleoid organization. We predicted that the phage genomes in each cell should excise from the host genome and be separated in space. We first imaged samples from an induction culture of our gpD-mNeongreen 24x*tetO* phage. Before the induction, the exponentially growing culture did not have particularly obvious phage DNA foci, which was expected because the tetO/TetR reporter does not have the single-

DNA-molecule sensitivity (Fig. 3.14). Over time after induction, we observed that cells have multiple red DNA clusters, which grow over time. We note that the localization patterns of these DNA foci do not match those from the infection movies, where there is much less preference to the polar and midcell regions. This is possibly because the prophages were part of the *E. coli* chromosome, so when they excised, they remained nearby the nucleoid, which is not typically at the poles or midcells. For infections, the phages adsorb preferentially to the poles and midcells, so their infection and development locations are expected to be different from during induction. The lytic reporter accumulates as foci near the phage DNA clusters, which are separate phactories, where they vary in size (Fig. 3.13). These data support that the location of the phage DNA as it undergoes initial gene expression organizes where the phactory is built.

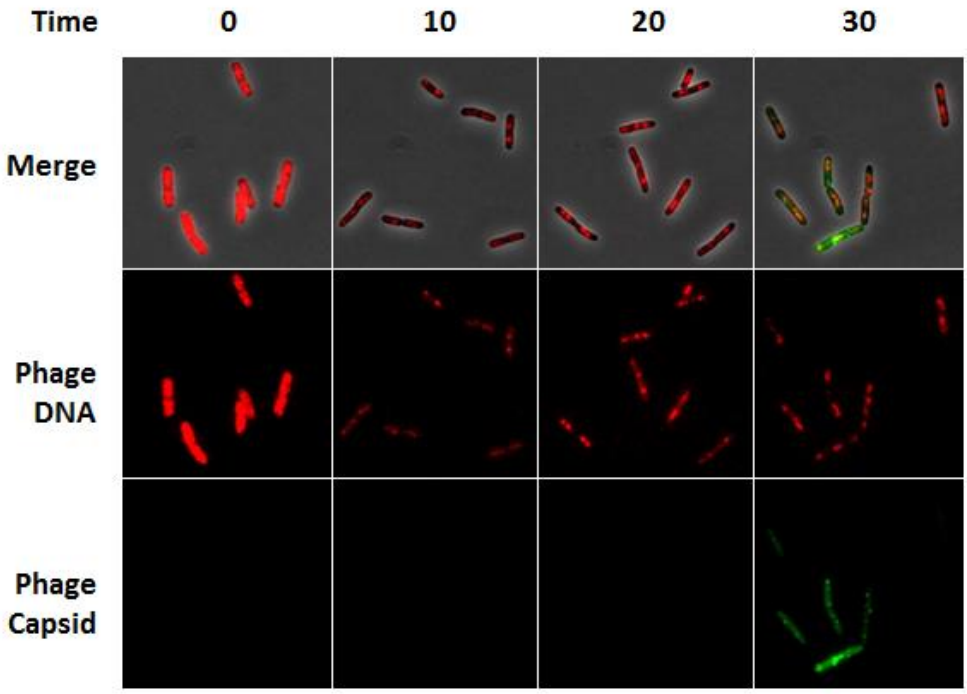

Figure 3.14 Phages develop in multiple separated areas during induction.
Lambda D-mNeonGreen cI_{857} 24xTetO lysogens bearing a TetR-mCherry plasmid and *dnaB-mTurquoise2* reporter were induced and imaged at given time points after induction. This is not a time lapse. Prior to induction, TetR is diffuse throughout the cell and most cells do not have DnaB-mTurquoise foci, although some cells have a single focus. 10 min after induction by heat shock, cells typically show multiple DnaB foci and each focus has a corresponding cluster of TetR signal, which shows that phage DNA is replicating at different locations. The phage DNA clusters grow in size over time and maintain DnaB at their locations. Green signal, which represents phage capsid assembly, accumulates near phage DNA clusters at later time points before lysis.

Discussion

As organization underpins biological processes of all lifeforms, we probed the paradigm of phage lambda with greater focus on spatial-temporal analysis than previous studies to resolve open questions about cellular decision-making. We found that the initial infecting lambda DNA functions to collect and spatially confine host DnaB nearby itself to enable viral replication. The sister phage genomes from replication prefer to remain in the vicinity of its predecessors, resulting in a distinct zone of replicating phage DNA. The major phage transcripts, early and late, prefer to reside in distinct zones as well, proximal to phage DNAs. The long length of some of these transcripts favors this localization because the mRNA is anchored to the template DNA during active transcription. This kinetic limitation combined with the short average lifetime of bacterial mRNAs might preclude rapid diffusion of transcripts, which helps generate high local concentrations of phage mRNAs in the location of phage DNAs. During lytic development, progeny phages assemble adjacent to the phage DNAs, as our reporter is on the gpD protein, which stabilizes the phage capsid only after DNA packaging. This is an expected result, and altogether demonstrates that these different phage processes coalesce into a specific area to function as a phage factory, or phactory as we call it.

The agent responsible for the organization appears to be the phage DNA, and the exact mechanism of how replicating phage DNAs remain in zones is unclear. This behavior is not absolute, as we observe that cells infected by a single phage can produce multiple phactories. We speculate that there may be a physical basis, but not a physical barrier, to the separation of developing phage DNAs. The agglomerate of phage DNA,

RNA, and protein does not appear to be separated by a wall of membrane or protein, so the phactories may behave more like membraneless compartments, such as nucleoli, Cajal bodies, or similar structures found in eukaryotic cells[194]. Certain types of these structures can form spontaneously when the proper components are present[195], and they serve as additional means to regulate biological activities in cells. Viewing these phactories from this perspective could elucidate the mechanisms of how they form and function.

One striking aspect of these phactories is that multiple can form in single cells, arising from either multiple phage co-infections or apparent separation of sister phage genomes. Different intracellular phactories resemble different phage "territories." The DNA, mRNA, and phage lytic reporter levels differ between intracellular segregations. This is significant because it begins to explain the mechanisms of individuality observed for phage lambda. Previous studies have concluded that individual phages, and even to the individual phage DNA level, are able to commit to cellular decisions. We were able to detect apparently separated zones of early phage gene expression, where the levels of transcription varied intracellularly to support asymmetrical development. Importantly, there are also cells where a single area committed to a lytic or lysogenic gene expression program whereas other intracellular areas do not, which evidences that the development of individual viruses can diverge the subcellular level. Additionally, we observed that the growing, replicating DNA clusters in cells become different sizes, or that individual DNAs may diffuse to different parts of the cell, but one may not form a replicating cluster. The lytic reporter follows a similar trend. This further underscores that phages

actively shape their environments causing differential development intracellular phages, where variations in DNA, mRNA, and protein in different phactories create viral individuality.

For all of the individuality or selfishness that occurs during phage lambda DNA replication and transcription, it is important to note that the actual proteins that are produced are not typically *cis*-acting, but rather, are diffuse throughout the cell and able to be shared with other intracellular phages. This is *trans*-action is needed for the complementation of mutations or cooperation observed in lysogeny, and is somewhat at odds with the viral individuality discussed so far. We point out that the lytic pathway is the primarily selfish pathway, as the onset of lytic gene expression is controlled by the Q protein, which was reported to have a *cis*-acting preference[31], meaning that one phactory may have a means to initiate lysis irrespective of any other intracellular phages. For lysogeny, the initiator of pRE is CII, which should be diffusible to activate CI for all infecting phages, to enforce lysogeny, so any independent pRE triggering is rare and likely transient. This sharing of proteins despite insular development of DNA and mRNA is curious, and may have an explanation for this temperate phage. Lysogeny is generally considered as the alternate pathway for lambda, and is favored when multiple phages infect. In a single infection, the sharing of proteins is irrelevant, because the only phage in the cell is "itself." This works against the notion that there should be any compartmentalization at all, except that the sequestration of resources may benefit the "offspring" of the original phage, allowing for rapid replication and perhaps quicker resolution of the infection. Another interpretation of this sequestration is that it may

defend against "cheater" or satellite phages, which cannot recruit their own resources, meaning they could only propagate if they can invade the resource-replete territory of the other phages. However, for lysogeny, the phage essentially requires the ability to sense or communicate with any other phages in the cell, and this is where the sharing of proteins might be important. If CII were fully cis-acting, then the main route for co-infecting phages to interact would be to occupy the same physical space, but since it is shared, separate locations in the cell can cooperate in that sense. This collective decision-making is in the "interest" of the phage that chooses lysogeny because a dissenting lytic vote dooms the cell, consequently dooming the non-lytic-voting phage. Conversely, for the phage choosing lysis, cis-acting properties promote an advantage for initiation. This set of interactions resembles the stag hunt or prisoner's dilemma games used in game theory. In these games, two players can choose to cooperate, where mutual cooperation results in a mutual gain. The players can also choose to dissent, and when both players dissent, a smaller reward is gained for both. Finally, when a player dissents and another cooperates, this betrayal provides a greater selfish reward for the dissenter, and a massively diminished one for the cooperator.

Organization for viral development has been previously characterized in other systems, which demonstrates that there are diverse strategies for viral propagation. One well-known example is Mimivirus, which is a giant virus which infects amoeba[107]. Its genome is over 1Mbp, encodes over 900 ORFs, including elements of translational machinery[196], and packages its own transcription machinery within its virion, making it more complex than many bacteria. Over the course of its infection, it builds virus

factories in its host, which do not appear to be membrane-bound. This virus' DNA replication, transcription, translation, and assembly occur in these cytoplasmic factories. This process is similar to how the poxvirus family develops as well. One of the largest known phages, the giant *Pseudomonas* phage, 201φ2-1, whose genome is over 300kbp encoding over 400 putative genes, was reported to build a nucleus-like, protein-walled compartment which houses its DNA and transcription during development[109]. By contrast, phage lambda has a genome of about 48.5kbp encoding over 70 genes. This relatively simple phage is capable of organizing an apparent virus factory similar to a much more complicated system, which indicates that strategies for spatial organization possibly evolved earlier, perhaps in less complex systems. Due to the co-evolution of bacteriophages and bacteria, it is unclear whether viral behaviors are obligatorily derived from pre-existing bacterial genes or if they can evolve in a novel manner, unrelated to existing bacterial genes. Our results suggest that using new tools to reexamine established systems could discover hidden phenomena to refine the understanding of our models.

The revelation of hidden variables has implications for systems-level understanding of biological processes. Technological advances have played a considerable role in illustrating remarkable complexity in simple systems, like bacteria and viruses, changing how we think about them. Previous notions that bacterial cells were bags of enzymes and genetic material or that viruses must be small and lack advanced features, we now consider anachronistic. By utilizing available tools, researchers have discovered individuality, nucleus-like functionalities, extracellular

communication, competition and cooperation in viruses[127]. These novel discoveries continue to accumulate, and this will continually bring up the debate of whether viruses are to be considered as bona-fide life, despite disagreement of what that term truly entails. Regardless of current opinions however, future efforts are guaranteed to contribute to our pool of knowledge, not detract from it, and as it is with science, more data will eventually change minds and ultimately shift paradigms.

#	Bacterial Strains	Comments	Source
-	MG1655	Wild type *E. coli*	Lab stock
-	LE392	sup^E and sup^F host	Lab stock
LZ1386	MG1655 *seqA-mKO2 Δdam::Kan^R Cm^R*	For methylated phage DNA labeling, *Kan^R Cm^R*	This work
LZ1555	MG1655 *seqA-mKO2 dnaB-mTurquoise2 CmR dam::Kan^R*	Strain to label single phage DNA and DnaB, *Cm^R Kan^R*	This work
LZ1557	MG1655 *seqA-mKO2 dnaB-mTurquoise2 CmR dam::Kan^R* [pACYC177 pFtsKi *tetR-mCherry*]	Triple reporter strain to label single and replicated phage DNA and DnaB, *Amp^R Cm^R Kan^R*	This work
LZ1575	MG1655 (λ*D-mNeongreen cI$_{857}$ bor::Cm^R* 24x*tetO*)[pBR322 pLate**D*]	Lysogen, induced to produce phage λLZ1575, *Amp^R Cm^R*	This work
LZ1576	MG1655 (λ*D-mNeongreen cI$_{857}$-mKO2 bor::Cm^R* 24x*tetO*)[pBR322 pLate**D*]	Lysogen, induced to produce phage λLZ1576, *Amp^R Cm^R*	This work
LZ1593	MG1655 (*λD-mNeongreen cI$_{857}$ bor::Cm^R* 24x*tetO*)[pACYC177 pFtsKi *tetR-mCherry*]	Lysogen for reporting phage DNA replication during induction	This work
λLZ613	λcI$_{857}$ bor::KanR	Wild type phage, non-fluorescent	This work
λLZ1575	λ*D-mNeongreen cI$_{857}$ bor::Cm^R* 24x*tetO*	Phage with gpD reporter and tetO array for replicated DNA reporter	This work
λLZ1576	λ*D-mNeongreen cI$_{857}$-mKO2 bor::Cm^R* 24x*tetO*	Phage with gpD reporter, cI reporter, and tetO array for replicated DNA reporter	This work

Table 3.1 Bacteria and phage strains used in this work.

Methods

Bacteria and phage strains

Bacteria and phage strains used in this study are listed in Table 3.1. The bacterial triple reporter strain was constructed by first inserting the *seqA-mKO2* construct into *E. coli* MG1655 using red recombination. The SeqA construct was marked by a chloramphenicol resistance cassette (CmR), which was flanked by FRT sites. After the construct was successfully inserted, the resulting strain was transformed with a plasmid, PCP20, which is used to recombine the FRT sites to "flip" out the CmR from the strain. PCP20 functions by having both its recombination activity and plasmid replication under temperature-sensitive control. Briefly, a TSS protocol was used to transform the cells with PCP20, and the cells were grown at 30C on LB plates supplemented with ampicillin, to select for PCP20, and in the absence of Cm. For the resulting colonies, PCP20 activity was induced by picking colonies and growing colonies in LB at 37C for about one hour to both activate its recombination function and to cure the cells of PCP20. These cells were diluted and plated on LB plates, and these colonies were tested to ensure that they lost their CmR marker, were cured of PCP20, and they were imaged to ensure that the *seqA-mKO2* construct remained. We then constructed a *dnaB-mTurquoise2* MG1655 strain using red recombination, where this reporter construct has a CmR marker. We then transduced this DnaB reporter into the markerless SeqA reporter strain using P1 transduction. We then transduced the Δ*dam::KanR* construct, described in chapter II, into this SeqA DnaB reporter strain. Finally, we transformed the pACYC177 pFtsKi

tetR-mCherry plasmid into this strain, to produce our strain with the triple TetR, SeqA, and DnaB reporter for infections.

To produce a reporter phage to use with the triple reporter strain, we constructed the phage similarly to the phage in chapter II. For this phage, the lytic reporter was *D-mNeonGreen* (D-mNG) and the lysogenic reporter was *cI-mKO2*, because these colors interfere the least with the cell reporters. We also constructed a version without the *cI* reporter. Briefly, we by constructing D-mNG phage with the bor::CmR marker. We then crossed this phage with *cI-mKO2* phage with the bor::KanR marker, or another bor::KanR phage without the *cI* reporter. We then use this *D-mNeonGreen cI-mKO2* (or lacking the CI reporter) bor::KanR phage and titer it onto cells with both a pLate*D plasmid and a plasmid with a 24x tetO array marked with bor::CmR, to recombine the array into the phage, producing a phages to use with the triple reporter cells.

RNA smFISH

pR (*cII*) probes were synthesized and labeled with Cy5 (GE Healthcare Life Sciences, #PA15000) following earlier protocols[197]. The pRE (*cI)* probes were designed following a previous study[186], pre-labeled with TAMRA (Biosearch Technologies). The pR′ probes were designed for the *S, R, Rz/Rz1* genes and labeled with AlexaFluor488.

To detect mRNA after infection, *E. coli* MG1655 was used as the host. The overnight culture was diluted 1:1000 into fresh LBMM (LB with 0.2% maltose and 10 mM $MgSO_4$) and grown at 37 ^oC with shaking at 265 rpm until reaching OD_{600} of ~0.4. The cells were then collected by centrifugation at 2000 ×g for 15 min and re-suspended in 1/10 volume of pre-chilled LBMM. For each sample to be collected, 1 ml of

concentrated cells was used for infection. Appropriate amount of phages were added to reach API of 0.1-0.2 and mixed well. For negative control, add the same volume of SM buffer (phage buffer, 100 mM NaCl, 10 mM $MgSO_4$, 0.01% gelatin, 50 mM Tris-Cl, pH 7.5) to the sample. The samples were incubated on ice for 30 min to allow phage adsorption, then transferred to 35 ^oC water bath and incubated for 5 min to allow phage DNA ejection. After this step, 750 μl of each sample was transferred to 7 ml of pre-warmed LBGM (LB with 0.2% glucose and 10 mM $MgSO_4$) and incubated in a 30 ^oC water bath with mild shaking at 225 rpm. At the specific time point, the sample was poured into a 50 ml tube with 860 μl of 37% formaldehyde (final concentration 3.7%) to allow quick fixation, and incubated for 30 min at room temperature using a nutator. The samples were then treated following protocols from previous reports[197].

Microscopy imaging

Information regarding the instrumentation of imaging is described in chapter II. The imaging protocol differs slightly from chapter II. The triple reporter cells are first grown as an overnight in M9M, and are then diluted about 1:1000 the next day in 5 ml of fresh M9M with all antibiotics. This culture is grown for about 16-18 hours overnight, to an OD600 ~ 0.2-0.4. One ml of the culture is centrifuged and resuspended in ~200 μl of room temperature M9M. 20 μl of this cell suspension is then mixed with 20 μl of the phage solution to make the infection mixture. The infection mixture is then incubated in a 35C water bath for 4 min, and 1 μl of the warmed infection mixture is spotted onto a M9M 1.5% agarose pad, on a long cover slip. When the spot dries into the pad, it is overlaid with a small coverslip and is ready for imaging.

The imaging program is similar as in chapter II, where the initial program to locate the phages is the same. For time-lapse imaging, images are taken every 10 min. To image the smFISH samples, after suspension of the cells in 2×SSC, 1 μl of the sample is placed on a cover slip and overlaid with a piece of 1.5% agarose pad (prepared with 1×PBS). The sample was then imaged immediately on our microscope. Images were taken using 100× objective (Plan Fluo, NA 1.40, oil immersion) with standard filter sets and a cooled EMCCD camera (iXon 3 897, Andor, Belfast, United Kingdom).

DNA FISH

For DNA FISH, probes were produced by PCR amplifying phage lambda (40-43kb region) and treating the purified PCR product with a PromoFluor labeling kit to generate DNA-dye fragments ranging from 100-500 bp. To perform DNA FISH on infection samples, cells were grown as described above and samples were collected at given time points by fixing the cells in a 3.7% formaldehyde solution. Further fixation, permeabilization, and hybridization was performed as described in a previous study[198]. Briefly, the cells were treated with lysozyme for 5 min, washed, and then applied to poly-L-lysine-treated slides. The cells were then dehydrated with ethanol and dried before hybridization. For hybridization, 160 ng of the labeled DNA fragments were denatured at 75 ^{o}C for 5 min and placed on ice. The probes were then applied onto the cell samples on the slide, overlaid with a coverslip and sealed with nail polish. The slide was then placed at 80-85 ^{o}C for 5 min and transferred to 0 ^{o}C briefly. The samples were then placed in a 37 ^{o}C incubator overnight to complete hybridization. The samples were then washed with SSC solution, and stained with DAPI before imaging.

CHAPTER IV

FLUORESCENT NANODIAMOND-BACTERIOPHAGE CONJUGATES MAINTAIN HOST SPECIFICITY

Introduction

Bacteria are found in almost every environmental niche [199]. In order to treat or avoid contracting bacterial illnesses, it is important to have tools to detect the presence of specific bacterial strains within samples[200,201]. Techniques such as ELISA and related sandwich immunoassays can detect bacteria based on specific antibody-antigen interactions [202]; however, antibody production is costly and time consuming. PCR-based approaches may require multiple steps to liberate bacterial DNA and often cannot robustly distinguish between pathogenic and non-pathogenic strains [203]. The enzymatic reagents for these assays may also be unstable or limited by shelf-life considerations.

To facilitate the simple analysis of samples, many diagnostic techniques utilize optical properties such as luminescence, color, or fluorescence [202]. There are multiple agents that can label samples to produce a fluorescent signal, including fluorescent proteins, chemical dyes, and fluorescent particles. Nanodiamonds with nitrogen vacancy defects are an example of a fluorescent particle, also referred to as fluorescent nanodiamonds (FNDs)[204]. They have attractive qualities as labeling agents, such as photostability and biological inertness[205]. Importantly, the nanometer-scale FNDs can be functionalized and then conjugated to different molecules, which confers new functions

to the FNDs. This enables the development of FNDs as useful bioimaging tools in biology and medicine[206].

The crucial issue is whether FNDs can be adapted for detection of specific bacteria. For this purpose, bacteriophages offer a promising approach. Bacteriophages (phages), the viruses of bacteria, are the most numerous and diverse genetic entities in the biosphere. There are many phages that are very specific, capable of precise selectivity of target hosts. A prime example is the bacteriophage lambda, which can infect *Escherichia coli* strains only if the maltoporin LamB is present as the receptor. In this work, we report studies in which we develop methods to conjugate FNDs to the lambda phage particle and use the product conjugates, termed as FND-phages, to detect *E. coli*. The results are discussed in terms of the potential for FNDs as extraordinarily sensitive and stable bio-detection agents.

Results

Functionalization of FND with streptavidin

To stably conjugate FNDs to phages, we sought to functionalize these components with proteins that have a strong interaction. Therefore, we chose to couple FNDs to phage lambda by exploiting the streptavidin-biotin interaction, one of the strongest non-covalent bonds known ($K_d < 10^{-15}$ M)(Fig. 4.1a)[207]. We first surface-labeled FNDs with reactive N-hydroxysuccinimide (NHS) esters, which are well-known amine-reactive esters, and then coupled the biotin-binding protein, streptavidin, to the FND surface. This resulted in streptavidin-functionalized FNDs (streptavidin-FNDs) with the ability to bind biotinylated substrates. We visualized the streptavidin-FNDs

using fluorescence microscopy, where they appear as fluorescent spots, or foci (Fig. 4.1e). We performed dynamic light scattering (DLS) on our FNDs after dilution with both pure water and SM buffer, our phage buffer for experiments (Fig. 4.1f). In water, we measured an average size of 105 nm with a standard deviation of 43 nm for our FNDs. In SM buffer, measured an average of 141 nm with standard deviation of 53 nm for our FNDs. We note that in addition to increased particle sizes in certain buffers, such as SM buffer, FNDs also sometimes form large fluorescent clusters which we observe under the microscope. Normally these can be removed from the FND solution by mild centrifugation prior to use. By incubating the streptavidin-FNDs with a biocytin-functionalized fluorescent dye, we confirmed that the streptavidin-FNDs retained their biotin-binding capabilities (Fig.4. 2a).

Production of biotinylated phage lambda particles

Next we produced phages with biotinylated capsids by exploiting the genetics of phage lambda, using complementation of phage capsid assembly. First, we constructed a plasmid (pLate*D-avitag) in which a modified allele of the lambda *D* capsid decoration gene is expressed from the native lambda late promoter (Fig. 4.1b). In pLate*D-avitag, the *D* allele has been modified to encode a gpD protein with a C-terminal biotinylation signal, or avitag, (amino acid sequence: GLNDIFEAQKIEWHE) following a 15-amino acid linker [208]. During expression, avitag-modified proteins are post-translationally biotinylated by the endogenous BirA activity in *E. coli* [209]. During induction of plasmid-bearing lysogens, transactivation of the plasmid-borne *D*-avitag allele should result in the decoration of progeny virions with the biotinylated gpD-avitag proteins [210]. Indeed, we found that Dam phages (λ1257) propagated in the presence of this plasmid form plaques on a non-permissive host bearing the plasmid, indicating that the modification of gpD does not impair morphogenesis (Fig. 4.1c). Notably, WT phages (λLZ613) form plaques similarly whether in the presence or absence of the plasmid, indicating that the modified gene product does not affect morphogenesis when an alternate source of functional gpD is present.

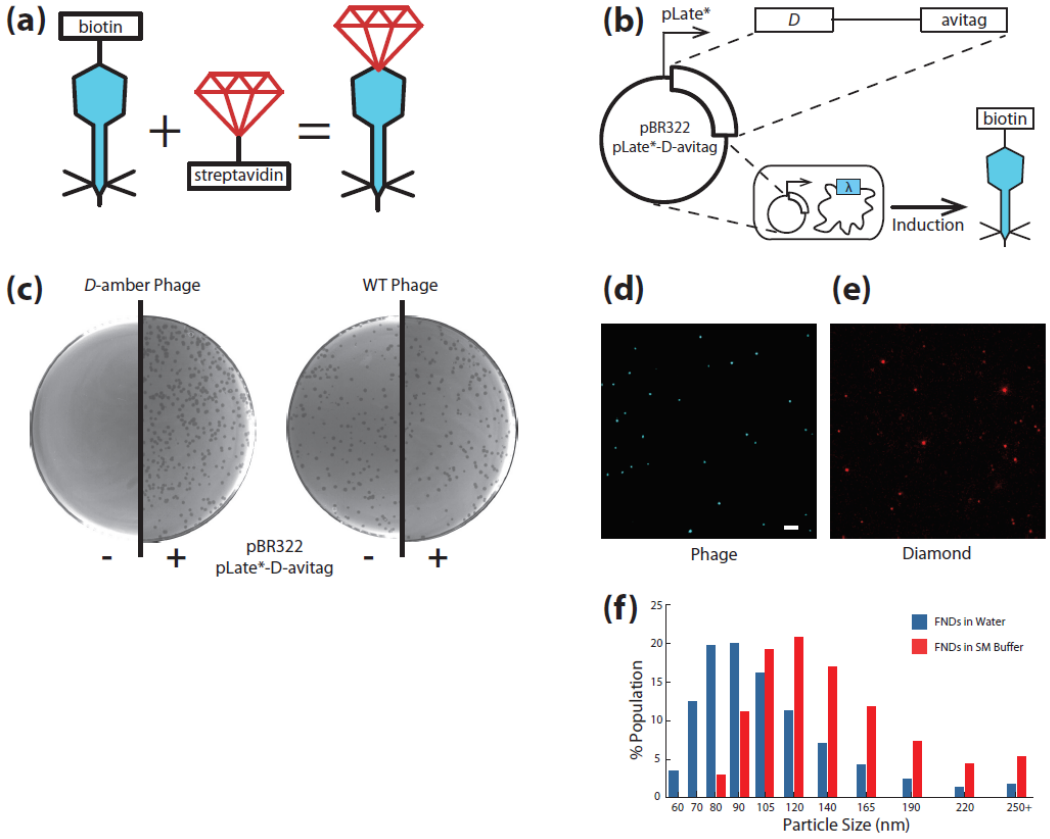

Figure 4.1 Producing biotinylated-phages for streptavidin-FND conjugation and visualization.
(a) Schematic of FND-phage conjugation. Streptavidin-FNDs are mixed with biotinylated phages to produce FND-phage conjugates from the streptavidin-biotin interaction. (b) Production of biotinylated phages from lysogen induction. A lambda *D* allele encoding a D protein modified with a biotinylation oligopeptide signal (avitag) was cloned under the native late gene promoter (pLate*) on a medium-copy plasmid, producing pBR322-pLate*D-avitag. The avitag-modified D protein is expressed by transactivation during the induction of the lambda prophage, post-transcriptionally biotinylated, and assembled onto the progeny virions. (c) Complementation of *Dam*. The lambda *Dam* phage (λ*LZ*1257) forms plaques on the host carrying the D-avitag plasmid mutant but not on the host without the plasmid. WT lambda phage forms plaques on hosts with or without the plasmid. (d and e) Visualization of biotinylated phage and FNDs. Purified phage lysate (λ*LZ*1476)(d) and streptavidin-FNDs (e) were imaged using a fluorescent microscope at 250x magnification with the proper filters. Phages and FNDs are visualized as fluorescent foci in their corresponding colors. Scale bar = 2 μm.
(f) Dynamic light scattering measurements of FNDs. The size of the streptavidin-FNDs were measured with DLS for FNDs suspended in water and SM buffer. In water, the FNDs had an average size of 105 ± 43 nm. In SM buffer, the FNDs had an average size of 141 ± 53 nm.

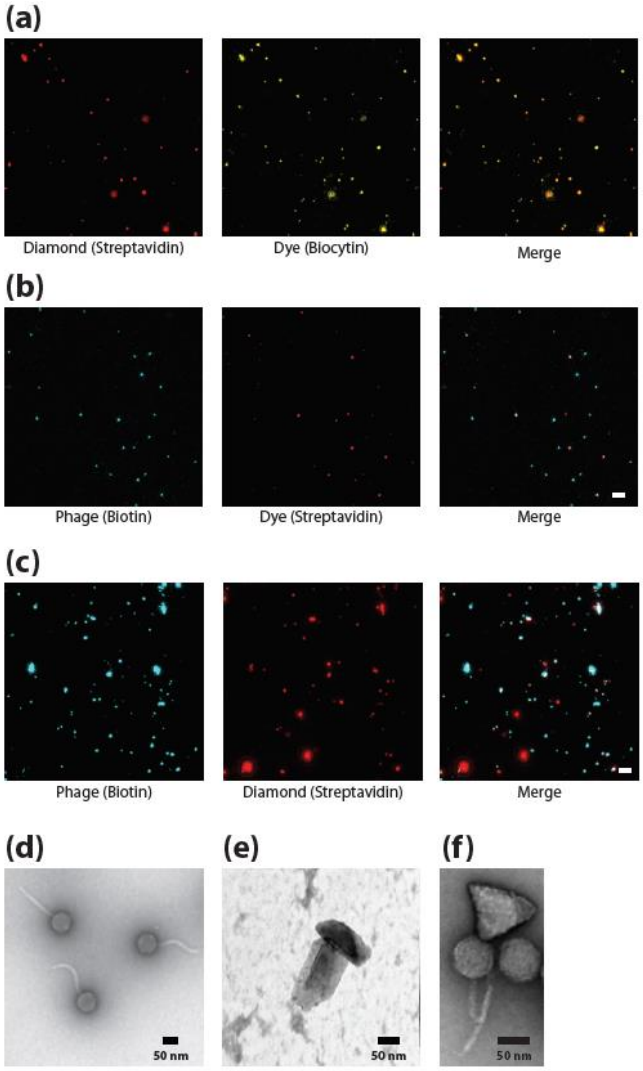

Figure 4.2 Biotin and streptavidin functionalized to phages and FNDs retain their ability to bind.
(a) Streptavidin-FNDs bind to biocytin-functionalized dye. A mixture of biocytin-AlexaFluor488 and streptavidin-FNDs was imaged using the proper filters (FNDs in red, dye in yellow). Co-localizing fluorescence signals indicates binding of dye to FNDs. (b) Biotinylated phages bind to streptavidin-functionalized dye. A mixture of streptavidin-AlexaFluor568 and biotinylated phages (λLZ1476) was imaged using the proper filters. Co-localizing fluorescence signals indicates binding of dye to phages. (c) Biotinylated phages bind to streptavidin-FNDs. A mixture of streptavidin-FNDs and biotinylated phages (λLZ1476) was imaged using the proper filters. Co-localizing fluorescence signals indicates binding of FNDs to phages. Scale bars in a-c = 2μm. (d – f) Transmission electron micrographs of phages, FNDs, and FND-phage. Representative image of biotinylated fluorescent phage lysate (λLZ1476)(d). Representative image of a suspension of streptavidin-FNDs (e). Representative image of a FND-phage conjugate from a biotinylated phage and streptavidin-FND mixture.

Production of FND-phage conjugates

To assess the efficiency of FND complexing with phage particles, we chose to biotinylate a phage carrying a fluorescent *D* gene (λLZ1476). This phage, established in our previous work, allows us to observe individual phages with fluorescence microscopy (Fig. 4.1d)[211]. Thus both the phages (Fig. 4.1d) and FNDs (Fig. 4.1e) could be visualized at the same magnification with different filter cubes [205]. Importantly, we purified our biotinylated phages prior to experimentation because crude phage lysates would contain an excess of biotinylated proteins, which would overwhelm the completed phage particles for FND conjugation. We confirmed that these biotinylated fluorescent phages retained the ability to bind to streptavidin by incubating the phages with a streptavidin-functionalized dye (Fig. 4.2b).

With these functional modifications in place, we then validated that streptavidin-FNDs and biotinylated fluorescent phages would form conjugates. We mixed the streptavidin-FNDs with a vast excess (approximately 50:1) of our purified biotinylated phage preparation. These conditions promoted the production of phages conjugated to single FNDs, as indicated by phage particles co-localizing with FND particles (Fig. 4.2c). As the FNDs agglomerate with some frequency, there are multiple phages around larger FND clusters. Of note and as expected, there were still unbound FNDs, and the large majority of the phages were not conjugated to FNDs. We suspect that the biotinylation efficiency of the phages was heterogeneous, due to limiting endogenous BirA activity, which may have contributed to the unbound FNDs. Transmission electron microscopy

revealed FND-phage conjugates in which neither the phage particles nor the FNDs showed morphological changes (Fig. 4.2d-f).

FND-phage conjugates adsorb to E. coli *cells*

In order to act a tool to identify bacteria, the FND-phages must retain their ability to bind to their host cells, so we assayed whether the FND-phages adsorb to *E. coli* cells using fluorescence microscopy. Lambda-sensitive host cells were incubated with FND-phages for 5 min at 35 ^{o}C, washed of free virions by centrifugation, and then visualized by fluorescence microscopy (Fig. 4.3a-b)[211]. We observed FND signals on host cells, where some cells have multiple FND foci (44 FND labeled cells of 108 cells observed); most of these individual FND foci (48 co-localized FND/phage foci on cells of 56 FND foci on cells in total) had a corresponding phage focus, suggesting that the actual FND-phage conjugate is bound to the cells (Fig. 4.3b). Similar results were obtained with phages lacking fluorescent proteins (λLZ1475)(Fig. 4.3c-d); 76 of 218 cells visualized had FND labeling under the same incubation and washing conditions. These data indicate that fluorescence-labeling of the phages was dispensable for the FND conjugation and subsequent cell labeling.

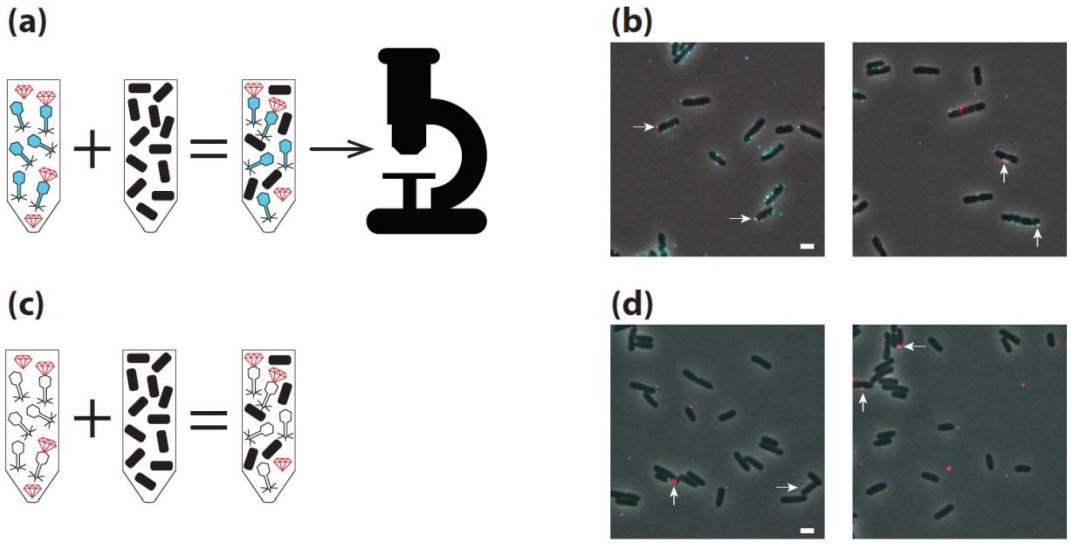

Figure 4.3 FND-phages bind to WT *E. coli* host cells.
(a) Schematic of FND-phage adsorption imaging, using fluorescent phages (λLZ1476).
(b) Representative images of FND-phage adsorption assay. FNDs are red foci and phages are cyan foci. Arrows point to FND-phage conjugates attached to cells. 44/108 cells have a red FND focus attached. 8/108 cells have a red FND focus attached without a co-localized cyan phage focus.
(c) Schematic of FND-phage adsorption imaging, using non-fluorescent phages (λLZ1475).
(d) Representative images of FND-phage adsorption assay using non-fluorescent phages. FNDs are red foci. Arrows point to FNDs attached to cells. 76/218 cells have a red FND focus attached. Scale bars = 2μm.

FND-phage conjugates retain receptor specificity

Phage lambda infection has an absolute requirement for the maltodextrin-specific outer membrane porin, LamB [14]. To demonstrate that the FND-phage retained this specificity, the adsorption experiments were repeated with isogenic *lamB*$^-$ mutant hosts. As expected, with the *lamB*$^-$ strain there were no FND-phages bound to the cells, and very few cells with phages adsorbed at all (Fig. 4.4a). We observed some cells with FNDs apparently attached (12/168), but these FNDs had no corresponding phage focus, indicating that there is a basal level of random co-localization of the FNDs to these *lamB*$^-$ *E. coli* cells, similarly to WT cells. We next tested whether the FND-phages could selectively bind to their proper host within a mixture of targets and non-targets. To distinguish the lambda-resistant cells from WT cells, we used isogenic *lamB*$^-$ mutants carrying a plasmid that expresses EYFP. When we infected a mixture of sensitive and resistant (*lamB*$^-$) cells with the FND-phage preparation, we found that lambda particles, irrespective of FND-conjugation, bound to the sensitive cells, as expected (Fig. 4.4c-d). These data indicate that these FND-phages were able to identify a specific target cell in a population, and in principle, suggest this selection could extend to more complex mixtures as well.

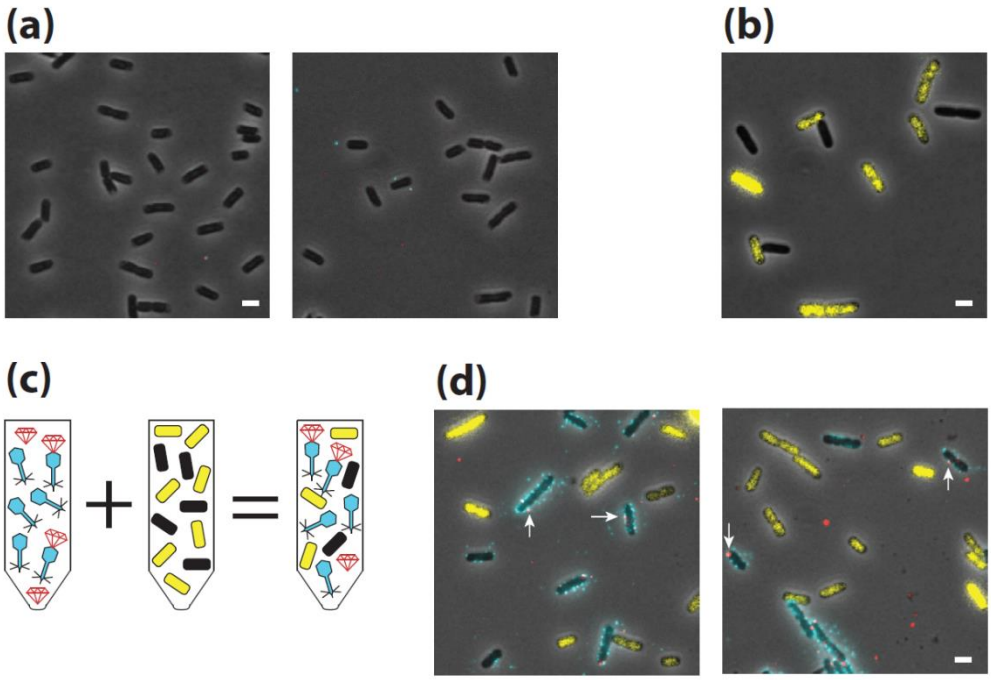

Figure 4.4 FND-phages properly target host cells in a bacterial mixture with non-target cells.

(a) FND-phages do not bind to cells lacking the phage receptor, LamB. FND-phages were mixed with isogenic *lamB*$^-$ mutants of MG1655 (LZ1561) and imaged. Phages, both free and FND-conjugated, require LamB to adsorb to cells.

(b) Visualizing target and non-target (*lamB*$^-$) bacteria of phage lambda. A plasmid that expresses an EYFP fusion protein was transformed into the *lamB*$^-$ mutant. Cultures of this plasmid-bearing mutant (LZ1564) were mixed with the WT host cells and imaged with the proper filters. Plasmid-bearing mutants appear as yellow cells and WT cells do not have yellow signal.

(c) Schematic of FND-phage adsorption assay using a mixture of target and non-target bacteria.

(d) Representative images of FND-phage adsorption assay, using target and non-target bacteria. FNDs are red foci and phages are cyan foci. The non-target *lamB*$^-$ cells (LZ1564) are yellow, whereas the target cells are not yellow. Arrows point to FND-phage conjugates attached to target host cells. Yellow cells are bound by fewer phage foci. Scale bars = 2 μm.

Discussion

In this study, we functionalized FNDs to conjugate to correspondingly modified phage particles and demonstrated that this technique can specifically label and identify the natural host bacteria of the phage. The FND-phages were able to distinguish their proper target from an isogenic, non-target *E. coli* strain. In theory, this system could confirm the presence of a given bacterial strain from a complex mixture of bacteria, from an environmental or clinical sample for example, and be used as a means to diagnose contamination or infection.

As a particle-based fluorescence method, FNDs are easily modified and have excellent physical properties. There are advantages for using FNDs as opposed to another particle-based labeling method, quantum dots (QD), for certain applications [212]. The FNDs have been reported to be generally non-toxic, although poorly cleaned detonation nanodiamonds with varying sizes or with certain surface groups have been reported to have antibacterial properties[213-215]. We use crushed HPHT nanodiamonds instead of detonation versions, which are cleaner to start with, coupled with oxidative cleaning, which has been shown to attenuate toxicity (Materials and Methods). Though we have not tested with bacteria, we have confirmed that nanodiamonds are not toxic to cultured animal cells and human leukocytes[216,217]. Regarding the toxicity of QDs, some may contain heavy metals, which have been reported to be toxic[218,219]. Furthermore, QDs have been shown to exhibit "blinking" behavior during imaging [220], whereas FNDs have been reported to fluoresce stably, which can improve imaging quality [221].

As a tool for bacterial identification, phages are versatile and abundant in nature. The specificity of the phages for bacteria is a tunable property with proper genetic tools. Whereas we used phage lambda, which has an extremely specific host, other phages are capable of attaching to a broad range of bacteria. For example, phage P1 infects and propagates in *E. coli*, but it is also able to adsorb and translocate its DNA into other bacteria such as *Salmonella typhimurium*, *Klebsiella aerogenes*, and *Myxococcus xanthus*[191,222]. This diversity among phages is advantageous for their development as tools. Consider the need to distinguish pathogenic bacteria from non-pathogenic strains, which might be very similar to each other. The presence of certain surface features such as specific pili or lipopolysaccharides may be among the minor differences between these strains[223,224]. For example, *E. coli* O157:H7 is a serotype that causes disease, and phage φV10 is specific for this strain, recognizing the O-antigen[225]. Variations in this antigen can confer resistance to phage infection to demonstrate the specificity of certain phages to specific strains [226].

We demonstrated one type of functionalization for our FND-phage conjugation technique in this study, and our method may be refined further. We did not separate the FND-phages from free FNDs and non-FND-phages prior to infection, but further purification may be useful for additional applications. For example, free, functionalized FNDs may have stronger affinities for unknown components in more complex samples, which could produce false positive results. Additionally, the non-FND-phages, if not removed, could cause problems in other applications where the FND-conjugation is the sole means of visualizing a non-fluorescent phage, because there would be "invisible"

phages present. Using our current protocol, we could not guarantee that each phage would have a biotinylated capsid. This is because each phage contains capsid components assembled randomly from three sources under our current system: in-*cis* fluorescent proteins from the phage, in-*trans* biotinylated proteins from the plasmid, and in-*trans* non-biotinylated proteins from the plasmid, as in-*vivo* biotinylation efficiency does not reach 100%. This effect may be mitigated by using a phage that cannot produce its own capsid decoration protein, which increases the probability of having biotinylated phages.

As a future direction, we propose to develop a protocol to quickly test samples without single-cell microscopy. We note that our current protocol displays some falsely positive FND-binding (Fig. 4.3 and 4.4), which may be alleviated with washing steps for samples affixed to a slide or in a plate. This would allow us to compare our method with other techniques, such as PCR-based or culture-based methods for bacterial identification [227]. Culture-based methods are theoretically capable of detecting a single colony-forming unit (CFU), as a single bacterium can grow into a colony over time. It may take up to a day to culture an observable colony. When bacterial culturing is combined with mass spectrometry, the time needed to achieve detection may be reduced[228,229]. Contamination is a potential cause of false positive results for cultures, and lack of bacterial growth (from cell death for example) might result in false negatives. PCR-based methods are also theoretically capable of single CFU or DNA detection. The preparation and running of PCR samples occurs over a few hours. False positives and

negatives can both occur due to the reactivity of primers or degradation and contamination of DNA.

We established that the streptavidin-biotin interaction functions as a conjugation method, but this required genetic manipulation of our phage, which may not always be a possibility when working with different phages. As a solution, the FNDs may be functionalized with a (bio)chemical group that will react with more promiscuity, as there are many possible chemical modifications for bioconjugation and FNDs are capable of being modified in many ways [230]. For example, maleimide will produce a chemical bond with cysteine, so it may be possible to bioinformatically search for phages with exposed cysteine residues for labeling other phages with maleimide-functionalized FNDs. Another possibility to bypass phage genetic engineering would be to functionalize the FND with an antibody, raised against a phage or phage protein, which would then enable the FND to specifically bind to the phage.

This fluorescent labeling of phages also has applications unrelated to diagnostics. This technique could add to the repertoire of labeling techniques for phages to use in live-cell experiments, which currently consists of various fluorescent protein, dye, and QD-based methods [12,133,137,211,231]. Because this technique may be modified to bind more generally to phages, it could eliminate the need for genetic modification of the viruses. This could enable the single-cell/virus characterization of many different phages, which may not have previously been possible. These FNDs do not photobleach after exposure to light like fluorescent proteins do, which may improve long-term imaging capabilities for certain applications. Additionally, FNDs may be produced with different defects to

fluoresce in different colors, such that multiple phage types can be labeled and imaged simultaneously[232,233].

FND-phage labeling is an adaptable technology with a great amount of potential. As a means to identify target bacteria, it is simple to handle and quick to produce, while also retaining incredible specificity, honed over millions of years of evolution. Our results, using a well-established system, showed that the natural behaviors of the system are maintained, which is an important conclusion for future work. The actual FNDs may be functionalized in a myriad of ways for a multitude of purposes, where we only characterized a single example. FNDs may also be used as sensors of properties such as temperature, magnetic fields, electric fields, among others, so there is much that may be explored by applying this technology[234-236].

Finally, we note that the nanodiamonds used in this experiment are similar in size to the phage heads which might affect labeling efficiency. We are actively developing smaller and brighter nanodiamonds [arXiv:1702.06854v1] to overcome this limitation, and to allow labeling of other parts of the phage (not just the head). This may eventually allow super-resolution imaging of the phage-bacteria interaction.

Strain #	Strain Name	Comments	Source
-	MG1655	Wild type *E. coli*	Lab Stock
LZ1467	MG1655 [pBR322-pLate**D*-avitag]	Wild type *E. coli* with gpD-avitag expression	This work
LZ1561	MG1655 *lamB*::Kan^R	*E. coli* with *lamB* knockout	Lab Stock
LZ1564	MG1655 *lamB*::Kan^R [pLAU52 *tetR-eyfp*]	*E. coli* with *lamB* knockout and *eyfp* expression	This work
LZ1476	MG1655 (λ*D-mTurquoise2 cI$_{857}$-mKO2 bor::Cm^R*)[pBR22-PLate**D*-avitag]	Lysogen, induced to produce biotinylated, fluorescent phage	This work
LZ1475	MG1655 (λ*Dam cI$_{857}$ bor::Kan^R*)[pBR322-PLate**D*-avitag]	Lysogen, induced to produce biotinylated, non-fluorescent phage	This work
λLZ613	*λcI$_{857}$ bor::Kan^R*	Parental phage	Lab Stock
λLZ1257	*λDam cI$_{857}$ bor::Kan^R*	*D* nonsense mutant	Lab Stock
λLZ1476	*λD-mTurquoise2 cI$_{857}$-mKO2 bor::Cm^R* (biotinylated gpD)	Fluorescent, biotinylated phage produced from LZ1476	This work
λLZ1475	*λDam cI$_{857}$ bor::Kan^R* (biotinylated gpD)	Non-fluorescent, biotinylated phage produced from LZ1475	This work

Table 4.1 Bacterial strains, plasmids and phages used in this work.

Materials and methods

Bacterial strains and phages used for this study are listed in Table 4.1.

Production of streptavidin-FNDs

The fluorescent nanodiamonds used in this study were prepared by Columbus NanoWorks Inc. Briefly, 100 nm crushed HPHT nanodiamonds, having a nitrogen concentration between 100 to 150 ppm, were submitted to electron irradiation as described by others[237,238]. Following electron irradiation, the diamonds were annealed under argon gas at 800 ^{o}C for 6 hours.

The FND particles were then refluxed at 70 ^{o}C for three days, then diluted with deionized H2O, and finally centrifuged at 900 rpm. After centrifugation, the pellets were extensively rinsed with deionized H2O. This cleaning procedure removes graphite from the FNDs and oxidizes the alcohol and carboxyl groups on the surface of the FNDs[239,240]. The FNDs were reacted with glycidol (Sigma-Aldrich, St. Louis, MO) according to published procedures to create a hydroxyl-terminated surface[241,242]. The FNDs were rinsed thrice with dimethylacetamide (DMAC, GFS Chemicals), and resuspended in the same solvent. This was diluted into dimethylformamide (DMF, GFS Chemicals) containing 200 mM N N'-disuccinimidyl carbonate (DSC, EMD Millipore, Billerica, MA) and allowed to react for 4 hours at room temperature. Unreacted DSC was removed by washing three times in DMAC then quickly rinsed once in cold 0.05 M 4-(2-hydroxyethyl)-1-piperazineethanesulfonic acid (HEPES, GFS Chemicals), pH 7.4, containing 0.05% Tween 20 (Sigma-Aldrich). The NHS-activated FNDs were resuspended in the same buffer containing 2 μmoles of streptavidin (Prozyme). The

reaction was incubated for 2 hours at room temperature, before quenching with ethanolamine for 30 minutes at room temperature. The streptavidin-FNDs were rinsed in and re-suspended in HEPES and stored at 4 ^{o}C.

Staining functionalized FNDs and phages with functionalized dyes

The streptavidin-FND (Columbus Nanoworks) suspension (concentration in the range of $10^9 – 10^{10}$ particles/ml) was mixed with AlexaFluor488-biocytin dye (2 μg/ml)(ThermoFisher) at a 1:1 volume ratio in a microcentrifuge tube for 10 minutes at room temperature to stain the FNDs. A dilution of biotinylated purified phage lysate (about $1x10^{10}$ pfu/ml in concentration) was mixed with AlexaFluor568-streptavidin (2 μg/ml)(ThermoFisher) at a 1:1 volume ratio in a microcentrifuge tube for 10 minutes at room temperature to stain the phages. The stained FNDs/phages were imaged under PBS-agarose pads.

FND conjugation to phages

10 μl of a streptavidin-FND suspension was mixed with 200 μl of purified phage lysate (over $2 x10^{11}$ pfu/ml in concentration) in a microcentrifuge tube and placed on a tube rotator for 30 minutes at room temperature. This FND-phage mixture was then stored at 4 ^{o}C when not in use. Over time, FNDs will settle to the bottom of the tube and they may be resuspended by gentle pipetting.

FND-phage adsorption imaging assay

A colony of wild type host *E. coli*, MG1655, is grown in LB+10mM $MgSO_4$+0.2% maltose (LBMM) overnight at 37 ^{o}C. This overnight culture is then diluted 1:100 into fresh LBMM and grown to OD_{600} ~0.4 at 37 ^{o}C, to reach exponential phase, and then

centrifuged at 4 ^{o}C. The pellet is then resuspended in one-tenth of the original volume using cold SM buffer. 30 µl of this cell suspension is mixed with 30 µl of the FND-phage mixture, and is then placed into a 35 ^{o}C water bath for 5 minutes. 500 µl of room temperature SM is added to this infection mixture and this new mixture is centrifuged at room temperature for 3 minutes 2000x g to pellet cells/infected cells. The pellet is then resuspended using 200 µl of room temperature SM buffer, and 1 µl of this suspension is placed onto a PBS-agarose pad for imaging.

For the *lamB*$^{-}$ infection, the same protocol as above was performed, with the addition of kanamycin (50 µg/ml) in the growth medium.

For the mixed WT and *lamB*$^{-}$ infection, the cells were grown as described above, and then mixed together following the initial resuspension in cold SM buffer, at an appropriate ratio. The FND-phage mixture infection remains the same as above.

Microscopy imaging

Imaging was performed on a Nikon Eclipse Ti inverted epifluorescence microscope using a 100x objective (Plan Fluo, NA 1.40, oil immersion) with a 2.5x TV relay lens, using a mercury lamp as the light source (X-Cite 200DC, Excelitas Technologies), within a cage incubator (InVivo Scientific) at 30 ^{o}C, and acquired using a cooled EMCCD (electron multiplying charge-coupled device) camera (iXon3 897, Andor, Belfast, United Kingdom). The fluorescent filters used in the study were as follows (Xnm, Yex [bandwidth] excitation filter/dichroic beamsplitter wavelength/Xnm, Yem [bandwidth] emission filter/company): cyan (436 nm, 20ex/455 nm/480 nm, 40em/Nikon), yellow (500 nm, 20ex/515 nm/535 nm, 30em/Nikon), and red (560 nm,

40ex/585 nm/630 nm, 75em/Nikon). The images are acquired with these exposures: phase-contrast (100 ms), red (500 ms), yellow (100 ms), and cyan (200 ms). These color names correspond to the filters used for the colors shown in the images.

TEM imaging

FNDs in water (10^9 FND/ml), phages in SM buffer (10^{10} pfu/ml), and the FND-phage mixture in SM buffer (10^{10} pfu/ml and 10^8 FND particles/ml) were stained with 0.2% uranyl acetate (in water) (Electron Microscopy Sciences, Hatfield, PA) prior to imaging. 1 µl of the mixture was placed onto a carbon grid (Dune Science, Eugene, OR) and allowed to attach for 2 minutes. The grid was investigated by a transmission electron microscope (TEM) at high (180kx-2571pixels/µm) and low (28kx-421pixels/µm) magnifications. The electron microscope operates at 80KV (Morgagni, FEI company, Hillsboro, OR). High-resolution images of the sample were collected by a MegaViewIII digital camera operated with iTEM software (Olympus Soft Imaging Systems, Germany).

CHAPTER V

SUMMARY AND CONCLUSIONS

In our work, we developed new tools to interrogate phage lambda development and decision-making at single cell/virus and subcellular levels to elucidate the hidden, detailed mechanisms that occur during this viral infection. Such mechanisms were clouded by limitations in technology before, but we were able to innovate new approaches to surpass these limits, and with future effort, we can further develop these tools to bring a full understanding of cellular decision-making closer to reality.

Cellular decisions emerge from subcellular interactions

The notion of individuality among viruses was suggested in a study on phage lambda, particularly with regards to how lambda commits to its decision-making. This provided us with the onus of investigating phages as separate entities during infection, which we accomplished by separating decision-making reporters in different phages. This technique granted phages individual "voices" despite ostensibly being identical, to allow us to track the viruses separately. We found a surprising set of interactions where different decisions show different behaviors. When different phages infect a cell, there is a competition, which typically results in one winner. With our new tools, we were able to directly observe that the phage develops itself, as the individual, at the cost of other phages. Our computational models suggested that cellular resources for DNA replication were the crux of the competition, where one phage can monopolize the resources to silence the other. This competition typically only played out in this manner during lysis

however, which is the pathway that produces many phage DNAs and new progeny. That the phage selfishly propagates "itself" in this situation was particularly interesting, as it implies that the phage somehow preferentially differentiates self from non-self. In contrast, during lysogeny, different phages display a sort of cooperation, where multiple phages will often propagate in one cell as multiply-integrated prophages. We concluded that this lack of competition was due to a reduced importance of phage DNA replication during lysogeny. Without the event that inspires competition, another interaction prevailed, which might promote diversification through cooperation to perhaps increase evolutionary fitness. Supporting that phages can be individuals in the cell, disagreements between cellular decisions occur as well, where both lytic and lysogenic pathways coincide. Of particular note, even a cell infected by a single phage could disagree with itself, which needed explanation. We concluded that replicated sister phage genomes had some degree of individuality, as there is no genetic difference between identical genomes arising from replication and genomes from co-infections. This suggests that viral individuality originates from the phage DNA level.

We may further explore phages as individuals by utilizing different phage mutants. From single-cell analysis of co-infections of different mutants, we expect to demonstrate how mutant phages develop in a biased manner, to support "themselves" in the cell. We hypothesize that certain proteins prefer in-cis action, such as reported for the Q protein, which we may characterize by using our fluorescent reporters. Whereas our results with mixed wild type phages show that phages dominate each other in lysis evenly, mutant phages, with cis-preferences should show skewed results for pure lysis

events. These specific protein behaviors may have evolved to allow phages to persist in nature. We can then explore how competition and cooperate affect phage populations, so we may directly test the effects of the interactions. By quantifying the composition of the lytic and lysogenic populations from mixed-phage infections at the ensemble level, we expect to find that different mutant phages will establish themselves in the populations differently, depending on the nature of their own proteins, and the other phages' specific mutations in the experiments. We can then collect the lytic progeny population, which represents the immediate change of infective phages over one generation, to re-infect naïve cells. By repeating this process, we will characterize how interactions change the population of phages over generations. We may vary our selection pressures as well, by collecting the lysogenic population, discarding the lytic population, and inducing the prophages to produce a new infective population. By changing our patterns of which type of progeny we collect, we can characterize the influence of competition and cooperation across different environmental conditions.

Phage-formed microenvironments mediate heterogeneous development

There is much unknown complexity in the simple lambda system. The results that we gained from examining phage interactions raised questions about how multiple phages, which are simply strands of DNA, can create and maintain individuality in a single cell. We realized the need for different tools to address these curiosities, and focused on investigating lambda development with special attention paid to spatial analysis. Organization permeates all strata of life, from ecosystems all the way down to the sub-subcellular levels. Phages, simpler than many eukaryotic viruses, which might

not even be considered actual life, also carry out life processes, so there is a high probability that phage development is organized. We combined multiple tools to target individual phage DNA molecules, replicated phage genomes, essential cellular resources, phage mRNAs, and phage decision-making to approach the study of spatial organization during lambda development. We found that single lambda genomes manipulate their subcellular environments to sequester resources and confine phage DNA replication to certain areas of the cell. We concluded that phages confine the bulk of their mRNA to these same areas, and assemble new progeny phages there as well. All of these processes comprise a phage factory, or "phactory" as we call it. This might be part the mechanism that explains our previous results, because multiple phactories can arise in the same cell, from different infecting phages, or from replicated phage DNAs that move around in the cell. These separate phactories are quantitatively different from each other at the DNA and RNA levels, and furthermore, separate areas of the cell are capable of executing different decision-making transcriptional programs, which could explain our phage voting phenomenon. This study underscores how the tools that we develop play important roles in tackling different problems.

For future directions, we recognize that our current characterization of separately functioning viral microenvironments is incomplete due to the limited resolution of our microscopy techniques. We believe that each phactory that we observe is a population of phage DNA and its related activity, and that phactories have additional structure. We propose to explore the architecture of a phactory using super-resolution microscopy. From these experiments we expect to quantify how many phage genomes make up the

microenvironments, as well as the number of transcripts and proteins. We will also be able to characterize if and how single strands of phage DNA develop differently in a phactory. Our data suggest that individuality may originate from single viral genomes, and these proposed experiments would support the notion and elaborate on the mechanisms by which this occurs. This line of experimentation will help us distinguish whether this observed individuality is due to deterministic local factors or stochasticity in biochemical activities. We might be able to ascertain the immediate local environment of each phage DNA via super-resolution microscopy, in terms of the level of transcripts and proteins by labeling key phage proteins. We may label phage genomes using click chemistry[243], label phage transcripts using a similar technique or with FISH probes[244], and label proteins with either fluorescent protein fusions or antibodies combined with fluorescent probes[245], for combined, targeted super-resolution studies. By comparing the microenvironment of different DNAs and their outcomes, we can define if the behaviors of different DNAs are determined by differences in their environment or if the behaviors may be random even with similar local environments. It has been characterized that membraneless organelles form based on differences in the physical properties of the organelle and its surrounding environment. We propose to discover the physical parameters of the phactory, such as the size of the components and how they diffuse, and relate them to the properties of the surrounding bacterial space. From this, we may show that phactories form due to similar mechanisms as other membraneless organelles in other systems. We can also disrupt the natural bacterial environment or the natural phage processes that we predict to define its physical properties, which should alter how

phactories behave. For example, we observed that different phactories were typically separated by bacterial DNA, as observed from DAPI-staining. Though bacterial DNA is not a barrier like a lipid membrane, it may play an important role in the dissociation of phage components from each other. If we disrupt the localization of *E. coli* DNA with a mutation such as the *dnaC2* mutation[101], the formation of phactories should change as well. Similarly, we could work with DNA-free *E. coli*, which should still support phage development, but would also be expected to display different phactory behavior due to a complete lack of the alleged barriers. Finally, we suggested that the tethering of long mRNA transcripts to phage DNA supports the formation of a local microenvironment. We propose to alter this system to have shorter transcripts to characterize the impact of more diffusible RNA on phactory formation. In theory, phactories should form in a plasmid-based system similarly to how it does in the phage system. If we insert a construct including key proteins from the pR and pR′ transcripts into a plasmid, we should produce phactories similar to actual phage lambda infections, at the DNA and mRNA levels. Furthermore, certain plasmids also localize to distinct areas of the cell, and this localization is based on partitioning systems encoded by the plasmid, which could be a useful tool to force the localization of a phactory to test hypotheses[246,247]. We may then divide the long phage transcripts into multiple short transcripts with single genes on a plasmid to characterize whether separate, small transcripts still localize and form microenvironments. These experiments would elucidate additional mechanistic details about the development of microenvironments.

Fluorescent nanodiamond-phage conjugates identify bacteria

With the ability to label single phage particles, we may actuate studies to delve into the mysteries of microbiological systems. There are other means of labeling virus particles, and there is much potential that can be realized by the development of additional tools. We attached nanodiamond particles to our lambda phage particles to fluorescently label phages to be used to fluorescently label bacteria. These nanodiamonds are remarkably stable, inert, and good for imaging. In principle, we can leverage the natural ability of phages to infect bacteria identify different bacteria, by labeling different phages. As a test case, we retained the desired properties of both the nanodiamonds and phages in an amicable union of engineering and evolution. Due to the facility for chemical modification of nanodiamonds, it is feasible to attach them to different phages, which do not have genetic tools as lambda does. For example, we may raise antibodies against purified, whole phage lysates, which is a process that is fairly reliable and independent of phage genetic modification. These antibodies can be conjugated to nanodiamonds and subsequently attached to phages for bacterial detection. This could enable an expansive range of studies on systems that are currently out of reach. We have demonstrated how we build different tools to solve a variety of problems, and hope to continue building more.

REFERENCES

1 Balazsi, G., van Oudenaarden, A. & Collins, J. J. Cellular decision making and biological noise: from microbes to mammals. *Cell* **144**, 910-925, doi:10.1016/j.cell.2011.01.030 (2011).

2 Mcfarland, D. J. Decision-making in animals. *Nature* **269**, 15-21, doi:Doi 10.1038/269015a0 (1977).

3 Zernicka-Goetz, M., Morris, S. A. & Bruce, A. W. Making a firm decision: multifaceted regulation of cell fate in the early mouse embryo. *Nature Reviews. Genetics* **10**, 467-477, doi:10.1038/nrg2564 (2009).

4 Spencer, S. L. *et al.* The proliferation-quiescence decision is controlled by a bifurcation in CDK2 activity at mitotic exit. *Cell* **155**, 369-383, doi:10.1016/j.cell.2013.08.062 (2013).

5 Malumbres, M. & Barbacid, M. To cycle or not to cycle: a critical decision in cancer. *Nat Rev Cancer* **1**, 222-231 (2001).

6 Sanchez, A. & Gore, J. Feedback between population and evolutionary dynamics determines the fate of social microbial populations. *PLoS Biology* **11**, e1001547, doi:10.1371/journal.pbio.1001547 (2013).

7 Zhou, J. X., Brusch, L. & Huang, S. Predicting pancreas cell fate decisions and reprogramming with a hierarchical multi-attractor model. *PloS One* **6**, e14752, doi:10.1371/journal.pone.0014752 (2011).

8 Bush, R. M. Predicting adaptive evolution. *Nature Reviews. Genetics* **2**, 387-392, doi:10.1038/35072023 (2001).

9 Oppenheim, A. B., Kobiler, O., Stavans, J., Court, D. L. & Adhya, S. L. Switches in lambda development. *Annu Rev Genet* **39**, 409-429, doi:10.1146/ (2005).

10 Ptashne, M. *A genetic switch: phage lambda revisited*. Third edn, (Cold Spring Harbor Press, 2004).

11 Court, D. L., Oppenheim, A. B. & Adhya, S. L. A new look at bacteriophage lambda genetic networks. *Journal of Bacteriology* **189**, 298-304, doi:10.1128/JB.01215-06 (2007).

12 Edgar, R. *et al.* Bacteriophage infection is targeted to cellular poles. *Molecular Microbiology* **68**, 1107-1116, doi:10.1111/j.1365-2958.2008.06205.x (2008).

13 Ptashne, M. Isolation of the lambda phage repressor. *PNAS* **57**, 306-313 (1967).

14 Randall-Hazelbauer, L. & Schwartz, M. Isolation of the bacteriophage lambda receptor from *Escherichia coli*. *Journal of Bacteriology* **116**, 1436-1446 (1973).

15 Gottesman, M. M., Hicks, M. L. & Gellert, M. Genetics and function of DNA ligase in *Escherichia coli*. *Journal of Molecular Biology* **77**, 531-547, doi:Doi 10.1016/0022-2836(73)90221-0 (1973).

16 Gellert, M., Mizuuchi, K., Odea, M. H. & Nash, H. A. DNA gyrase - enzyme that introduces superhelical turns into DNA. *Proceedings of the National Academy of Sciences of the United States of America* **73**, 3872-3876, doi:DOI 10.1073/pnas.73.11.3872 (1976).

17 Mizuuchi, K. & Nash, H. A. Restriction assay for integrative recombination of bacteriophage lambda DNA in vitro - requirement for closed circular DNA substrate. *Proceedings of the National Academy of Sciences of the United States of America* **73**, 3524-3528, doi:DOI 10.1073/pnas.73.10.3524 (1976).

18 Johnson, A., Meyer, B. J. & Ptashne, M. Mechanism of action of the cro protein of bacteriophage lambda. *Proceedings of the National Academy of Sciences of the United States of America* **75**, 1783-1787 (1978).

19 Kobiler, O. *et al.* Quantitative kinetic analysis of the bacteriophage genetic network. *PNAS* **102**, 4470-4475 (2005).

20 Roberts, J. W. Termination factor for RNA synthesis. *Nature* **224**, 1168-&, doi:Doi 10.1038/2241168a0 (1969).

21 Luzzati, D. Regulation of lambda exonuclease synthesis - role of N-gene product and lambda repressor. *Journal of Molecular Biology* **49**, 515-&, doi:Doi 10.1016/0022-2836(70)90261-5 (1970).

22 Learn, B. A., Um, S. J., Huang, L. & McMacken, R. Cryptic single-stranded-DNA binding activities of the phage lambda P and *Escherichia coli* DnaC replication initiation proteins facilitate the transfer of *E. coli* DnaB helicase onto DNA. *Proceedings of the National Academy of Sciences of the United States of America* **94**, 1154-1159, doi:DOI 10.1073/pnas.94.4.1154 (1997).

23 Tsurimoto, T. & Matsubara, K. Purified bacteriophage lambda O protein binds to four repeating sequences at the lambda replication origin. *Nucleic Acids Research* **9**, 1789-1799 (1981).

24 Lebowitz, J. H. & Mcmacken, R. The *Escherichia coli* DnaB replication protein is a DNA helicase. *Journal of Biological Chemistry* **261**, 4738-4748 (1986).

25 Better, M. & Freifelder, D. Studies on the replication of *E. coli* phage lambda DNA. *Virology* **126**, 168-182 (1983).

26 Wickner, S. H. DNA replication proteins of *Escherichia coli* and phage lambda. *Cold Spring Harb Symp Quant Biol* **43 Pt 1**, 303-310 (1979).

27 Grayhack, E. J., Yang, X. J., Lau, L. F. & Roberts, J. W. Phage lambda gene-Q antiterminator recognizes RNA polymerase near the promoter and accelerates it through a pause site. *Cell* **42**, 259-269, doi:Doi 10.1016/S0092-8674(85)80121-5 (1985).

28 Grayhack, E. J. & Roberts, J. W. The phage lambda Q gene product - activity of a transcription anti-terminator in vitro. *Cell* **30**, 637-648, doi:Doi 10.1016/0092-8674(82)90260-4 (1982).

29 Deighan, P. & Hochschild, A. The bacteriophage lambda Q anti-terminator protein regulates late gene expression as a stable component of the transcription elongation complex. *Molecular Microbiology* **63**, 911-920, doi:10.1111/j.1365-2958.2006.05563.x (2007).

30 Wang, I. N., Smith, D. L. & Young, R. Holins: the protein clocks of bacteriophage infections. *Annual Review of Microbiology* **54**, 799-825, doi:10.1146/annurev.micro.54.1.799 (2000).

31 Burt, D. & Brammar, W. The cis-specificity of the Q gene product of bacteriophage lambda. *Mol Gen Genet* **185**, 468-472 (1982).

32 Echols, H., Court, D. L. & Green, L. On the nature of cis-acting regulatory proteins and genetic organization in bacteriophage: the example of gene Q of bacteriophage lambda. *Genetics* **33**, 5-10 (1976).

33 Datta, A. B., Panjikar, S., Weiss, M. S., Chakrabarti, P. & Parrack, P. Structure of lambda CII: implications for recognition of direct-repeat DNA by an unusual tetrameric organization. *Proceedings of the National Academy of Sciences of the United States of America* **102**, 11242-11247, doi:10.1073/pnas.0504535102 (2005).

34 Reichardt, L. & Kaiser, A. Control of lambda repressor synthesis. *PNAS* **68**, 2185-2189 (1971).

35 Johnson, A. D., Meyer, B. J. & Ptashne, M. Interactions between DNA-bound repressors govern regulation by the lambda phage repressor. *Proceedings of the National Academy of Sciences of the United States of America* **76**, 5061-5065, doi:DOI 10.1073/pnas.76.10.5061 (1979).

36 Dodd, I. B. *et al.* Cooperativity in long-range gene regulation by the lambda CI repressor. *Gene Dev* **18**, 344-354, doi:Doi 10.1101/Gad.1167904 (2004).

37 Anderson, L. M. & Yang, H. DNA looping can enhance lysogenic CI transcription in phage lambda. *Proceedings of the National Academy of Sciences of the United States of America* **105**, 5827-5832, doi:10.1073/pnas.0705570105 (2008).

38 Nickels, B. E., Dove, S. L., Murakami, K. S., Darst, S. A. & Hochschild, A. Protein–protein and protein–DNA interactions of σ70 region 4 Involved in

transcription activation by λcI. *Journal of Molecular Biology* **324**, 17-34, doi:10.1016/s0022-2836(02)01043-4 (2002).

39 Jain, D., Nickels, B. E., Sun, L., Hochschild, A. & Darst, S. A. Structure of a ternary transcription activation complex. *Molecular Cell* **13**, 45-53 (2004).

40 Maurer, R., Meyer, B. J. & Ptashne, M. Gene regulation at the right operator (oR) of bacteriophage lambda. I. Or3 and autogenous negative control by repressor. *Journal of Molecular Biology* **139**, 147-161, doi:Doi 10.1016/0022-2836(80)90302-2 (1980).

41 Schindler, D. & Echols, H. Retroregulation of the int gene of bacteriophage lambda: control of translation completion. *Proceedings of the National Academy of Sciences of the United States of America* **78**, 4475-4479 (1981).

42 Kotewicz, M., Chung, S., Takeda, Y. & Echols, H. Characterization of the integration protein of bacteriophage lambda as a site-specific DNA-binding protein. *Proceedings of the National Academy of Sciences of the United States of America* **74**, 1511-1515 (1977).

43 Ho, Y. S. & Rosenberg, M. Characterization of a third, cII-dependent, coordinately activated promoter on phage lambda involved in lysogenic development. *The Journal of Biological Chemistry* **260**, 11838-11844 (1985).

44 Shotland, Y. *et al.* Proteolysis of the phage lambda CII regulatory protein by FtsH (HflB) of *Escherichia coli*. *Molecular Microbiology* **24**, 1303-1310 (1997).

45 Kihara, A., Akiyama, Y. & Ito, K. Host regulation of lysogenic decision in bacteriophage lambda: transmembrane modulation of FtsH (HflB), the cII

degrading protease, by HflKC (HflA). *Proceedings of the National Academy of Sciences of the United States of America* **94**, 5544-5549 (1997).

46 Herman, C., Thevenet, D., DAri, R. & Bouloc, P. The HflB protease of *Escherichia coli* degrades its inhibitor lambda cIII. *Journal of Bacteriology* **179**, 358-363, doi:DOI 10.1128/jb.179.2.358-363.1997 (1997).

47 Arkin, A., Ross, J. & McAdams, H. Stochastic kinetic analysis of developmental pathway bifurcation in phage lambda infected *E. coli* cells. *Genetics* **149**, 1633-1648 (1998).

48 Gillespie, D. T. Exact stochastic simulation of coupled chemical reactions. *Journal of Physical Chemistry*, 2340 – 2361 (1977).

49 Kourilsky, P. Lysogenization by bacteriophage lambda-I. multiple infection and the lysogenic response. *Mol Gen Genet* **122**, 183-195 (1973).

50 Kourilsky, P. & Knapp, A. Lysogenization by bacteriophage lambda. III. Multiplicity dependent phenomena occuring upon infection by lambda. *Biochimie* **56**, 1517-1523 (1974).

51 St-Pierre, F. & Endy, D. Determination of cell fate selection during phage lambda infection. *Proceedings of the National Academy of Sciences of the United States of America* **105**, 20705-20710, doi:10.1073/pnas.0808831105 (2008).

52 Kourilsky, P. Lysogenization by bacteriophage lambda-II. identification of genes involved in the multiplicity dependent processes. *Biochimie* **56**, 1511-1515 (1974).

53 Belfort, M. & Wulff, D. The roles of the lambda c3 gene and the Escherichia coli catabolite gene activation system in the establishment of lysogeny by bacteriophage lambda. *Proceedings of the National Academy of Sciences of the United States of America* **71**, 779-782 (1974).

54 Grodzicker, T., Arditti, R. R. & Eisen, H. Establishment of repression by lambdoid phage in catabolite activator protein and adenylate cyclase mutants of *Escherichia coli*. *Proceedings of the National Academy of Sciences of the United States of America* **69**, 366-370 (1972).

55 Slominska, M., Neubauer, P. & Wegrzyn, G. Regulation of bacteriophage lambda development by guanosine 5'-diphosphate-3'-diphosphate. *Virology* **262**, 431-441, doi:10.1006/viro.1999.9907 (1999).

56 Cotman, C. Apoptosis decision cascades and degeneration in Alzheimers disease. *Neurobiology of Aging* **19**, 29-32 (1998).

57 van Gaalen, M. M., van Koten, R., Schoffelmeer, A. N. & Vanderschuren, L. J. Critical involvement of dopaminergic neurotransmission in impulsive decision making. *Biological Psychiatry* **60**, 66-73, doi:10.1016/j.biopsych.2005.06.005 (2006).

58 Rahman, S., B, J. S., R, N. C., Rogers, R. & Robbins, T. Decision making and neuropsychiatry. *Trends in Cognitive Sciences* **5**, 271-277 (2001).

59 Starcke, K. & Brand, M. Decision making under stress: a selective review. *Neuroscience and Biobehavioral Reviews* **36**, 1228-1248, doi:10.1016/j.neubiorev.2012.02.003 (2012).

60 Clapham, D. E. TRP channels as cellular sensors. *Nature* **426**, 517-524, doi:10.1038/nature02196 (2003).

61 Story, G. M. *et al.* ANKTM1, a TRP-like channel expressed in nociceptive neurons, is activated by cold temperatures. *Cell* **112**, 819-829 (2003).

62 Galperin, M. Y. Bacterial signal transduction network in a genomic perspective. *Environmental Microbiology* **6**, 552-567, doi:10.1111/j.1462-2920.2004.00633.x (2004).

63 Stock, J. B., Stock, A. M. & Mottonen, J. M. Signal transduction in bacteria. *Nature* **344**, 395-400, doi:10.1038/344395a0 (1990).

64 Sanders, D. A., Gillece-Castro, B. L., Burlingame, A. L. & Koshland, D. E., Jr. Phosphorylation site of NtrC, a protein phosphatase whose covalent intermediate activates transcription. *Journal of Bacteriology* **174**, 5117-5122 (1992).

65 Parkinson, J. S. Signal transduction schemes of bacteria. *Cell* **73**, 857-871 (1993).

66 Briggman, K. L., Abarbanel, H. D. & Kristan, W. B., Jr. Optical imaging of neuronal populations during decision-making. *Science* **307**, 896-901, doi:10.1126/science.1103736 (2005).

67 Kristan, W. B. Neuronal decision-making circuits. *Current Biology : CB* **18**, R928-932, doi:10.1016/j.cub.2008.07.081 (2008).

68 Losick, R. & Desplan, C. Stochasticity and cell fate. *Science* **320**, 65-68, doi:10.1126/science.1147888 (2008).

69 Beaumont, H. J., Gallie, J., Kost, C., Ferguson, G. C. & Rainey, P. B. Experimental evolution of bet hedging. *Nature* **462**, 90-93, doi:10.1038/nature08504 (2009).

70 Veening, J. W., Smits, W. K. & Kuipers, O. P. Bistability, epigenetics, and bet-hedging in bacteria. *Annual Review of Microbiology* **62**, 193-210, doi:10.1146/annurev.micro.62.081307.163002 (2008).

71 Mangel, M. Game theory and animal behaviour. *Nature* **395**, 32-32, doi:Doi 10.1038/25651 (1998).

72 Wood, R. I., Kim, J. Y. & Li, G. R. Cooperation in rats playing the iterated Prisoner's Dilemma game. *Anim Behav* **114**, 27-35, doi:10.1016/j.anbehav.2016.01.010 (2016).

73 Gore, J., Youk, H. & van Oudenaarden, A. Snowdrift game dynamics and facultative cheating in yeast. *Nature* **459**, 253-256, doi:10.1038/nature07921 (2009).

74 Wolf, D. M. & Arkin, A. P. Motifs, modules and games in bacteria. *Current Opinion in Microbiology* **6**, 125-134 (2003).

75 Avlund, M., Dodd, I. B., Szabolcs, S., Sneppen, K. & Krishna, S. Why do phage play dice? *Journal of Virology* **83**, 11416-11420, doi:10.1128/Jvi.01057-09 (2009).

76 Turner, P. E. & Chao, L. Prisoner's dilemma in an RNA virus. *Nature* **398**, 441-443, doi:10.1038/18913 (1999).

77 Turner, P. E. & Chao, L. Escape from prisoner's dilemma in RNA phage phi6. *The American Naturalist* **161**, 497-505, doi:10.1086/367880 (2003).

78 Lewis, K. Persister cells, dormancy and infectious disease. *Nature Reviews Microbiology* **5**, 48-56, doi:10.1038/nrmicro1557 (2007).

79 Balaban, N. Q., Merrin, J., Chait, R., Kowalik, L. & Leibler, S. Bacterial persistence as a phenotypic switch. *Science* **305**, 1622-1625, doi:10.1126/science.1099390 (2004).

80 Moreira, D. & Lopez-Garcia, P. Ten reasons to exclude viruses from the tree of life. *Nature Reviews. Microbiology* **7**, 306-311, doi:10.1038/nrmicro2108 (2009).

81 Claverie, J. M. & Ogata, H. Ten good reasons not to exclude giruses from the evolutionary picture. *Nature Reviews Microbiology* **7**, doi:10.1038/nrmicro2108-c3 (2009).

82 Bonabeau, E., Theraulaz, G., Deneubourg, J. L., Aron, S. & Camazine, S. Self-organization in social insects. *Trends in Ecology & Evolution* **12**, 188-193 (1997).

83 Dussutour, A., Fourcassie, V., Helbing, D. & Deneubourg, J. L. Optimal traffic organization in ants under crowded conditions. *Nature* **428**, 70-73, doi:10.1038/nature02345 (2004).

84 Malamy, J. E. & Benfey, P. N. Organization and cell differentiation in lateral roots of *Arabidopsis thaliana*. *Development* **124**, 33-44 (1997).

85 Shubin, N. H. & Alberch, P. A Morphogenetic approach to the origin and basic organization of the tetrapod limb. *Evol Biol* **20**, 319-387 (1986).

86 Ehret, C. F. Organelle systems and biological organization. Structural and developmental evidence leads to a new look at our concepts of biological organization. *Science* **132**, 115-123 (1960).

87 Flemming, H. C. & Wingender, J. The biofilm matrix. *Nature Reviews. Microbiology* **8**, 623-633, doi:10.1038/nrmicro2415 (2010).

88 Prindle, A. *et al.* Ion channels enable electrical communication in bacterial communities. *Nature* **527**, 59-63, doi:10.1038/nature15709 (2015).

89 Typas, A., Banzhaf, M., Gross, C. A. & Vollmer, W. From the regulation of peptidoglycan synthesis to bacterial growth and morphology. *Nature Reviews. Microbiology* **10**, 123-136, doi:10.1038/nrmicro2677 (2011).

90 Sham, L. T. *et al.* MurJ is the flippase of lipid-linked precursors for peptidoglycan biogenesis. *Science* **345**, 220-222, doi:10.1126/science.1254522 (2014).

91 Chamakura, K. R. *et al.* A viral protein antibiotic inhibits lipid II flippase activity. *Nature Microbiology* **2**, 1480-1484, doi:10.1038/s41564-017-0023-4 (2017).

92 Shapiro, L., McAdams, H. H. & Losick, R. Why and how bacteria localize proteins. *Science* **326**, 1225-1228, doi:10.1126/science.1175685 (2009).

93 Wang, W., Li, G. W., Chen, C., Xie, X. S. & Zhuang, X. Chromosome organization by a nucleoid-associated protein in live bacteria. *Science* **333**, 1445-1449, doi:10.1126/science.1204697 (2011).

94 Wang, X., Possoz, C. & Sherratt, D. J. Dancing around the divisome: asymmetric chromosome segregation in *Escherichia coli*. *Genes Dev* **19**, 2367-2377, doi:10.1101/gad.345305 (2005).

95 Bi, E. F. & Lutkenhaus, J. FtsZ ring structure associated with division in *Escherichia coli*. *Nature* **354**, 161-164, doi:10.1038/354161a0 (1991).

96 Bernhardt, T. G. & de Boer, P. A. SlmA, a nucleoid-associated, FtsZ binding protein required for blocking septal ring assembly over chromosomes in *E. coli*. *Molecular Cell* **18**, 555-564, doi:10.1016/j.molcel.2005.04.012 (2005).

97 Justice, S. S., Garcia-Lara, J. & Rothfield, L. I. Cell division inhibitors SulA and MinC/MinD block septum formation at different steps in the assembly of the *Escherichia coli* division machinery. *Molecular Microbiology* **37**, 410-423, doi:DOI 10.1046/j.1365-2958.2000.02007.x (2000).

98 Danilova, O., Reyes-Lamothe, R., Pinskaya, M., Sherratt, D. & Possoz, C. MukB colocalizes with the oriC region and is required for organization of the two *Escherichia coli* chromosome arms into separate cell halves. *Molecular Microbiology* **65**, 1485-1492, doi:10.1111/j.1365-2958.2007.05881.x (2007).

99 de boer, P. A. J., Crossley, R. E., Hand, A. R. & Rothfield, L. I. The MinD protein is a membrane ATPase required for the correct placement of the *Escherichia coli* division site. *Embo Journal* **10**, 4371-4380 (1991).

100 Raskin, D. M. & deBoer, P. A. J. The MinE ring: an FtsZ-independent cell structure required for selection of the correct division site in *E. coli*. *Cell* **91**, 685-694, doi:Doi 10.1016/S0092-8674(00)80455-9 (1997).

101 Parry, B. R. *et al.* The bacterial cytoplasm has glass-like properties and is fluidized by metabolic activity. *Cell* **156**, 183-194, doi:10.1016/j.cell.2013.11.028 (2014).

102 Huang, K. C., Mukhopadhyay, R., Wen, B., Gitai, Z. & Wingreen, N. S. Cell shape and cell-wall organization in Gram-negative bacteria. *Proceedings of the National Academy of Sciences of the United States of America* **105**, 19282-19287, doi:10.1073/pnas.0805309105 (2008).

103 Ursell, T. S. *et al.* Rod-like bacterial shape is maintained by feedback between cell curvature and cytoskeletal localization. *Proceedings of the National Academy of Sciences of the United States of America* **111**, E1025-E1034, doi:10.1073/pnas.1317174111 (2014).

104 Ingerson-Mahar, M., Briegel, A., Werner, J. N., Jensen, G. J. & Gitai, Z. The metabolic enzyme CTP synthase forms cytoskeletal filaments. *Nature Cell Biology* **12**, 739-746, doi:10.1038/ncb2087 (2010).

105 O'Neill, R. E., Talon, J. & Palese, P. The influenza virus NEP (NS2 protein) mediates the nuclear export of viral ribonucleoproteins. *The EMBO Journal* **17**, 288-296, doi:10.1093/emboj/17.1.288 (1998).

106 Claverie, J. M. & Abergel, C. Mimivirus: the emerging paradox of quasi-autonomous viruses. *Trends in Genetics : TIG* **26**, 431-437, doi:10.1016/j.tig.2010.07.003 (2010).

107 Claverie, J. M. & Abergel, C. Mimivirus and its virophage. *Annu Rev Genet* **43**, 49-66, doi:10.1146/annurev-genet-102108-134255 (2009).

108 Legendre, M. *et al.* mRNA deep sequencing reveals 75 new genes and a complex transcriptional landscape in Mimivirus. *Genome Research* **20**, 664-674, doi:10.1101/gr.102582.109 (2010).

109 Chaikeeratisak, V. *et al.* Assembly of a nucleus-like structure during viral replication in bacteria. *Science* **355**, 194-197, doi:10.1126/science.aal2130 (2017).

110 Hallick, L., Boyce, R. P. & Echols, H. Membrane association by bacteriophage lambda DNA - possible direct role of regulator gene N. *Nature* **223**, 1239-&, doi:Doi 10.1038/2231239a0 (1969).

111 Kolber, A. R. & Sly, W. S. Association of lambda bacteriophage DNA with a rapidly sedimenting *Escherichia coli* component. *Virology* **46**, 638-654 (1971).

112 Stracy, M. *et al.* Live-cell superresolution microscopy reveals the organization of RNA polymerase in the bacterial nucleoid. *Proceedings of the National Academy of Sciences of the United States of America* **112**, E4390-4399, doi:10.1073/pnas.1507592112 (2015).

113 Bakshi, S., Siryaporn, A., Goulian, M. & Weisshaar, J. C. Superresolution imaging of ribosomes and RNA polymerase in live *Escherichia coli* cells. *Molecular Microbiology* **85**, 21-38, doi:10.1111/j.1365-2958.2012.08081.x (2012).

114 Castellana, M., Hsin-Jung Li, S. & Wingreen, N. S. Spatial organization of bacterial transcription and translation. *Proceedings of the National Academy of*

Sciences of the United States of America **113**, 9286-9291, doi:10.1073/pnas.1604995113 (2016).

115 Mueller, U. G., Rehner, S. A. & Schultz, T. R. The evolution of agriculture in ants. *Science* **281**, 2034-2038 (1998).

116 Caldwell, M. M., Dawson, T. E. & Richards, J. H. Hydraulic lift: consequences of water efflux from the roots of plants. *Oecologia* **113**, 151-161, doi:10.1007/s004420050363 (1998).

117 Neumann, R. B. & Cardon, Z. G. The magnitude of hydraulic redistribution by plant roots: a review and synthesis of empirical and modeling studies. *The New Phytologist* **194**, 337-352, doi:10.1111/j.1469-8137.2012.04088.x (2012).

118 Carlson, M. & Botstein, D. Two differentially regulated mRNAs with different 5' ends encode secreted with intracellular forms of yeast invertase. *Cell* **28**, 145-154 (1982).

119 Hueck, C. J. Type III protein secretion systems in bacterial pathogens of animals and plants. *Microbiology and Molecular Biology Reviews : MMBR* **62**, 379-433 (1998).

120 Christie, P. J. & Vogel, J. P. Bacterial type IV secretion: conjugation systems adapted to deliver effector molecules to host cells. *Trends in Microbiology* **8**, 354-360 (2000).

121 Bingle, L. E., Bailey, C. M. & Pallen, M. J. Type VI secretion: a beginner's guide. *Current Opinion in Microbiology* **11**, 3-8, doi:10.1016/j.mib.2008.01.006 (2008).

122 Cascales, E. *et al.* Colicin biology. *Microbiology and Molecular Biology Reviews : MMBR* **71**, 158-229, doi:10.1128/MMBR.00036-06 (2007).

123 Liu, J. T. *et al.* Coupling between distant biofilms and emergence of nutrient time-sharing. *Science* **356**, 638-641, doi:10.1126/science.aah4204 (2017).

124 Humphries, J. *et al.* Species-independent attraction to biofilms through electrical signaling. *Cell* **168**, 200-+, doi:10.1016/j.cell.2016.12.014 (2017).

125 Iida, S., Streiff, M. B., Bickle, T. A. & Arber, W. Two DNA antirestriction systems of bacteriophage P1, darA, and darB: characterization of darA- phages. *Virology* **157**, 156-166 (1987).

126 Pedruzzi, I., Rosenbusch, J. P. & Locher, K. P. Inactivation in vitro of the *Escherichia coli* outer membrane protein FhuA by a phage T5-encoded lipoprotein. *FEMS Microbiology Letters* **168**, 119-125 (1998).

127 Erez, Z. *et al.* Communication between viruses guides lysis-lysogeny decisions. *Nature* **541**, 488-493, doi:10.1038/nature21049 (2017).

128 Toothman, P. & Herskowitz, I. Rex-dependent exclusion of lambdoid phages. *Virology* **102** (1980).

129 Labrie, S. J., Samson, J. E. & Moineau, S. Bacteriophage resistance mechanisms. *Nature Reviews. Microbiology* **8**, 317-327, doi:10.1038/nrmicro2315 (2010).

130 Golding, I. Single-Cell Studies of Phage λ: hidden treasures under Occam's rug. *Annu Rev Virol* **3**, 1-20, doi:10.1146/annurev-virology-110615-042127 (2016).

131 Bednarz, M., Halliday, J. A., Herman, C. & Golding, I. Revisiting bistability in the lysis/lysogeny circuit of bacteriophage lambda. *PloS One* **9**, e100876, doi:10.1371/journal.pone.0100876 (2014).

132 Alvarez, L. J., Thomen, P., Makushok, T. & Chatenay, D. Propagation of fluorescent viruses in growing plaques. *Biotechnology and Bioengineering* **96**, 615-621, doi:10.1002/bit.21110 (2007).

133 Zeng, L. *et al.* Decision making at a subcellular level determines the outcome of bacteriophage infection. *Cell* **141**, 682-691, doi:10.1016/j.cell.2010.03.034 (2010).

134 Shao, Q. *et al.* Lysis-lysogeny coexistence: prophage integration during lytic development. *MircrobiologyOpen*, doi:10.1002/mbo3.395 (2016).

135 Shao, Q., Hawkins, A. & Zeng, L. Phage DNA dynamics in cells with different fates. *Biophysical Journal* **108**, 2048-2060, doi:10.1016/j.bpj.2015.03.027 (2015).

136 Golding, I. Infection by bacteriophage lambda: an evolving paradigm for cellular individuality. *Current Opinion in Microbiology* **43**, 9-13, doi:10.1016/j.mib.2017.09.014 (2017).

137 Van Valen, D. *et al.* A single-molecule Hershey-Chase experiment. *Current Biology : CB* **22**, 1339-1343, doi:10.1016/j.cub.2012.05.023 (2012).

138 Clarke, M., Maddera, L., Harris, R. L. & Silverman, P. M. F-pili dynamics by live-cell imaging. *Proceedings of the National Academy of Sciences of the United States of America* **105**, 17978-17981, doi:10.1073/pnas.0806786105 (2008).

139 van Ditmarsch, D. *et al.* Convergent evolution of hyperswarming leads to impaired biofilm formation in pathogenic bacteria. *Cell Reports* **4**, 697-708, doi:10.1016/j.celrep.2013.07.026 (2013).

140 Gonzalez, C. *et al.* Stress-response balance drives the evolution of a network module and its host genome. *Molecular Systems Biology* **11**, 827, doi:10.15252/msb.20156185 (2015).

141 Sneppen, K., Krishna, S. & Semsey, S. Simplified models of biological networks. *Annu Rev Biophys* **39**, 43-59, doi:10.1146/annurev.biophys.093008.131241 (2010).

142 Dressler, D. & Potter, H. Molecular mechanisms in genetic recombination. *Annual Review of Biochemistry* **51**, 727-761, doi:10.1146/annurev.bi.51.070182.003455 (1982).

143 Dodd, I. B., Shearwin, K. E. & Egan, J. B. Revisited gene regulation in bacteriophage lambda. *Current Opinion in Genetics & Development* **15**, 145-152, doi:10.1016/j.gde.2005.02.001 (2005).

144 West, S. A., Griffin, A. S. & Gardner, A. Evolutionary explanations for cooperation. *Current Biology : CB* **17**, R661-672, doi:10.1016/j.cub.2007.06.004 (2007).

145 Yurtsev, E. A., Chao, H. X., Datta, M. S., Artemova, T. & Gore, J. Bacterial cheating drives the population dynamics of cooperative antibiotic resistance plasmids. *Molecular Systems Biology* **9**, 683, doi:10.1038/msb.2013.39 (2013).

146 Goedhart, J. *et al.* Structure-guided evolution of cyan fluorescent proteins towards a quantum yield of 93%. *Nature Communications* **3**, 751, doi:10.1038/ncomms1738 (2012).

147 Shaner, N. C. *et al.* A bright monomeric green fluorescent protein derived from *Branchiostoma lanceolatum*. *Nature Methods* **10**, 407-409, doi:10.1038/nmeth.2413 (2013).

148 Sakaue-Sawano, A. *et al.* Visualizing spatiotemporal dynamics of multicellular cell-cycle progression. *Cell* **132**, 487-498, doi:10.1016/j.cell.2007.12.033 (2008).

149 Shcherbo, D. *et al.* Far-red fluorescent tags for protein imaging in living tissues. *The Biochemical Journal* **418**, 567-574, doi:10.1042/BJ20081949 (2009).

150 Bæk, K., Svenningsen, S., Eisen, H., Sneppen, K. & Brown, S. Single-cell analysis of λ Immunity Regulation. *Journal of Molecular Biology* **334**, 363-372, doi:10.1016/j.jmb.2003.09.037 (2003).

151 Révet, B., von Wilcken-Bergmann, B., Bessert, H., Barker, A. & Müller-Hill, B. Four dimers of lambda repressor bound to two suitably spaced pairs of lambda operators form octamers and DNA loops over large distances. *Current Biology* **9**, 151-154 (1999).

152 Gussin, G. & Peterson, V. Isolation and properties of rex- mutants of bacteriophage lambda. *Virology* **10**, 760-765 (1972).

153 Engelberg-Kulka, H. & Kumar, S. Yet another way that phage lambda manipulates its *Escherichia coli* host: lambda rexB is involved in the lysogenic-

lytic switch. *Molecular Microbiology* **96**, 689-693, doi:10.1111/mmi.12969 (2015).

154 Ueda, K., McMacken, R. & Kornberg, A. DnaB protein of *Escherichia coli*. Purification and role in the replication of phiX174 DNA. *The Journal of Biological Chemistry* **253**, 261-269 (1978).

155 Wegrzyn, G. & Taylor, K. Inheritance of the replication complex by one of two daughter copies during lambda plasmid replication in *Escherichia coli*. *J Mol Biol* **226**, 681-688 (1992).

156 Kaiser, A. Mutations in a temperate bacteriophage affecting its ability to lysogenize *E. coli*. *Virology* **3**, 42-61 (1957).

157 Dove, W. F. Action of the lambda chromosome. I. control of functions late in bacteriophage development. *J Mol Biol* **19**, 187-201 (1966).

158 Brooks, K. Studies in the physiological genetics of some suppressor-sensitive mutants of bacteriophage lambda. *Virology* **26**, 489-499 (1965).

159 Babic, A., Lindner, A. B., Vulic, M., Stewart, E. J. & Radman, M. Direct visualization of horizontal gene transfer. *Science* **319**, 1533-1536, doi:10.1126/science.1153498 (2008).

160 Baranska, S. *et al.* Regulation of the switch from early to late bacteriophage lambda DNA replication. *Microbiology* **147**, 535-547 (2001).

161 Weitz, J. S., Mileyko, Y., Joh, R. I. & Voit, E. O. Collective decision making in bacterial viruses. *Biophysical Journal* **95**, 2673-2680, doi:10.1529/biophysj.108.133694 (2008).

162 Ripp, S. & Miller, R. V. The role of pseudolysogeny in bacteriophage-host interactions in a natural freshwater environment. *Microbiol-Uk* **143**, 2065-2070 (1997).

163 Wu, Y. H., Franden, M. A., Hawker, J. R., Jr. & McHenry, C. S. Monoclonal antibodies specific for the alpha subunit of the *Escherichia coli* DNA polymerase III holoenzyme. *The Journal of Biological Chemistry* **259**, 12117-12122 (1984).

164 Lynch, M. The evolution of genetic networks by non-adaptive processes. *Nature Reviews. Genetics* **8**, 803-813, doi:10.1038/nrg2192 (2007).

165 Ohashi, M. & Dove, W. F. Lethal lysogenization by coliphage lambda. *Virology* **72**, 299-307 (1976).

166 Svenningsen, S. L. & Semsey, S. Commitment to lysogeny is preceded by a prolonged period of sensitivity to the late lytic regulator Q in bacteriophage lambda. *Journal of Bacteriology* **196**, 3582-3588, doi:10.1128/JB.01705-14 (2014).

167 Marinus, M. G. & Morris, N. R. Biological function for 6-methyladenine residues in the DNA of *Escherichia coli* K12. *J Mol Biol* **85**, 309-322 (1974).

168 Wadhams, G. H. & Armitage, J. P. Making sense of it all: bacterial chemotaxis. *Nature Reviews. Molecular Cell Biology* **5**, 1024-1037, doi:10.1038/nrm1524 (2004).

169 Bode, W. Lysis inhibition in *Escherichia coli* infected with bacteriophage T4. *Journal of Virology* **1**, 948-955 (1967).

170 Six, E. W. & Klug, C. A. Bacteriophage P4: a satellite virus depending on a helper such as prophage P2. *Virology* **51**, 327-344 (1973).

171 Suttle, C. A. Viruses in the sea. *Nature* **437**, 356-361, doi:10.1038/nature04160 (2005).

172 Zinder, N. D. RNA phages. *Annual Review of Microbiology* **19**, 455-472, doi:10.1146/annurev.mi.19.100165.002323 (1965).

173 Shirogane, Y., Watanabe, S. & Yanagi, Y. Cooperation: another mechanism of viral evolution. *Trends in Microbiology* **21**, 320-324, doi:10.1016/j.tim.2013.05.004 (2013).

174 Rizzetto, M. Hepatitis D: thirty years after. *Journal of Hepatology* **50**, 1043-1050, doi:10.1016/j.jhep.2009.01.004 (2009).

175 Datsenko, K. A. & Wanner, B. L. One-step inactivation of chromosomal genes in *Escherichia coli* K-12 using PCR products. *Proceedings of the National Academy of Sciences of the United States of America* **97**, 6640-6645, doi:10.1073/pnas.120163297 (2000).

176 Sussman, R. & Jacob, F. On a thermosensitive repression system in the *Escherichia coli* lambda bacteriophage. *C.R. Acad. Sci.* **254** (1962).

177 Roberts, J. W. & Devoret, R. in *Lambda II* (eds RW Hendrix, J. W. Roberts, FW Stahl, & RA Weisberg) (Cold Spring Harbor Laboratory, 1983).

178 Zhang, N. & Young, R. Complementation and characterization of the nested Rz and Rz1 reading frames in the genome of bacteriophage lambda. *Mol Gen Genet* **262**, 659-667 (1999).

179 Szyf, M. *et al.* DNA methylation pattern is determined by the intracellular level of the methylase. *Proceedings of the National Academy of Sciences of the United States of America* **81**, 3278-3282 (1984).

180 Sambrook, J., and Russell, D.W. *Molecular cloning: a laboratory manual*. Third edn, (Cold Spring Harbor Press, 2001).

181 Gillespie, D. T. Approximate accelerated stochastic simulation of chemically reacting systems. *Journal of Chemical Physics*, 1716-1733 (2001).

182 Yao, N. Y. & O'Donnell, M. SnapShot: The replisome. *Cell* **141**, 1088, 1088 e1081, doi:10.1016/j.cell.2010.05.042 (2010).

183 Wegrzyn, A., Wegrzyn, G., Herman, A. & Taylor, K. Protein inheritance: lambda plasmid replication perpetuated by the heritable replication complex. *Genes to Cells : Devoted to Molecular & Cellular Mechanisms* **1**, 953-963 (1996).

184 Kelman, Z. & O'Donnell, M. DNA polymerase III holoenzyme: structure and function of a chromosomal replicating machine. *Annual Review of Biochemistry* **64**, 171-200, doi:10.1146/annurev.bi.64.070195.001131 (1995).

185 Maki, H. & Kornberg, A. The polymerase subunit of DNA polymerase III of *Escherichia coli*. II. purification of the alpha subunit, devoid of nuclease activities. *The Journal of Biological Chemistry* **260**, 12987-12992 (1985).

186 Zong, C., So, L. H., Sepulveda, L. A., Skinner, S. O. & Golding, I. Lysogen stability is determined by the frequency of activity bursts from the fate-determining gene. *Molecular Systems Biology* **6**, 440, doi:10.1038/msb.2010.96 (2010).

187 Cooke, J. The emergence and regulation of spatial organization in early animal development. *Annual Review of Biophysics and Bioengineering* **4**, 185-217, doi:10.1146/annurev.bb.04.060175.001153 (1975).

188 Munro, S. Organelle identity and the organization of membrane traffic. *Nature Cell Biology* **6**, 469-472, doi:10.1038/ncb0604-469 (2004).

189 Klein, A., Lanka, E. & Schuster, H. Isolation of a complex between the P protein of phage lambda and the DnaB protein of *Escherichia coli*. *Eur J Biochem* **105**, 1-6, doi:DOI 10.1111/j.1432-1033.1980.tb04467.x (1980).

190 Biswas, S. B. & Biswas, E. E. Regulation of dnaB function in DNA replication in *Escherichia coli* by dnaC and lambda P gene products. *The Journal of Biological Chemistry* **262**, 7831-7838 (1987).

191 Tyler, B. M. & Goldberg, R. B. Transduction of chromosomal genes between enteric bacteria by bacteriophage P1. *Journal of Bacteriology* **125**, 1105-1111 (1976).

192 Dodson, M., Roberts, J., McMacken, R. & Echols, H. Specialized nucleoprotein structures at the origin of replication of bacteriophage lambda: complexes with lambda O protein and with lambda O, lambda P, and *Escherichia coli* DnaB proteins. *Proceedings of the National Academy of Sciences of the United States of America* **82**, 4678-4682 (1985).

193 Vogel, U. & Jensen, K. F. The RNA chain elongation rate in *Escherichia coli* depends on the growth rate. *Journal of Bacteriology* **176**, 2807-2813 (1994).

194 Mao, Y. S., Zhang, B. & Spector, D. L. Biogenesis and function of nuclear bodies. *Trends in Genetics : TIG* **27**, 295-306, doi:10.1016/j.tig.2011.05.006 (2011).

195 Weber, S. C. & Brangwynne, C. P. Getting RNA and protein in phase. *Cell* **149**, 1188-1191, doi:10.1016/j.cell.2012.05.022 (2012).

196 Abergel, C., Rudinger-Thirion, J., Giege, R. & Claverie, J. M. Virus-encoded aminoacyl-tRNA synthetases: structural and functional characterization of mimivirus TyrRS and MetRS. *Journal of Virology* **81**, 12406-12417, doi:10.1128/JVI.01107-07 (2007).

197 Skinner, S. O., Sepulveda, L. A., Xu, H. & Golding, I. Measuring mRNA copy number in individual *Escherichia coli* cells using single-molecule fluorescent in situ hybridization. *Nature Protocols* **8**, 1100-1113, doi:10.1038/nprot.2013.066 (2013).

198 Bates, D. & Kleckner, N. Chromosome and replisome dynamics in *E. coli*: loss of sister cohesion triggers global chromosome movement and mediates chromosome segregation. *Cell* **121**, 899-911, doi:10.1016/j.cell.2005.04.013 (2005).

199 Whitman, W. B., Coleman, D. C. & Wiebe, W. J. Prokaryotes: the unseen majority. *Proceedings of the National Academy of Sciences of the United States of America* **95**, 6578-6583 (1998).

200 Molbak, K., Hojlyng, N., Jepsen, S. & Gaarslev, K. Bacterial contamination of stored water and stored food: a potential source of diarrhoeal disease in West Africa. *Epidemiology and Infection* **102**, 309-316 (1989).

201 Crump, J. A., Griffin, P. M. & Angulo, F. J. Bacterial contamination of animal feed and its relationship to human foodborne illness. *Clinical Infectious Diseases : an Official Publication of the Infectious Diseases Society of America* **35**, 859-865, doi:10.1086/342885 (2002).

202 de Boer, E. & Beumer, R. R. Methodology for detection and typing of foodborne microorganisms. *International Journal of Food Microbiology* **50**, 119-130 (1999).

203 Mozola, M. A. Genetics-based methods for detection of *Salmonella* spp. in foods. *Journal of AOAC International* **89**, 517-529 (2006).

204 Chang, Y. R. *et al.* Mass production and dynamic imaging of fluorescent nanodiamonds. *Nature Nanotechnology* **3**, 284-288, doi:10.1038/nnano.2008.99 (2008).

205 Yu, S. J., Kang, M. W., Chang, H. C., Chen, K. M. & Yu, Y. C. Bright fluorescent nanodiamonds: no photobleaching and low cytotoxicity. *Journal of the American Chemical Society* **127**, 17604-17605, doi:10.1021/ja0567081 (2005).

206 Hsiao, W. W., Hui, Y. Y., Tsai, P. C. & Chang, H. C. Fluorescent nanodiamond: a versatile tool for long-term cell tracking, super-resolution imaging, and nanoscale temperature sensing. *Accounts of Chemical Research* **49**, 400-407, doi:10.1021/acs.accounts.5b00484 (2016).

207 Chaiet, L. & Wolf, F. J. The properties of streptavidin, a biotin-binding protein produced by *Streptomycetes*. *Archives of Biochemistry and Biophysics* **106**, 1-5 (1964).

208 Beckett, D., Kovaleva, E. & Schatz, P. J. A minimal peptide substrate in biotin holoenzyme synthetase-catalyzed biotinylation. *Protein Science : a Publication of the Protein Society* **8**, 921-929, doi:10.1110/ps.8.4.921 (1999).

209 Barker, D. F. & Campbell, A. M. The birA gene of *Escherichia coli* encodes a biotin holoenzyme synthetase. *J Mol Biol* **146**, 451-467 (1981).

210 Calendar, R. Viral transactivation. *Bio-Technol* **4**, 1074-1077, doi:Doi 10.1038/Nbt1286-1074 (1986).

211 Trinh, J. T., Szekely, T., Shao, Q., Balazsi, G. & Zeng, L. Cell fate decisions emerge as phages cooperate or compete inside their host. *Nature Communications* **8**, 14341, doi:10.1038/ncomms14341 (2017).

212 Michalet, X. *et al.* Quantum dots for live cells, in vivo imaging, and diagnostics. *Science* **307**, 538-544, doi:10.1126/science.1104274 (2005).

213 Wehling, J., Dringen, R., Zare, R. N., Maas, M. & Rezwan, K. Bactericidal activity of partially oxidized nanodiamonds. *Acs Nano* **8**, 6475-6483, doi:10.1021/nn502230m (2014).

214 Turcheniuk, V. *et al.* Antimicrobial activity of menthol modified nanodiamond particles. *Diam Relat Mater* **57**, 2-8, doi:10.1016/j.diamond.2014.12.002 (2015).

215 Beranova, J. *et al.* Sensitivity of bacteria to diamond nanoparticles of various size differs in Gram-positive and Gram-negative cells. *FEMS Microbiology Letters* **351**, 179-186, doi:Doi 10.1111/1574-6968.12373 (2014).

216 Suarez-Kelly, L. P. *et al.* Fluorescent nanodiamonds engage innate immune effector cells: a potential vehicle for targeted anti-tumor immunotherapy. *Nanomed-Nanotechnol* **13**, 909-920, doi:10.1016/j.nano.2016.12.005 (2017).

217 Mohan, N., Chen, C. S., Hsieh, H. H., Wu, Y. C. & Chang, H. C. In vivo imaging and toxicity assessments of fluorescent nanodiamonds in *Caenorhabditis elegans*. *Nano Letters* **10**, 3692-3699, doi:10.1021/nl1021909 (2010).

218 Kirchner, C. *et al.* Cytotoxicity of colloidal CdSe and CdSe/ZnS nanoparticles. *Nano Letters* **5**, 331-338, doi:10.1021/nl047996m (2005).

219 Yong, K. T. *et al.* Nanotoxicity assessment of quantum dots: from cellular to primate studies. *Chemical Society Reviews* **42**, 1236-1250, doi:10.1039/c2cs35392j (2013).

220 Mahler, B. *et al.* Towards non-blinking colloidal quantum dots. *Nature Materials* **7**, 659-664, doi:10.1038/nmat2222 (2008).

221 Fu, C. C. *et al.* Characterization and application of single fluorescent nanodiamonds as cellular biomarkers. *Proceedings of the National Academy of Sciences of the United States of America* **104**, 727-732, doi:10.1073/pnas.0605409104 (2007).

222 Kaiser, D. & Dworkin, M. Gene transfer to myxobacterium by *Escherichia coli* phage P1. *Science* **187**, 653-654 (1975).

223 Kaper, J. B., Nataro, J. P. & Mobley, H. L. Pathogenic *Escherichia coli*. *Nature Reviews. Microbiology* **2**, 123-140, doi:10.1038/nrmicro818 (2004).

224 Donnenberg, M. S. Pathogenic strategies of enteric bacteria. *Nature* **406**, 768-774, doi:10.1038/35021212 (2000).

225 Perry, L. L. *et al.* Sequence analysis of *Escherichia coli* O157:H7 bacteriophage PhiV10 and identification of a phage-encoded immunity protein that modifies the O157 antigen. *FEMS Microbiology Letters* **292**, 182-186, doi:10.1111/j.1574-6968.2009.01511.x (2009).

226 Knirel, Y. A. *et al.* Variations in O-antigen biosynthesis and O-acetylation associated with altered phage sensitivity in *Escherichia coli* 4s. *Journal of Bacteriology* **197**, 905-912, doi:10.1128/JB.02398-14 (2015).

227 Culbreath, K. & Petti, C. A. Balancing enthusiasm for innovative technologies with optimizing value: an approach to adopt new laboratory tests for infectious diseases using bloodstream infections as exemplar. *Open Forum Infectious Diseases* **2**, ofv075, doi:10.1093/ofid/ofv075 (2015).

228 Stevenson, L. G., Drake, S. K. & Murray, P. R. Rapid identification of bacteria in positive blood culture broths by matrix-assisted laser desorption ionization-time of flight mass spectrometry. *Journal of Clinical Microbiology* **48**, 444-447, doi:10.1128/JCM.01541-09 (2010).

229 Ferroni, A. *et al.* Real-time identification of bacteria and *Candida* species in positive blood culture broths by matrix-assisted laser desorption ionization-time

of flight mass spectrometry. *Journal of Clinical Microbiology* **48**, 1542-1548, doi:10.1128/JCM.02485-09 (2010).

230 Koniev, O. & Wagner, A. Developments and recent advancements in the field of endogenous amino acid selective bond forming reactions for bioconjugation. *Chemical Society Reviews* **44**, 5495-5551, doi:10.1039/c5cs00048c (2015).

231 Edgar, R. *et al.* High-sensitivity bacterial detection using biotin-tagged phage and quantum-dot nanocomplexes. *Proceedings of the National Academy of Sciences of the United States of America* **103**, 4841-4845, doi:10.1073/pnas.0601211103 (2006).

232 Mkandawire, M. *et al.* Selective targeting of green fluorescent nanodiamond conjugates to mitochondria in HeLa cells. *Journal of Biophotonics* **2**, 596-606, doi:10.1002/jbio.200910002 (2009).

233 Mochalin, V. N. & Gogotsi, Y. Wet chemistry route to hydrophobic blue fluorescent nanodiamond. *Journal of the American Chemical Society* **131**, 4594-4595, doi:10.1021/ja9004514 (2009).

234 Kucsko, G. *et al.* Nanometre-scale thermometry in a living cell. *Nature* **500**, 54-58, doi:10.1038/nature12373 (2013).

235 Balasubramanian, G. *et al.* Nanoscale imaging magnetometry with diamond spins under ambient conditions. *Nature* **455**, 648-651, doi:10.1038/nature07278 (2008).

236 Schirhagl, R., Chang, K., Loretz, M. & Degen, C. L. Nitrogen-vacancy centers in diamond: nanoscale sensors for physics and biology. *Annual Review of Physical Chemistry* **65**, 83-105, doi:10.1146/annurev-physchem-040513-103659 (2014).

237 Dantelle, G. *et al.* Efficient production of NV colour centres in nanodiamonds using high-energy electron irradiation. *J Lumin* **130**, 1655-1658, doi:10.1016/j.jlumin.2009.12.003 (2010).

238 Boudou, J. P. *et al.* High yield fabrication of fluorescent nanodiamonds. *Nanotechnology* **20**, doi:Artn 23560210.1088/0957-4484/20/23/235602 (2009).

239 Ushizawa, K. *et al.* Covalent immobilization of DNA on diamond and its verification by diffuse reflectance infrared spectroscopy. *Chem Phys Lett* **351**, 105-108, doi:Doi 10.1016/S0009-2614(01)01362-8 (2002).

240 Li, Y. S. *et al.* Electrochemistry of carboxylated nanodiamond films. *Sci China Chem* **55**, 2445-2449, doi:10.1007/s11426-012-4619-5 (2012).

241 Boudou, J. P., David, M. O., Joshi, V., Eidi, H. & Curmi, P. A. Hyperbranched polyglycerol modified fluorescent nanodiamond for biomedical research. *Diam Relat Mater* **38**, 131-138, doi:10.1016/j.diamond.2013.06.019 (2013).

242 Zhao, L. *et al.* Chromatographic separation of highly soluble diamond nanoparticles prepared by polyglycerol grafting. *Angew Chem Int Edit* **50**, 1388-1392, doi:10.1002/anie.201006310 (2011).

243 Ferullo, D. J., Cooper, D. L., Moore, H. R. & Lovett, S. T. Cell cycle synchronization of *Escherichia coli* using the stringent response, with

fluorescence labeling assays for DNA content and replication. *Methods* **48**, 8-13, doi:10.1016/j.ymeth.2009.02.010 (2009).

244 Jao, C. Y. & Salic, A. Exploring RNA transcription and turnover in vivo by using click chemistry. *Proceedings of the National Academy of Sciences of the United States of America* **105**, 15779-15784, doi:10.1073/pnas.0808480105 (2008).

245 Jungmann, R. *et al.* Multiplexed 3D cellular super-resolution imaging with DNA-PAINT and exchange-PAINT. *Nature Methods* **11**, 313-U292, doi:10.1038/Nmeth.2835 (2014).

246 Pogliano, J., Ho, T. Q., Zhong, Z. & Helinski, D. R. Multicopy plasmids are clustered and localized in *Escherichia coli*. *Proceedings of the National Academy of Sciences of the United States of America* **98**, 4486-4491, doi:10.1073/pnas.081075798 (2001).

247 Pogliano, J. Dynamic cellular location of bacterial plasmids. *Current Opinion in Microbiology* **5**, 586-590 (2002).